UNLV | UNIVERSITY LIBRARIES

UNLV Theses, Dissertations, Professional Papers, and Capstones

8-2010

The Effects of contact metamorphism on the host rocks for Carlin-type mineralization at the Getchell Development, Nevada, USA

Nathan C. Eck
University of Nevada, Las Vegas

Follow this and additional works at: https://digitalscholarship.unlv.edu/thesesdissertations

 Part of the Geology Commons

Repository Citation

Eck, Nathan C., "The Effects of contact metamorphism on the host rocks for Carlin-type mineralization at the Getchell Development, Nevada, USA" (2010). *UNLV Theses, Dissertations, Professional Papers, and Capstones*. 879.
http://dx.doi.org/10.34917/2228977

This Thesis is protected by copyright and/or related rights. It has been brought to you by Digital Scholarship@UNLV with permission from the rights-holder(s). You are free to use this Thesis in any way that is permitted by the copyright and related rights legislation that applies to your use. For other uses you need to obtain permission from the rights-holder(s) directly, unless additional rights are indicated by a Creative Commons license in the record and/or on the work itself.

This Thesis has been accepted for inclusion in UNLV Theses, Dissertations, Professional Papers, and Capstones by an authorized administrator of Digital Scholarship@UNLV. For more information, please contact digitalscholarship@unlv.edu.

THE EFFECTS OF CONTACT METAMORPHISM ON THE HOST ROCKS FOR CARLIN-TYPE MINERALIZATION AT THE GETCHELL DEPOSIT, NEVADA, USA

by

Nathan Charles Eck

Bachelor of Science
University of Wisconsin - Madison
2008

A thesis submitted in partial fulfillment
of the requirements for the

Master of Science in Geoscience
Department of Geoscience
College of Sciences

Graduate College
University of Nevada, Las Vegas
August 2010

Copyright by Nathan Eck 2010
All Rights Reserved

UNLV
UNIVERSITY OF NEVADA LAS VEGAS

THE GRADUATE COLLEGE

We recommend the thesis prepared under our supervision by

Nathan Charles Eck

entitled

The Effects of Contact Metamorphism on the Host Rocks for Carlin-Type Mineralization at the Getchell Development, Nevada, USA

be accepted in partial fulfillment of the requirements for the degree of

Master of Science in Geoscience

Adam Simon, Committee Co-chair

Jean Cline, Committee Co-chair

Wanda Taylor, Committee Member

John Muntean, Committee Member

Barbara Luke, Graduate Faculty Representative

Ronald Smith, Ph. D., Vice President for Research and Graduate Studies
and Dean of the Graduate College

August 2010

ABSTRACT

The Effects of Contact Metamorphism on Host Rocks for Carlin-Type Mineralization at the Getchell Deposit, Nevada, USA

by

Nathan Charles Eck

Dr. Adam Simon, Examination Committee Co-chair
Assistant Professor
University of Nevada, Las Vegas

Dr. Jean Cline, Examination Committee Co-chair
Professor
University of Nevada, Las Vegas

Carlin-type gold deposits (CTGDs) result from low to moderate temperature hydrothermal systems which form replacement bodies in carbonate or calcareous host rocks. The Getchell CTGD is located on the Getchell trend in north central Nevada. The Eocene age mineralization is locally hosted within the metamorphic aureole of the Cretaceous age Osgood stock. Previous studies have noted that the effects of the contact metamorphism can be heterogeneous, with strongly calc-silicate altered carbonates transitioning to relatively pristine limestone over short distances. The main finding of this study was that the variability in calc-silicate alteration is largely dependent on the differing host lithologies at the deposit. Strong calc-silicate alteration from contact metamorphism commonly exists in rocks composed of argillaceous mudstone inter-bedded with limestone while the rocks composed of siliceous carbonaceous mudstones and limestones just a few meters away show no evidence of calc-silicate alteration.

The different ways in which these rock types respond to the contact metamorphism plays an important role in ore control at the deposit. The strongly calc-silicate altered rocks are poor hosts for Carlin-type gold deposition. The ore fluids which were

moderately acidic, pH 3-4, required carbonates to generate porosity and permeability, as well as to liberate iron for the ore fluids to sulfidize to form the Au-bearing pyrite. As such the strongly calc-silicate altered lithologies are not receptive to the Carlin ore fluids, due to most of the carbonate being replaced by calc-silicate minerals. The limestones inter-bedded with siliceous carbonaceous mudstones which have not been altered to calc-silicates, are the best hosts for Carlin-type mineralization. This study observed several locations where strong mineralization is present in this rock type up to the contact with the strongly calc-silicate altered argillaceous mudstones inter-bedded with limestones.

Additionally mineralization is restricted to areas adjacent to conduits for ore fluids, most commonly faults, but also along dikes. Where conduits transporting ore fluids contact the receptive areas host rock mineralization permeates outward away from the conduit. The best hosts, those which are dominantly limestone, contain grades >1.000 ounce Au per ton (oz/t). Sections composed dominantly of siliceous carbonaceous mudstones have little to no calcareous material for the ore fluids to replace aside from calcite filled fractures. Gold grade in mineralized sections of siliceous carbonaceous mudstone are <0.100 oz/t Au. Faults which cut the strongly calc-silicate altered rocks typically have mineralization which is confined to the fault gouge and does not permeate into the surrounding rock, although in heavily faulted areas there can be significant intervals of fault gouge and breccia with ore grade mineralization (>0.300 oz/t Au).

The secondary focus of this study examined the distribution of iron-bearing carbonate proximal to the Osgood stock to determine if the stock was responsible for adding iron to the surrounding carbonates. Iron-bearing carbonates have been proposed to be better hosts for Carlin mineralization, providing a source of iron for the ore fluids to sulfidize

and precipitate Au-bearing pyrite. This study revealed no systematic distribution of ferroan carbonate that would indicate the iron was sourced from the stock. Rather, the distribution of ferroan carbonate is found to be largely controlled by lithology. The limestones with a silty component were found to be iron-rich while pure limestones associated with the siliceous carbonaceous mudstones were iron-poor.

TABLE OF CONTENTS

LIST OF TABLES

LIST OF FIGURES

CHAPTER 1

INTRODUCTION

The state of Nevada in the western United States is the type locality for the world class Carlin-type gold deposits (Fig. 1). The total gold in Nevada's Carlin-type deposits, including past production and current reserves is in excess of 200 million ounces (Moz) (Sillitoe, 2008). These deposits account for much of the 5.6 Moz of gold produced in Nevada during 2008, which made up 76% of U.S. gold production that year (The Nevada Mineral Industry, 2008). This made Nevada alone the world's 4th largest gold producer behind China, Australia and South Africa (The Nevada Mineral Industry, 2008).

Carlin-type deposits are large sediment-hosted gold deposits which typically contain structurally and/or stratigraphically controlled, disseminated gold-bearing pyrite mineralization (Cline et al., 2005). Host rocks for these types of systems are dominantly pyritic, carbonaceous, silty carbonates and less commonly calcareous shales (Cline et al., 2005 and references therein). These deposits occur along linear trends in north central Nevada (Fig. 1), which are thought to overlie deep crustal scale faults (Tosdal et al., 2000; Crafford and Grauch, 2002; Cline et al., 2005). The main trends are the NW trending Carlin Trend, the NW trending Battle Mountain – Eureka Trend and the NNE trending Getchell Trend (Figs. 1 and 2).

Several large Carlin-type deposits, including the Betze-Post and Getchell deposits, occur in host rocks adjacent to Mesozoic intrusions (Figs. 2 and 3). During subsequent deformation events after their emplacement these Mesozoic plutons are thought to have acted as rigid bodies, resulting in the generation of enhanced fracture networks around the plutons providing fluid pathways for the later Eocene aged Carlin mineralization

event (Cline et al., 2005). However, the contact metamorphism associated with the intrusion of these plutons also caused calc-silicate alteration; which replaced the reactive, favorable, carbonate host rocks near these stocks with less favorable, unreactive, calc-silicate minerals such as wollastonite. Due to this replacement the Carlin ore fluids could not generate porosity and permeability in the rocks via dissolution of carbonate by acidic fluids. Additionally the dissolution of carbonates is hypothesized as necessary to liberate iron vital for the ore fluids to sulfidize and form gold bearing pyrite. As a result calc-silicate rocks are generally poor host rocks for Carlin-type mineralization.

The Getchell Property has been the site of large scale gold mining since 1938. The site contains three deposits; 1) The Getchell Open Pits were mined along the surface exposure of the Getchell fault intermittently from 1938-1998 (Joralemon, 1951; Chevillon et al., 2000) 2) the Getchell Main Underground mineralization in the footwall of the Getchell fault was mined from 1994-2008 (Tretbar, 2004), and 3) the Turquoise Ridge underground mine, the only current mining activity on the property, is targeting mineralization in the hanging wall above the Getchell fault and has been mined from 1997-present (Cline et al., 2008).

The purpose of this study is to determine how contact metamorphism, in particular, calc-silicate alteration, caused by Mesozoic intrusions, impacts the ability of various lithologies to host Carlin-type gold mineralization at the Getchell deposit. This study is focused on an area of mineralization located in the hanging wall of the Getchell fault to the south-southwest of the Turquoise Ridge deposit (Fig. 4). This mineralization occurs within the metamorphic aureole of the Osgood stock and is adjacent to a lobe of the Osgood stock located in the hanging wall.

The primary goal of this study was to constrain the effects of calc-silicate alteration on the various lithologies potential for hosting Eocene aged Carlin type mineralization within the metamorphic aureole of the Cretaceous Osgood stock on the Getchell Property (Fig. 2). The secondary goals of this project were to 1) conduct carbonate staining for the presence of iron in non or minimally calc-silicate altered limestones in order to determine if the Osgood stock was responsible for adding iron to the surrounding carbonates, and 2) better develop the stratigraphy in this area and relate it to the stratigraphy that has been established at Turquoise Ridge.

CHAPTER 2

GEOLOGIC HISTORY

The complex geologic history of Nevada played a vital role in creating favorable host rocks, structures to transport ore fluids, and traps to localize the mineralization. Beginning in the Late Proterozoic, rifting generated deep seated basement faults in the thinned continental crust along the western margin of North America (Tosdal et al., 2000; Crafford and Grauch, 2002). Above this rifted margin a sedimentary sequence developed, initially dominantly composed of clastic material which built up to a thickness of >6 km from the Neoproterozoic to the Cambrian (Stewart, 1980; Emsbo et al., 2006). From the Cambrian to the Devonian a carbonate platform developed along this passive margin generating a package of sedimentary rocks consisting largely of shelf and slope carbonate rocks (Cook, 2005). These rocks transition from dominantly shallow water carbonates in eastern Nevada to deep water siliciclastic mudstones, and cherts locally inter-bedded with carbonates, transported off the Paleozoic carbonate shelf as turbidites, in western Nevada (Cook, 2005).

In the late Devonian, compressional tectonics began as a subduction zone developed along the western margin of North America culminating in the Devonian-Mississippian Antler Orogeny (Crafford and Grauch, 2002; Dickinson, 2004; Metcalf, 2004). The orogeny thrust the deep water siliciclastic sediments and basalts of the Roberts Mountain Allochthon, referred to as the upper plate, over the slope and shelf carbonate sequences, referred to as the lower plate, along the Roberts Mountain Thrust (Roberts, 1960). Active compressional tectonics continued from the Triassic into the Tertiary with the Sonoma

and Sevier Orogenies (Dickinson, 2004). These events resulted in further thrusting and folding of the sedimentary rocks along the western margin of North America.

During the Mesozoic, east dipping subduction of the Farallon plate generated magmatism which gave rise to the Sierra Nevada batholiths as well as the intrusion of several back arc plutons (Crafford and Grauch, 2002; Dickinson, 2004; Emsbo et al., 2006). The distribution of these plutons along linear trends suggests that they were emplaced along the earlier crustal scale faults (Tosdal et al., 2000; Emsbo et al., 2006). These Mesozoic plutons include the Jurassic Goldstrike diorite on the Carlin Trend and the Mesozoic Osgood stock on the Getchell trend (Ressel et al., 2000). Magmatism shutdown as the angle of subduction became increasingly shallow eventually resulting in the slab becoming coupled to the base of the continental crust (Humphreys, 1995).

Magmatism resumed in the Eocene with the introduction of hot asthenospheric mantle to the base of the crust. In the northern Basin and Range this magmatism began in Idaho around 50 Ma and swept south through Nevada as the Farallon plate, which had been previously coupled to the base of the crust, was removed (Humphreys, 1995). The timing of the onset of extension and magmatism in northern Nevada is consistent with the age of formation for the Carlin-type gold deposits at 43-37 Ma (Ressel et al., 2000; Tretbar, 2004; Cline et al., 2005; Emsbo et al., 2006).

The extension opened and/or reactivated favorably oriented structures from previous tectonic events, providing pathways for ore fluids (Cline et al., 2005). These fluids exploited areas of crustal weakness and moved upward into areas of receptive carbonate host rocks. The Eocene magmatism provided at the minimum a heat source for the hydrothermal system which generated the Carlin-type deposits and may have contributed

the metals as well (Ressel et al. 2000; Cline et al., 2005; Ressel and Henry, 2006). Subsequent uplift and erosion since the Eocene has exhumed Carlin deposits, which are proposed to have formed at depths of 1-3 km, to their present location at or near the surface (Cline et al., 2005).

CHAPTER 3

PREVIOUS WORK AT GETCHELL

Stratigraphy

The host rocks for the Carlin-type gold deposits on the Getchell trend consist of Late Cambrian through Ordovician carbonates, silty carbonates, calcareous shales, and shales. Historically these host rocks have been mapped as the Cambrian Preble Formation and the Cambro-Ordovician Comus Formation (Holtz and Willden, 1964) (Fig. 3). Fossils are uncommon in the area and where they have been located they have been significantly altered by the metamorphism associated with the intrusion of the Osgood stock (Boskie, 2001). These factors have made precise dating of the units difficult. Where trace fossils have been recovered they yield Cambrian to early Ordovician ages (Holtz and Wilden, 1964; Boskie, 2001). In the vicinity of Getchell and Turquoise Ridge the sedimentary sequence is capped by Ordovician basalt (Breit et. al, 2005)

These formations were later intruded in the Cretaceous, first by dacite dikes dated 115 ± 2.3 Ma and later by the Osgood granodiorite stock at 92 Ma (Groff et al., 1997; Breit et al. 2005; Cline et al. 2008). The intrusion of the Osgood stock altered many of the surrounding carbonates and mudstones the calc-silicates and hornfels within a metamorphic aureole extending out 2000-3000 feet from the stock (Cline et. al, 2008). The deposits along the Getchell trend lack evidence of the Eocene magmatism which is ubiquitous on the Carlin Trend, in the form of dikes and sills, further to the east (Ressel and Henry, 2006).

Controversy still exists over which formation or formations are present along the eastern flank of the Osgood Mountains, and host the Carlin-type gold deposits of the

Getchell trend. It has been suggested that the units mapped as the Comus Formation along the eastern flank of the Osgood Mountains more closely resemble the lithology and structural deformation observed in the Preble Formation than the Comus Formation at its type locality (Madden-Maguire and Marsh, 1991; Boskie, 2001). Further, Boskie (2001) concluded, based on litho-geochemistry of samples, that the units mapped as Comus Formation and Preble Formation along the Osgood Mountains were chemically indistinguishable.

The stratigraphy at Turquoise Ridge and Getchell is further complicated by lack of conspicuous stratigraphic marker horizons and discontinuity of units over short distances (Joralemon, 1951; Cline et al., 2008). Boskie (2001) mapped the eastern flank of the Osgood Mountains in and around the Getchell and Pinson mines and concluded that no stratigraphic continuity exists between the units in the area. The study proposed that the rocks on the eastern flank of the Osgood Mountains are part of a tectonic mélange. This mélange incorporated slices of differing lithologies and juxtaposed them resulting in the complex geology that is observed in the area (Boskie, 2001).

Geologists working on the Getchell/Turquoise Ridge deposit for Placer Dome, and later Barrick Gold, as well as research conducted by Cline et al. (2008) have interpreted this complex stratigraphy as an olistostrome, based on the interpretation of thousands of feet of core drilled on the property. This unit consists of a series of one or more large scale debris flow deposits or soft sediment slumps occurring on the slope of the Paleozoic continental margin. The thickness of the unit is unknown but has been drilled to depths of 5000 feet at Turquoise Ridge in the hanging wall of the Getchell fault (Keith Wood, per. comm., 2009).

Structure

The key structural feature of the property is the Getchell fault, located along the eastern flank of the Osgood Mountains (Figs. 2 and 3). The fault strikes NNW and dips 30°-50° to the east. The fault is observed as a gouge zone ranging from 50-200 feet thick. The history of movement on the fault is long and complex. Many dikes in the area are emplaced along Getchell parallel structures suggesting the fault existed prior to the emplacement of the 92 Ma Osgood stock. The early motion on the fault was dominated by left-lateral strike-slip movement, based on the presence of large horizontal mullions (Boskie, 2001). A second, later stage of movement was normal displacement, inferred from vertical slickenlines overprinting the horizontal mullions, was associated with extension in the Basin and Range (Boskie, 2001). Slickenlines of the late stage ore mineral realgar, and offset of alluvial fans suggest post-mineralization movement on the fault (Boskie, 2001; Tom Chadwick, per. comm. 2010).

The surface expression of the fault consists of a series of splays which diverge and coalesce along the strike of the fault. The resulting fault zone expands out to 400 feet in thickness where the splays diverge in the south pit, and necks down to 20 feet where the splays coalesce between the Main and North Pits (Fig. 4; Tom Chadwick, Per. Comm. 2009) The Getchell fault was the primary conduit for the ore forming fluids during mineralization (Joralemon, 1951; Cline, 2001; Tretbar, 2004; Cline et al., 2008). The early mining at Gechell focused on the surface exposures of the altered carbonaceous fault gouge, which were developed into open pits (Joralemon, 1951). Later underground mining at Turquoise Ridge has focused on mineralization in the hanging wall above the Getchell fault (Cline et al., 2008).

Mineralization

The Carlin-type mineralization has been extensively studied at the Getchell and Turquoise Ridge deposits (Joralemon, 1951; Cline and Hofstra, 2000; Cline, 2001; Tretbar, 2004; Longo et al., 2008; Cline et al., 2008). Fluid inclusion and geochemical data from Getchell indicate that mineralizing fluids precipitated gold-bearing trace element rich pyrite at temperatures between 180º and 220º C, had bulk salinities of 4 to 5 wt. % NaCl eq., and contained H_2S with which the gold may have been complexed as a gold-bisulfide species (Cline and Hofstra, 2000; Cline, 2001; Cline et al., 2005). These characteristics are salient features of most Carlin-type deposits. The ore fluids were mildly acidic, having inferred pH ranging from 3 to 4.5, which allowed them to react with and dissolve the calcareous host rock, creating further permeability for ore fluids (Cline et al., 2005).

Cline (2001) proposed that Carlin-style mineralization occurred during a single ore-fluid event at each deposit. After the hydrothermal system collapsed and cooled, marked by the precipitation of late ore-stage minerals such as realgar, there were no further overprinting gold mineralization events (Cline, 2001). Electron probe microanalysis (EPMA) and laser ablation inductively coupled plasma mass spectrometry (LA-ICP-MS) analyses of ore-stage pyrite from the Getchell deposit show chemical variation occurred over the duration of the hydrothermal system (Cline et al., 2005; Longo et al., 2008). These later studies report and discuss data that are consistent with mineralizing fluids that evolved chemically in space and time throughout the Getchell deposit (Longo et al., 2008). New research using high resolution Secondary Ion Mass Spectrometer (nanoSIMS) analysis of ore stage pyrite from Turquoise Ridge conducted by Barker et al.

(2009) suggests that there were two pulses of chemically distinct ore fluids separated by a low gold event.

CHAPTER 4

METHODS

Drill Core Logging

During the summer of 2009 approximately 9000 feet of 63.5 mm diameter drill core was logged for this study, noting lithology, alteration, and mineralization. The drill holes selected are within 100 feet of either side of two cross section planes, A-A' and B-B', extending outward from the lobe of the Osgood stock in the hanging wall of the Getchell fault (Fig. 4). The cross section lines were chosen to examine the effects of calc-silicate alteration on the host rocks extending outward from the lobe of the Osgood stock in the hanging wall of the Getchell fault (Fig. 4). The goals of producing these cross sections were to 1) determine the extent and intensity of calc-silicate alteration in the area; 2) identify areas of mineralization and see how they are spatially related to the areas of calc-silicate alteration; and 3) clarify the stratigraphy south of Turquoise Ridge.

The drill core that was logged and sampled came from eleven drill holes as well as rock chips from one reverse circulation drill hole. Five of the core holes were logged completely and portions of six holes were logged in and around areas that intersected mineralization due to preservation of only the mineralized portions of core. Core logs for the rest of the holes were used to construct the cross sections as well. Gold grades and multi-element assays were provided by Barrick.

Optical Petrography

Twenty-five polished thin sections were cut from core samples for petrographic analysis. These samples represented a wide range in rock types and degrees of calc-

silicate alteration as well as varying degrees of mineralization. The thin sections were analyzed by both standard transmitted and reflected light microscopy.

X-Ray Diffraction

Many of the samples contained very fine grained mineral assemblages which made mineral identification with optical petrography difficult. X-ray diffraction (XRD) was utilized to identify the mineralogy of the fine-grained assemblages in samples. Twenty-five samples of varying lithologies and with varying amounts of calc-silicate alteration, including several samples of mineralized material, were taken from drill core hand samples for XRD analysis. Samples were ground to a fine powder with a corundum mortar and pestle. These powders were mounted onto 10 mm sample discs and analyzed with a PANalytical X'PERT Pro X-ray Diffraction Spectrometer in the University of Nevada, Las Vegas XRD/XRF Laboratory. Data were collected in twenty minute runs analyzed from 10-84 2θ. Analysis of the XRD spectra for mineral identification and semi-quantitative mineral abundances were conducted using the X'pert Highscore Plus software package.

Carbonate Staining

Staining of carbonates for the presence of iron was completed following methods outlined in Hitzman (1999) and Cline et al. (2008). Staining in this study was conducted to determine if there is any spatial distribution of iron-rich carbonates which would suggest that the iron was sourced from the Osgood stock or fluids related to its intrusion. Three staining solutions were prepared: 1) a solution of potassium ferricyanide was prepared using 125 mL of 2% HCl and 0.625 g of potassium ferricyanide; 2) a solution of Alizarin Red S was prepared using 125 mL of 2% HCl and 0.15 g of alizarin red S; 3) a

solution was made by combining equal parts of the alizarin red S and potassium ferricyanide solutions. The potassium ferricyanide stains iron-bearing phases blue and the Alizarin Red S stains calcite red. The composite solution stains pure limestone red, ferroan limestone purple, ferroan dolomite blue, and dolomite has no stain. Care was taken during staining to avoid areas of limestone with iron sulfides which may cause a false iron positive result.

CHAPTER 5

DATA

Core Logging and Cross Sections

Footwall Section

This study primarily deals with the rocks in the hanging wall of the Getchell fault; however in the drill core examined for Cross Section B, rocks in the footwall of the Getchell fault were encountered. These rocks are the lowest unit encountered in core; however, due to the substantial offset caused by the Getchell fault, their stratigraphic relationship to the rocks in the hanging wall remains uncertain. These footwall rocks consist dominantly of light to dark gray carbonaceous limestones with lesser inter-bedded dark gray to black calcareous carbonaceous mudstones and lesser amounts of siliceous carbonaceous mudstone (Fig. 5-A and 6). The limestone beds can range in thickness from <1 cm to >1 m but generally range in thickness from 2-6 cm. The calcareous and siliceous mudstone beds are generally thinner and <2 cm. The limestone beds in these rocks are commonly weakly to moderately altered to calc-silicate minerals, dominantly wollastonite. The footwall rocks appear to be fairly homogeneous with consistent bedding angles in the upper 200-300 feet encountered by the core in Cross Section B, unlike the rocks in the hanging wall described below.

Hanging Wall Section

The hanging wall above the Getchell fault, the stratigraphy becomes far more complex. As described previously in the deposit geology section, the rocks in this area have no lateral continuity and exhibit rapid/abrupt changes in lithology over very short intervals. As such, logging these rocks and correlating them between drill holes even

100-200 feet apart was difficult. The rocks of the hanging wall can be divided into two distinct groups by the composition of the mudstones. One group consists of siliceous carbonaceous mudstones and the other consists of argillaceous mudstones. Both groups of mudstones are inter-bedded with variable amounts of limestone and locally are dominantly limestone. The siliceous carbonaceous mudstones with limestone are best thought of as clasts ranging in some cases up to 300 feet in thickness that are found in a matrix of argillaceous mudstone. Contacts between the two rock types are commonly broken in core, but locally are found intact (Figs. 7 and 8). The boundary between the clast and matrix consists of fragments of limestone and siliceous mudstone locally mixed with the argillaceous mudstone. These fragments have a sheared fabric near the contact and become chaotic and jumbled with distance away from the contact (Fig. 7). Further into the siliceous carbonaceous mudstone clasts the chaotic jumble of fragments transitions to more regular bedding.

Siliceous Carbonaceous Mudstone and Limestone

The black siliceous carbonaceous pyritic mudstones are commonly inter-bedded with gray to dark gray limestone turbidites (Fig. 9). Intervals vary from dominantly mudstone to, less commonly, dominantly limestone. The bedding in the mudstone is generally 1-3 cm thick and typically bounded by thin, 1-3 mm, carbon-rich mudstone inter-beds (Fig. 10). The limestone beds generally range from a few centimeters to several meters in thickness. In some cases the limestone turbidites contain a basal conglomerate with rip-up clasts of mudstone near the contact with the underlying mudstone bed (Fig. 11).

A distinctive feature of these rocks is the occurrence of calcite veins, oriented perpendicular to beds of carbonaceous mudstone; these are generally restricted to a single

bed (Figs. 10 & 12). The calcite veins terminate at the thin inter-beds of carbon-rich mudstone (Figs. 10 and 13). These thin carbon-rich mudstone inter-beds appear to have behaved in a ductile manner during deformation. In some samples these carbon-rich mud inter-beds are observed partially filling the tension fractures (Fig. 10). In contrast the partially lithified siliceous beds between them behaved in a brittle manner and fractured, generating space for calcite veins. In addition to the tension gashes the siliceous carbonaceous mudstones and limestones are often deformed by folding of the bedding observed as changes in bedding orientation within one clast in core (Fig. 14). Differences in bedding angles are also commonly observed between clasts (Fig. 15).

The mineralogy of the siliceous carbonaceous mudstones is difficult to determine via optical microscopy; due to their high carbon content they are typically opaque in thin section. With the exception of veins filled with coarse calcite, analysis by XRD shows that these mudstone units are comprised dominantly of quartz with lesser amounts of feldspar and diagenetic pyrite (Fig. 16).

In thin section the limestone portions of these units are dominantly pure calcite, often finely recrystalized. There are locally small grains of quartz, ranging from ~0.5-1 mm in diameter, commonly near the base of the limestone bed associated with the basal conglomerate containing rip-up clasts of the siliceous carbonaceous mudstone from the underlying bed. Analysis by XRD confirms the observations via optical petrography of dominantly pure calcite with small amounts of quartz (Fig. 16).

Argillaceous Mudstone and Limestone

The second group of rocks in the debris flow consists of argillaceous mudstones, often with inter-beds of limestone. Less commonly some sections are dominantly

limestone with thin inter-beds of argillaceous mudstone. In the area of this study, the intrusion of the Osgood stock has metamorphosed the argillaceous mudstones to fine-grained biotite hornfels, which are characteristically maroon to brown in color (Fig. 17). The bedding in the mudstones varies from finely laminated, often with soft sediment deformation, to massive. The limestones associated with the argillaceous mudstones are generally more thinly bedded than those found in association with the siliceous carbonaceous mudstones, ranging from 1-3 cm. The limestones are commonly cut by a developed cleavage fabric, defined by bands of biotite. These planes commonly cut and produce minor offsets in the bedding in the limestones (Fig 18).

The argillaceous mudstones are very fine grained. Their mineralogy is difficult to determine in hand-sample. Under a microscope the argillaceous mudstones are revealed to be composed of fine-grained biotite and quartz. Analysis of samples of argillaceous mudstone by XRD indicates that these mudstones are composed of equal amounts of biotite and quartz with a small component of orthoclase, which was not observed under optical petrography (Table 1). Locally there are lenses that are composed dominantly of fine grained quartz.

Samples of limestone are fine-grained calcite and commonly have thin beds of mudstone composed of biotite and quartz similar to the sections dominantly composed of argillaceous mudstone. Samples of limestone analyzed with XRD show they are composed of dominantly calcite, with a smaller component of orthoclase (Table 1). These limestones also commonly contain variable amounts of calc-silicate minerals which will be discussed below.

In core the argillaceous mudstones and limestones show pronounced soft sediment deformation with ductile folding in comparison to the more blocky and brittle deformation observed in the siliceous carbonaceous mudstones. The argillaceous mudstones also commonly have a fragmental texture with a matrix composed of dominantly argillaceous mudstones and small clasts of limestone ranging up to tens of centimeters in size, but typically 3-5 cm (Fig. 19). Some of the fragmental fabrics have limestone clasts with flow patterns around them suggesting that these rocks behaved in a ductile manner during the formation of the debris flow. These fragmental fabrics are often found on the borders of larger sections, tens of meters, of argillaceous limestone (Fig 19).

Both groups of rocks, siliceous carbonaceous mudstones and argillaceous mudstones along with their associated limestones, occur together in the lower portions of the debris flow (Plates 1 and 2). Moving upward through the hanging wall section the amount of the siliceous carbonaceous mudstones and associated limestones decreases. The clasts of siliceous carbonaceous mudstone and limestone no longer occur above a broadly defined horizon at 4000’- 4200’ a.s.l in Cross Section B and 3600’- 3800’a.s.l in Cross Section A (Plates 1 and 2). The variations in the contact elevations suggest this horizon dips shallowly to the north.

The upper portion of the debris flow is composed only of argillaceous mudstones and associated limestones (Fig. 5-D). The upper section also contains thicker intervals composed dominantly of limestone with thin layers of argillaceous mudstone, although clasts of the same limestone may also be found in the lower portions of the section. These larger intervals of dominantly limestone with thin inter-beds of argillaceous mudstone

also appear to be clasts in a dominantly argillaceous mudstone matrix. Along the margins of such clasts, fragments of the limestone are ripped off and incorporated into the mud matrix (Fig. 19).

Upper Siliceous Carbonaceous Mudstone

Above the upper portion of the debris flow deposit there is a continuous unit of siliceous carbonaceous black mudstone (Fig. 5-E). This layer ranges from 25-150 feet thick, with thicker intervals in Cross Section A as opposed to Cross Section B to the south, suggesting the unit may thicken to the north. Individual mudstone beds measure 1-3 cm thick although they are locally finely laminated on a millimeter scale (Fig. 20). Diagenetic pyrite is also common along bedding planes. Unlike the rock in the siliceous carbonaceous mudstone that occurs as clasts in the lower parts of the stratigraphy, these siliceous carbonaceous mudstones form a continuous layer traceable across and between both cross sections. In addition these upper siliceous carbonaceous mudstones lack limestone inter-beds which are common in the similar rocks lower in the stratigraphy; however, these upper mudstone beds locally contain small clasts of limestone.

Analysis of a sample of this material by XRD shows that it is dominantly composed of quartz with lesser amounts of orthoclase, plagioclase, biotite, and pyrite (Table 1). This composition is a distinctly different from the argillaceous mudstones which underlie this unit. Overall this unit is more similar in mineralogy to the siliceous carbonaceous mudstones found lower in the section.

Within the upper siliceous carbonaceous mudstones there are inter-beds, or small debris flows, of hyaloclastite with clasts of vesiculated basalt (Fig. 21). These inter-beds range up to tens of meters in thickness (Plates 1 and 2). In some areas these inter-beds are

fine grain hyaloclastite "tuff". In other areas the units consist of a mix of rounded siliceous mudstone clasts 1-3 cm in diameter and wispy irregular clasts of vesiculated basalt scoria up to 3 cm across. In these more conglomeratic sections there are commonly significant amounts of sulfides, locally ~5% by volume, dominantly pyrrhotite with lesser amounts of pyrite.

Upper Basalt

The uppermost unit in the area is basalt, referred to as the upper basalt or Valmy Basalt (Fig. 5-F). The basalt generally extends from the surface to depths of 500-700 feet in the Cross Section B and as deep as 1200 feet in the eastern portions of Cross Section A where it is down dropped by a large normal fault. The unit varies from green (due to chlorite alteration) to brown (due to biotite hornfels alteration) in color. The upper basalt locally is vesiculated and pillow margins are observed in core (Fig. 22). There are also intervals of hyaloclastite material which is generally tan to brown in color, and varies from very fine grained "tuff" to clasts of vesiculated basalt.

Igneous Intrusive Units

The sedimentary rocks in the area are cut by dikes and sills of two compositions, the earlier of which are the diabase dikes. The diabase dikes are fine grained mafic dikes typically dark gray to dark green (chlorite alteration) in hand sample (Fig. 23). These dikes are commonly cut by sulfide veins composed of pyrite or pyrrhotite. These dikes range in thickness from <1 m to >20 m. Diabase dikes are only found in the upper portions of the cross sections (Plates 1 and 2) which suggests they are near horizontal in orientation.

The other group of dikes is the dacite dikes, which are more variable in their appearance than the diabase dikes. The dacite dikes are fine to coarse grained felsic dikes. The dikes range in thickness up to 10-20 m and are commonly gray-pink in color and have an aphanitic matrix with plagioclase, hornblende and locally biotite phenocrysts. In several locations these dikes appear to be emplaced along structures parallel to the Getchell fault (Plate 1).

Calc-Silicate Alteration

The major effect of the contact metamorphism resulting from the intrusion of the Osgood stock is the calc-silicate alteration of the limestones and calcareous units in the study area. The distribution of calc-silicate alteration is variable throughout the study area. Cross Section A shows a general decrease in the intensity of calc-silicate alteration from west to east, with increasing distance away from the stock, although non calc-silicate altered rock can be observed in drill core closer to the stock (Fig. 24). Cross Section B does not show this trend; rather, strongly calc-silicate altered rocks are still present in the eastern most drill core sampled, farthest from the stock (Fig. 25). Although similar to Cross Section A, there are still zones/pods of reactive limestone within this area.

The rocks composed of argillaceous mudstone and limestone are more commonly calc-silicate altered than those composed of siliceous carbonaceous mudstone and limestone. This variability in the intensity of calc-silicate alteration is often abrupt and can be observed over as short a distance as the contact between the two rock types (Figs. 8 and 26). The argillaceous mudstones and limestones are altered to calc-silicate minerals

while the limestones inter-bedded with siliceous carbonaceous mudstones in contact with the argillaceous mudstones are not though they may be recrystallized.

Siliceous Assemblage

In hand samples, contact metamorphism seems to have little visible effect on the siliceous carbonaceous mudstones. Locally the black carbon-rich mudstone is bleached to off-white/tan near the limestone beds, or early calcite veins, which have been altered to calc-silicate minerals (Fig. 27). The limestones inter-bedded with the siliceous carbonaceous mudstones are commonly recrystallized. Locally however, they are strongly calc-silicate altered to white, coarse-bladed to acicular, wollastonite. Analyses of calc-silicate altered siliceous carbonaceous mudstone and limestone by XRD indicates alteration to an assemblage of dominantly wollastonite, minor vesuvianite, trace quartz, and locally trace diopside (Fig. 28, Table 1).

In thin section samples of siliceous carbonaceous mudstone and limestones contain variable amounts of calc-silicate alteration. In samples of limestone inter-bedded with siliceous carbonaceous mudstone the calc-silicate alteration commonly starts at the contact between the limestone and mudstone and extends into the limestone. One thin section shows strong calc-silicate alteration in limestone at the contact between siliceous carbonaceous mudstones and an inter-bed of limestone, with decreasing calc-silicate alteration moving away from the contact (Fig. 29). The calcite filled veins in siliceous carbonaceous mudstone have also been altered to calc-silicate minerals, dominantly wollastonite.

Argillaceous Assemblage

In hand sample the argillaceous mudstones are altered to fine grained maroon to brown biotite hornfels with no grains visible with a hand lens. Limestones associated with the argillaceous mudstones tended to alter to an assemblage of wollastonite, garnet, fine green minerals (likely diopside), coarse recrystallized calcite, and pyrrhotite, which rarely occurs in the siliceous carbonaceous rocks. These limestones inter-bedded with argillaceous mudstones commonly have weak to moderate calc-silicate alteration throughout the bed taking on a pink/purple grey color in hand sample. In areas of less intense calc-silicate alteration there is typically a rind on the contact between the limestone and inter-bedded mudstone with limestone remaining less altered away from the contact (Fig. 30). Smaller beds or limestone clasts in matrix in these areas are commonly completely altered to calc-silicate minerals.

Analysis by XRD indicates that the argillaceous limestones are variably altered by metamorphism to an assemblage of wollastonite, diopside, garnet, vesuvianite, and calcite, and locally, amphiboles tremolite and hornblende (Table 1). All samples of the limestone inter-bedded with argillaceous mudstone showed some evidence of calc-silicate alteration, and even weakly altered samples contain some diopside (Table 1). Overall diopside is more common in the argillaceous limestones, imparting the common green color. The argillaceous limestones also have a more diverse calc-silicate assemblage than the limestone associated with the siliceous carbonaceous mudstones.

Structure

The dominant structural feature in the study area is the NNW striking Getchell fault. This fault is observed in core as a strongly sheared, carbon-rich gouge zone generally

ranging from 50-150 feet thick (Fig. 31). The fault zone dips 30-50 degrees to the east. The Getchell fault was only encountered in drill holes on Cross Section B. The drill holes in Cross Section A did not penetrate deep enough to reach the fault; the position of the Getchell fault is projected on Cross Section A from other drill core in the database. In some locations there are splays along the main fault strand with intervening slices of competent rock of various lithologies between the splays (Plate 2).

Several other major faults in the hanging wall were identified and correlated from core logging. One major fault runs approximately parallel to the Getchell fault. The fault zone, a series of smaller faults and splays, is located ~100-200 feet above the main Getchell fault. It is observed in core as broken rubble zone where encountered in the siliceous carbonaceous mudstones and strongly sheared gouge in the argillaceous mudstones (Plate 2). The fault has a series of small strands and splays and is not as well developed as the Getchell fault. There appears to be a small normal offset on the fault (Plate 2), however strike-slip offset could not be determined. This fault is not observed in Cross Section A.

A large unnamed west dipping fault is present in Cross Section A. The fault is responsible for down dropping the Upper Basalt 600-700 feet in the western portion of the Cross Section (Plate 1). In core the fault is observed as a heavily sheared gouge zone. There is also a series of splays of this fault branching off to the east of the main fault. A smaller west dipping feature is also observed in Cross Section B, although it does not appear to be the same fault as it does not have any apparent normal offset. Numerous other small faults were observed in the cores for this study, but could not be correlated between drill holes with any confidence.

Carlin Alteration and Mineralization

Location and Controls

Alteration associated with Carlin-type gold mineralization was identified in all drill core examined for this study. The dominant controls on the location of mineralization are the presence of conduits for ore fluids and reactive host rocks which are receptive to the mineralization (Figs. 32 and 33). Ore fluid conduits include dikes and faults. Traditional Carlin-style mineralization, defined by replacement of carbonate or calcareous host rocks, was most prevalent in areas of inter-bedded limestones and siliceous carbonaceous mudstones unaffected by calc-silicate alteration. The strongly decalcified and silicified limestones are commonly dark grey to black in hand sample with a pitted and porous texture. These porous areas are commonly filled with realgar.

The siliceous mudstones themselves remain visibly unaltered by the Carlin fluids due to the lack of calcareous material to alter. Fractures and veins in the siliceous mudstone which were formerly filled with calcite commonly have had the calcite removed in and around areas of Carlin-type mineralization. These formerly calcite filled fractures and veins are now voids which are commonly filled with late ore-stage quartz or realgar (Fig. 34 and 35). Commonly, realgar fills pore spaces, fractures, and locally cements breccias (Fig. 36). Late stage veins commonly have late stage calcite and orpiment/realgar (Fig. 37).

The grade of mineralization encountered in the siliceous carbonaceous mudstone is largely dependent on the amount of inter-bedded limestone. The units consisting of dominantly siliceous carbonaceous mudstone generally had the lowest grades, <0.100 oz/t Au. Sections with larger fractions of limestone typically contained higher grades,

locally >1.000 oz/t Au. Mineralization occurred where these receptive rocks are cut by structures such as the Getchell fault or other faults or dikes, which were transporting ore fluids (Figs. 32, 33, 38a and 38b). In these receptive host rocks, mineralization spreads out from the ore fluid conduits. In many places, potential host rock that was not altered to calc-silicates has not been mineralized owing to the lack of intersecting ore fluid conduits.

Calc-silicate altered rocks, including those which showed evidence for exposure to Carlin-type ore fluids, were typically poor hosts; i.e., realgar replacing calcite on fracture surfaces or along mineralized faults. In areas of less receptive calc-silicate altered host rocks, mineralization occurs locally, but is generally restricted to heavily fractured rock within the fault gouge and fluids did not alter or move into the surrounding calc-silicate rocks (Fig. 38a). Wider areas of mineralization in these rocks are associated with fault intersections and fault jogs (Fig. 39). Mineralization in these highly faulted areas is not dependent on rock type or lack of calc-silicate alteration because it is largely contained within the fault material. Mineralization in these zones can be high grade, >1.000 oz/t Au.

Mineralogy

The mineralogy of the ore is dependent largely on the alteration type. The strongly decalcified and silicified limestones of the siliceous carbonaceous mudstone and limestone are altered to dark gray to black porous silica. Locally, realgar or white to tan clay fills in the pores and voids (Fig. 36). In some locations there are dissolution breccias in the limestone inter-beds.

In thin section, mineralized areas of limestone show complete replacement of calcite by fine grained jasperoid quartz with lesser fine grained sulfides (Fig. 34). Analysis by

XRD of mineralized samples of units formerly composed of limestone are now composed dominantly of quartz, with lesser realgar, kaolinite, pyrite, marcasite, and locally stibnite (Figs. 40 and 41). Locally there are sections of less altered limestone bounded by areas of mineralization. Samples of these less altered limestones analyzed by XRD show evidence for minor silicification by the Carlin-type ore fluids, but no evidence for calc-silicate alteration (Fig. 42, Table 1).

The zones that are dominated by argillization show alteration of maroon-brown biotite hornfels to white-tan clays with abundant sulfides. These sulfides are often concentrated along former foliation/cleavage in the biotite hornfels (Fig. 18). Analysis by using XRD of a sample of argillized biotite hornfels from above an area of mineralization in drill hole 07-GC-020 on Cross Section B shows alteration to kaolinite + quartz + marcasite (Fig. 43, Table 1).

Chemistry

The chemistry of the mineralized zones examined in this study is consistent with the chemistry associated with Au mineralization in other CTGDs. Common elements associated with Au mineralization include As, Hg, Sb, Se, Te, and Tl. Variability in the chemistry of the ore mineralization is apparent in whole rock multi-element assays of various ore intercepts encountered in this study. The amount of gold in relation to other trace metals commonly found in CTGD's (e.g. Hg, Sb, and Tl) is quite variable. In some areas ratios Au to Hg, Sb, and Tl are approximately 1:1 while in other areas the values are 1:100 or less. However, patterns emerge when mineralization is divided into three broad types: I, II and III (Fig. 44). These divisions were based primarily on the ratio of Au to Ag in the samples. See Appendix B for full whole rock geochemistry data.

Type I mineralization is characterized by moderate amounts of Ag resulting in Au:Ag of 2:1 to 1:1. Additionally values of Hg, Sb, and Tl are also high relative to Au (Figs. 45 and 46). Type I mineralization is most common in the mineralized limestone inter-bedded with siliceous carbonaceous mudstone adjacent to the Getchell fault or the Getchell parallel fault in Cross Section B (Fig. 44). Alteration associated with Type I mineralization is commonly strong decalcification and silicification. The ore grade associated with this mineralization type is low in comparison to Turquoise Ridge where grades are commonly >1.000 oz/t Au. However economic gold grades (>0.300 oz/t Au) are possible in the areas of low Au:Ag ratios. For example, Type I mineralization averages 0.354 oz/t Au over 78.3 feet, including 5 feet at 1.110 oz/t Au in drill hole 08-GC-035 (Fig. 38b).

A correlation matrix produced using 24 sampled intervals of Type I mineralization with grades >0.300 oz/t Au shows strong correlation ($R>0.75$) of Au with Cu, Hg, and Tl; moderate correlation ($0.50<R<0.75$) of Au with Te; and a weak but notable correlation ($0.40<R<0.50$) of Au with Ag and S (Table 2).

Type II mineralization is characterized by essentially no added Ag above background levels resulting in very high Au:Ag values (Figs. 45 and 46). In addition to low Ag values Type II mineralization also has much lower Hg, Sb, and Tl values than are found in Type I mineralization (Figs. 45 and 46). The mineralization type occurs along a west dipping hanging wall fault in Cross Section B (Fig. 44). Type II mineralization is associated with strong argillization and weak silicification of the gouge material in this fault. Additionally there is a large amount of bleaching and argillization in the non-mineralized

rock adjacent to the fault zone (Fig. 47). Type II mineralization has the highest gold grades sampled in this study, locally >2.000 oz/t Au (Fig. 46).

A correlation matrix evaluated 13 sampled intervals of Type II mineralization grading >0.300 oz/t Au, and indicates strong correlation (R>0.75) of Au with As, Hg, Se and Tl; moderate correlation (0.50<R<0.75) of Au with Cr, Cu, In, Mg, Mn, Ni, Sb, Sc, Te, and W; and a weak but notable correlation (0.40<R<0.50) of Au with Ge, Sn, and Ta (Table 3).

Type III mineralization is characterized by Au<Ag. In addition to having high Ag values, values of Hg and Tl are also higher than values in Type I and II. However, Tl values for Type III mineralization are similar to those for Type I mineralization (Figs. 45 and 46). This mineralization is typically low grade <0.1 oz/t Au. It is associated with alteration in areas of siliceous carbonaceous mudstone lacking limestone, which is typically a poor host lithology. In these areas, mineralization is largely restricted to replacement of formerly calcite filled fractures and tension gashes with quartz, minor sooty pyrite, and late realgar. No samples of mineralization with this signature contained >0.300 oz/t Au.

A correlation matrix produced with the lower grade intercepts (ranging from 0.01 to 0.244 oz/t Au) indicated a moderate correlation of Au with Tl with an R value of 0.549 and a weak but notable correlation of Au with Te and S with R values of 0.442 and 0.426 respectively (Table 4).

Locally some ore zones display multiple mineralization types within one zone (Appendix – 08-GC-037). In other locations such as ore zones associated with the jog in the Getchell fault in Cross Section B, the ore chemistry reflects aspects of type I and type

II mineralization; with high concentrations of Hg, Sb, and Tl and low to absent Ag respectively (Fig. 44; Appendix B drill hole 07-GC-023).

Carbonate Staining

For this study a total of 144 samples of carbonate from drill core were stained for the presence of iron. See Appendix C for full staining data. Limestones associated with the argillaceous mudstones generally stained purple indicating the presence of iron (62/68) (Fig. 48). Limestones associated with the siliceous carbonaceous mudstones generally stained red/pink (48/59) indicating they lacked iron-bearing calcite (Fig. 48). Limestones in the footwall rocks all stained red/pink (17/17). Overall the upper portions of the cross sections, hanging wall to the Getchell fault, tended to have carbonates that were more ferroan while the lower portions had limestones which were iron poor. This correlates to the distribution of the limestone associated with the siliceous carbonaceous mudstones (Figs. 49 and 50).

Carbonate staining was complicated by the large amount of calc-silicate alteration from the contact metamorphism; in particular in areas closest to the Osgood stock (Figs 24 and 25). The units of argillaceous mudstone containing fragments of limestone were often intensely calc-silicate altered throughout drill holes in both sections. These rocks composed large portions of the cores for these sections. The lack of available reactive limestone due to the prevalence of these calc-silicate altered units in these areas limited staining coverage.

CHAPTER 6

DISCUSSION AND INTERPRETATION

Stratigraphy

Logging of drill core for this study indicates that the complex stratigraphy established at the Turquoise Ridge deposit, consisting of one or more debris flows and soft-sediment slumps resulting in the physical mixing of two discrete lithologies, can in large part be extended to this study area further to the south. The dominant architecture of blocky, brittle clasts of siliceous carbonaceous mudstone and limestone in a matrix of poorly lithified, strongly soft-sediment deformed, argillaceous mudstone and limestone in the lower portions of the hanging wall, and 2) argillaceous mudstone and limestone in the upper portions of the section, is consistent with the stratigraphy at Turquoise Ridge (Cline et al., 2008).

Although they are generally similar, several differences are observed between the stratigraphy in this study area and at Turquoise Ridge further north. Most notable is the lack of the carbonaceous shear texture breccia unit, which is a major host for mineralization at Turquoise Ridge. At Turquoise Ridge this siliceous carbonaceous mudstone unit with limestone fragments occurs above the lower portions of the debris flow deposit, defined by the upper occurrence of the siliceous carbonaceous mudstone and limestone clasts (Cline et al., 2008; Keith Wood, per. comm. 2009). This unit has been observed to thin to the south and the lack of observation of the shear texture breccia unit in this study confirms that finding (Cline et al., 2008; Keith Wood, per. comm., 2009). The upper extent of clasts of the siliceous carbonaceous mudstone and limestone lithology is at a higher elevation in this study area, typically 3800’ to 4200’ a.s.l., in

comparison to elevations of 2500 feet a.s.l. where observed at Turquoise Ridge, suggesting that this boundary dips to the north (Cline et al., 2008).

The current study also documented a siliceous carbonaceous mudstone unit below the Upper Basalt. This mudstone unit is observed as the upper sedimentary layer in both cross sections, suggesting that these rocks were deposited after and above the discontinuous stratigraphy of the debris flow below them. The upper carbonaceous mudstone unit locally contains small inter-beds or flows of hyaloclastite material. These inter-beds suggests that the upper basalt is in depositional contact with this unit and not faulted in via the Roberts Mountain Thrust as some previous studies have suggested.

Calc-Silicate Alteration

The key focus of this study was to elucidate the effects of calc-silicate alteration, owing to the intrusion of the Osgood stock at 92 Ma, on host rock potential at the Getchell and Turquoise Ridge deposits. Overall the study found that extent and intensity of calc-silicate alteration within the metamorphic aureole is variable. Variability in the intensity of calc-silicate alteration has been previously noted by Boskie (2001) even in areas within ten of meters from the stock. The effects of contact metamorphism observed in this study are variable with moderate calc-silicate alteration locally present out to approximately 2,000 ft from the stock. In Cross Section A the intensity of calc-silicate alteration generally decreases away from the stock. In Cross Section B a clear pattern is not discernable, with strongly calc-silicate altered rocks occurring locally in the drill holes most distant from the lobe of the stock in the hanging wall. This more intense calc-silicate alteration may be due to the closer proximity of Cross Section B, which is located further to the south, to the main body of the Osgood stock (Fig. 4).

The key finding of this study was that variability in the intensity of calc-silicate alteration is strongly influenced by lithology. The limestone inter-bedded with argillaceous mudstone was found to alter to calc-silicate minerals more readily than the limestone inter-bedded with the siliceous mudstones (Fig. 26). The limestone associated with the argillaceous mudstone commonly contains a small silty component, evidenced by the small feldspar signature observed in the XRD spectra. This silty component would provide the necessary constituents to create the more diverse calc-silicate assemblage, including abundant diopside, garnet, and vesuvianite, observed in the argillaceous limestones. In comparison, the relatively silt-free limestone inter-bedded with the siliceous carbonaceous mudstone is altered to a wollastonite dominated calc-silicate assemblage.

Structure

The major structural feature of the deposit is the Getchell fault, observed as a gouge zone 50-100 feet thick that dips approximately 30°-50° to the east. Numerous other small faults occur in the hanging wall. Overall there appears to be two main orientations of faults in the hanging wall, the east-dipping Getchell-parallel structures and the west-dipping faults. The major west dipping fault in Cross Section A, responsible for down dropping the Upper Basalt, may correspond to the NNE striking structures which have been previously mapped in the area (Fig. 4; Tom Chadwick per. comm. 2010). Additional smaller west dipping structures are observed in both cross sections. The other major structure is the east dipping Getchell-parallel fault in Cross Section B, which may be similar to a structure along which dacite dikes were emplaced in Cross Section A. As

discussed below both sets of structures in the hanging wall played an important role in transporting ore fluids.

Mineralization

Controls

The dominant control on ore mineralization is the presence of reactive host rocks in contact with ore fluid conduits. Ore fluids were dominantly mobilized along the Getchell fault which is weakly to moderately mineralized where encountered in this study, with grades typically ranging from 0.01 oz/t Au up to 0.20 oz/t Au. Fluids moved upward from the Getchell fault into the hanging wall, either into zones of reactive carbonate in direct contact with the fault or along faults and dikes intersecting the Getchell fault (Figs. 32 and 33). Mineralization is generally not present in the footwall of the fault even in areas where reactive host rock is present. These findings are consistent with the findings of Cline et al. (2008).

Where the faults intersect receptive clasts of siliceous carbonaceous mudstones with inter-bedded limestone, mineralization extends beyond these subsidiary hanging wall structures. However where the fault intersects calc-silicate altered rocks the mineralization remains tightly restricted to the gouge zone, as is the case with the major west dipping structures observed in this study. Although the Getchell fault appears to have been the primary local conduit for the Carlin-type ore fluids, it typically hosts only lower grade mineralization that grades <0.100 oz/t Au (Plate 1).

As noted in previous studies (Heitt et al., 2003), rocks which have been altered to calc-silicates and hornfels are typically poor hosts for Carlin-type mineralization. This is largely due to the lack of carbonate mineralogy for the acidic Carlin ore fluids to dissolve

and create enhanced permeability and porosity of the hydrothermal system and perhaps to liberate and sulfidize reactive Fe. In addition to being poor hosts for Carlin-type mineralization, the calc-silicate altered rocks also acted as an aquitard to the migration of the Carlin-type fluids. In many places (Figs. 38a and 38b) mineralization stops at the contact between the calc-silicate and non calc-silicate altered rocks. Potentially receptive and reactive rocks which are surrounded by calc-silicate altered rocks remain non-mineralized unless they are intersected by structures that carried ore fluids.

Zones of calc-silicate altered argillaceous mudstone and limestone near mineralization in the limestone and siliceous carbonaceous mudstone preserve evidence that they were exposed to the ore fluids, however they are not well mineralized. They commonly contain realgar on fractures or are cut by faults with ore-grade mineralization. However, no mineralization extends beyond the fractures or fault gouge (Fig. 38a). Evidence, apparent in hand samples, for a lack of calc-silicate alteration in limestone inter-bedded with siliceous carbonaceous mudstone includes the visible alteration by Carlin ore fluids of strong decalcification and silicification that produced porous silica along former limestone beds. These observations, of a lack of calc-silicate minerals in the mineralized limestone units, were confirmed by thin section petrography and XRD analyses of samples of ore grade mineralization.

Although the siliceous carbonaceous mudstones themselves are typically poor hosts due to their lack of carbonate material for the ore fluids to mineralize, they appear to play an important role in the transport of ore fluids. These mudstone beds commonly have a well developed fracture network of small tension fractures filled with calcite (Figs. 10 and 12). The Carlin-type ore fluids removed the calcite from these fractures and

generated permeability through a rock type that would otherwise be very impermeable and difficult to alter. Further, because the mudstones are dominantly composed of quartz they generally remain relatively unaltered, unlike the argillaceous mudstones, which became argillized where they reacted with ore fluids, generating voids which remained open, possibly for the duration of the Carlin hydrothermal system. This porosity is evidenced by late stage realgar and quartz filling these voids, some of which locally remain open (Fig. 34).

Chemistry

The variations in the chemistry determined for the ore zones in this area have been classified into Type I, II, and III mineralization (Table 5). These variations in chemistry most likely reflect the whole-rock signature response to pulses of ore fluids with different trace metal chemistries. Previous studies by Longo et al. (2008) and Barker et al. (2009) have identified discrete zonations in pyrite rims which have distinct elemental signatures. These studies conclude that the variations observed in the ore-stage pyrite chemistry reflect changes in the chemistry of the ore fluid as the hydrothermal system evolved and as new pulses of ore-fluids were introduced to the system.

Type I mineralization has much lower Au:Ag ratios, typically 2:1 to 1:1, than is common in most Carlin-type ore deposits, which typically have ratios of 10:1 and as high as 100:1 (Kretschmer, 1990; Emsbo et al., 2006). Type I mineralization appears to be associated with later stage mineralization. These ore zones commonly contain abundant late-stage realgar and there tends to be very little alteration adjacent to these mineralized zones possibly reflecting cooler ore fluids (Figs. 38a and 38b).

Type II mineralization typically has wider areas of alteration, such as bleaching and argillization, associated with it and realgar is much less common (Fig. 47). Additionally, Type II mineralization appears to be able to alter and mineralize less favorable host rocks than Type I mineralization. Further, Longo et al. (2008) reported that the early fluids have low Tl, consistent with the much lower Tl present in Type II mineralization in comparison to Type I mineralization. This suggests the Type II fluids may possibly represent the early fluids in the system.

Type III mineralization is commonly adjacent to zones of Type I mineralization, and typically occurs in areas of limestone poor siliceous carbonaceous mudstone. The chemistry most closely resembles that of Type I mineralization. Type III mineralization therefore may represent more distal portions of the Type I mineralization or may be the result of Type I mineralization altering a different, less receptive, rock type.

Carbonate Staining

The results of the staining of limestone in the area showed no discernable pattern that would suggest the source of iron in carbonates was from fluids evolved from the Osgood stock. Rather, the distribution of ferroan carbonate seems to be dominantly controlled by the pre-stock lithology. The ferroan limestone is far more commonly inter-bedded with the argillaceous mudstones. Alternatively, little to no ferroan limestone is inter-bedded with the siliceous carbonaceous mudstones.

In this study the majority of the ferroan limestone occurs in the limestone below the Upper Basalt. This is similar to the distribution of ferroan carbonate observed in other studies at Turquoise Ridge to the north (Cline et al., 2008). However, the distribution observed in the present study also correlates with the distribution of the argillaceous

limestone that is more common in the upper portions of the section. Further, the presence of the argillaceous limestone which also stained for iron deeper in the section, likely indicates that the iron in the limestone is intrinsic to the limestone of that lithology rather than an addition of iron by some post depositional process.

With respect to iron-bearing carbonates being better hosts for Carlin-type mineralization, owing to the tendency for the argillaceous limestones to readily alter to calc-silicates, these limestones are typically not the best host rocks in this study area. However, locally where they are mineralized, generally in areas of Type II mineralization, the argillaceous limestones host the highest gold grades (e.g., drill hole 07-GC-027 with 25 feet grading 1.439 oz/t Au). This is in comparison to the more commonly mineralized siliceous carbonaceous mudstones and limestones, which are generally lower grade (e.g., drill hole 08-GC-035 with 78 feet grading 0.354 oz/t Au). Whether this is a result of the presence or absence of iron bearing carbonates or different ore fluids is difficult to distinguish, owing to the small sampling of ore zones associated with iron-rich carbonates.

CHAPTER 7

CONCLUSIONS

Effects of Calc-Silicate Alteration

The major focus of this study was to determine how calc-silicate alteration of Cambro-Ordovician sediments by a Mesozoic intrusion affected host rock receptivity for younger Eocene-age Carlin mineralization at the Getchell Deposit. With regards to calc-silicate alteration caused by the intrusion of the Osgood stock, this study found the following: 1) the intensity and extent of calc-silicate alteration of host rocks is quite variable within the greater extent of the metamorphic aureole; 2) within the aureole, limestones and calcareous shales inter-bedded with siliceous carbonaceous mudstones are less likely to become calc-silicate altered compared to those limestones and calcareous mudstones inter-bedded with the argillaceous mudstones, and limestones and calcareous shales inter-bedded with siliceous carbonaceous mudstones are therefore more likely to remain receptive host rocks for Carlin-type mineralization; 3) the calc-silicate altered rocks are poor hosts for Carlin-type mineralization, with the exception of heavily faulted areas; and 4) the boundaries between these two rock types exhibit strong lithologic control on mineralization, and grades range from >0.300 oz/t Au to background levels across the contact.

Mineralization documented in this study within the metamorphic aureole of the Osgood stock occurs primarily within zones or pods of re-crystallized limestone which have not been altered to calc-silicate minerals. These areas are most commonly the limestone and calcareous mudstone inter-bedded with siliceous carbonaceous mudstone. Mineralization in these units is associated with strong decalcification and silicification of

the formerly calcareous units. Argillization is not a dominant alteration in the siliceous mudstones host likely due to the small amount of aluminum-silicate minerals present in these units.

Mineralization locally occurs in calc-silicate or otherwise non-reactive rocks in areas that are strongly structurally deformed; such locations include jogs or intersections of faults. Similar mineralization restricted largely to fault gouge and breccia zones has been documented at other deposits, such as Deep Star, which occur in strongly calc-silicate altered host rocks (Heitt et al., 2003). In these areas the alteration is dominated by argillization with local silicification. Minor mineralization also occurs in the upper siliceous carbonaceous mudstone, just below the base of the Upper Basalt. Mineralization is associated with strong silicification and bleaching, and gold grades in these areas are generally low (i.e., <0.100 oz/t Au) again due to the lack of receptive carbonate.

Stratigraphy

In an effort to understand the effects of calc-silicate alteration, which has been shown to be influenced by lithology, it was important to understand the stratigraphy of the area and how it relates to Turquoise Ridge to the north. This study demonstrates that the stratigraphy in this study area is very similar to the stratigraphy observed at Turquoise Ridge. The large debris flow(s) is observed with the inter-mixing of two distinct groups of rocks: 1) clasts of siliceous carbonaceous mudstones inter-bedded with limestones; and 2) a matrix of argillaceous mudstones inter-bedded with limestones in the lower portions of the hanging wall section. The upper portions of the stratigraphy in this field area consist of another siliceous and carbonaceous unit of mudstone. Unlike similar rocks lower in the stratigraphy, these rocks are continuous, contain no limestone, and exhibit

less brittle deformation. Locally, these rocks contain small clasts of limestone. The major distinction of the stratigraphy in the study area in comparison to Turquoise Ridge to the north is the lack of the carbonaceous shear texture breccias and the North Pillow Basalt. Both of these units strongly influence the mineralization at Turquoise Ridge, with the shear texture breccia as a common host and the North Pillow Basalt commonly serving as a cap and focus for mineralization.

Staining

The results from the iron staining indicate no discernable spatial pattern that would suggest that iron in the carbonates was sourced from the Osgood stock or related metamorphic fluids. However, there is a correlation of iron-bearing carbonate with certain lithologies. Limestones inter-bedded with argillaceous mudstones tend to be more iron rich, staining purple, than the limestones inter-bedded with the siliceous carbonaceous mudstones, that typically stain red indicating no iron.

The majority of the carbonates staining purple for the presence of iron are in the upper parts of the sections below the Upper Basalt. However, I conclude that this has more to do with the distribution of the argillaceous limestone, which is also more common in the upper parts of the hanging wall section, than the proximity to the Upper Basalt. In the lower parts of the section where iron-free carbonates are more common, a few samples of limestone which stain for purple iron do occur, however they are typically in lithologies identified as argillaceous limestone. A few sections of limestone inter-bedded with the siliceous carbonaceous mudstones do stain for iron; these samples are commonly on the boundary between the two lithologies. Further the limestones that are

inter-bedded with siliceous carbonaceous mudstones in the footwall all stain red indicating no iron in the carbonate.

Future Work

The stratigraphy of the Osgood Mountains which hosts the Carlin-type gold mineralization at Getchell/Turquoise Ridge and Twin Creeks is very complex and remains poorly understood. The understanding of the stratigraphy is further complicated by different nomenclatures and naming systems used by different investigators and mining companies in the area over the last 70 years. A comprehensive stratigraphic model of the rocks would greatly help in elucidating how the rocks along the eastern flank of the Osgood Mountains formed and came to be in their present complex arrangement. This would potentially lead to a better understanding of the rocks which host the gold deposits along the Getchell trend and perhaps provide insight for targeting new deposits along this trend.

The variation in the whole rock geochemistry of the ore zones was a secondary but interesting result of this study. The observation that ore zones with certain chemistries tend to be higher grade, have wider zones of alteration, and can potentially mineralize less favorable hosts is a topic worth exploring. A study to expand on this idea, detailing how ore zone geochemistry varies across the deposit would be useful. Further correlation between whole rock geochemistry and ore-stage pyrite zoning using EPMA along the lines of the work conducted by Longo et al. (2008) to trace out the evolution of the ore fluids through the deposit could also provide new insight to deposit formation.

Core ID	Quartz	Calcite	Biotite	Muscovite	Kaolinite	Plagioclase	Orthoclase	Grossular	Marcasite
007-1621	Major	Major							
020-1048	Major				Major		Trace		Trace
035-1494									
035-1564	Trace	Minor							
035-2012	Major				Trace				
037-1352	Trace	Minor							
037-1668									
037-1704a		Major				Minor	Minor		
037-1704b	Trace					Major	Minor		
037-1797	Major				Trace				Trace
037-1878	Minor	Major					Minor		
037-1887a	Minor	Major					Minor		
037-1887	Major				Trace				Trace
037-1913		Minor					Minor	Minor	
088-1620	Major								
094-2152		Major				Minor			
094-2724a	Minor	Major							
094-2724b	Major						Minor		
142-1620	Major	Trace				Trace			
148-1007	Major		Minor				Major		Trace
148-1216		Major				Minor	Minor		
148-1269	Major	Trace	Major				Minor		
151-1622a	Minor	Trace		Major					
151-1622b	Minor	Trace	Major		Minor				
151-1822		Trace						Minor	

Core ID	Realgar	Diopside	Pyrite	Stibnite	Dolomite	Wollastonite	Vesuvianite	Tremolite	Hornblende
007-1621									
020-1048									
035-1494									
035-1564	Minor								
035-2012	Trace								
037-1352						Major	Minor		
037-1668									
037-1704a		Minor							
037-1704b									Minor
037-1797	Trace								
037-1878									
037-1887a									
037-1887	Trace								
037-1913		Minor							Minor
088-1620	Minor			Trace					
094-2152		Minor							
094-2724a									
094-2724b			Trace					Trace	
142-1620		Minor							
148-1007									
148-1216		Minor							
148-1269									
151-1622a			Trace		Minor				
151-1622b									
151-1822		Minor				Major	Major		

Table 1. Mineral identification and abundance data from XRD runs with major (>50%) minor (50-10%) trace (<10%) as determined by the X'pert Highscore Plus software program.

Type I	Au	Ag	Al	As	B	Ba	Be	Bi	Ca	Cd	Ce	Co
Au	1.000											
Ag	0.418	1.000										
Al	-0.305	-0.214	1.000									
As	0.119	0.274	-0.136	1.000								
B	0.107	-0.119	0.256	0.075	1.000							
Ba	-0.259	-0.353	0.186	0.038	0.095	1.000						
Be	-0.390	-0.371	0.276	-0.078	0.057	0.513	1.000					
Bi	-0.082	0.086	0.289	0.077	0.233	-0.260	-0.084	1.000				
Ca	-0.408	-0.116	0.463	0.070	-0.095	0.115	0.620	-0.014	1.000			
Cd	0.153	0.614	0.194	0.162	0.093	-0.182	-0.310	-0.085	0.098	1.000		
Ce	-0.303	-0.234	0.452	-0.499	0.032	0.015	0.424	0.317	0.383	-0.108	1.000	
Co	-0.432	-0.444	0.380	-0.633	0.031	0.236	0.486	0.274	0.194	-0.318	0.794	1.000
Cr	-0.076	-0.065	0.065	0.060	0.130	0.178	-0.123	-0.171	0.002	0.136	0.017	-0.194
Cs	-0.221	0.266	0.003	-0.066	0.002	0.263	0.513	-0.242	0.303	0.342	0.031	0.092
Cu	0.751	0.432	0.013	0.138	0.234	-0.050	-0.290	0.071	-0.379	0.476	-0.126	-0.249
Fe	0.212	-0.251	0.352	-0.538	0.334	0.233	0.307	0.217	-0.040	-0.118	0.595	0.687
Ga	-0.223	-0.161	0.908	-0.246	0.416	0.140	0.210	0.389	0.317	0.228	0.616	0.482
Ge	0.197	0.637	0.026	0.066	0.032	-0.341	-0.547	0.099	-0.183	0.552	-0.004	-0.193
Hf	-0.187	-0.007	0.658	-0.026	0.231	-0.151	-0.063	0.573	0.165	0.338	0.261	0.141
Hg	0.776	0.589	-0.114	0.180	0.155	-0.198	-0.326	-0.033	-0.329	0.580	-0.277	-0.455
In	0.306	0.761	-0.077	0.136	-0.034	-0.386	-0.338	0.075	-0.088	0.785	-0.106	-0.319
K	-0.261	-0.284	0.302	-0.072	0.317	0.683	0.708	-0.122	0.185	-0.136	0.073	0.363
La	-0.286	-0.197	0.459	-0.518	0.044	-0.035	0.323	0.333	0.329	-0.041	0.991	0.769
Li	-0.331	-0.300	0.832	-0.401	-0.029	0.241	0.356	0.102	0.558	-0.007	0.588	0.527
Mg	-0.161	-0.169	0.254	0.061	-0.089	0.576	0.590	-0.203	0.327	-0.212	0.004	0.167
Mn	-0.372	-0.309	0.467	0.018	-0.032	0.369	0.744	-0.054	0.877	-0.162	0.327	0.301
Mo	-0.065	0.189	0.224	0.125	0.135	-0.294	-0.619	0.491	-0.382	0.339	0.004	-0.064
Na	-0.163	-0.098	0.693	-0.225	-0.017	0.417	0.470	-0.227	0.486	0.199	0.446	0.436
Nb	0.015	0.561	0.258	0.150	0.035	-0.177	-0.296	0.178	0.203	0.735	-0.045	-0.225
Ni	-0.258	-0.014	0.438	-0.127	0.134	-0.163	-0.255	0.649	-0.154	0.194	0.443	0.416
P	0.125	0.482	0.269	0.240	0.015	-0.227	-0.445	0.351	-0.131	0.430	0.065	-0.200
Pb	-0.034	-0.034	0.238	-0.405	-0.172	0.048	0.236	-0.218	0.092	0.017	0.260	0.464
Rb	-0.219	-0.312	0.316	-0.125	0.320	0.665	0.724	-0.099	0.187	-0.148	0.210	0.456
Re	-0.153	0.192	0.305	0.199	0.086	-0.301	-0.438	0.620	-0.161	0.339	-0.051	-0.138
S	0.431	0.750	-0.177	0.048	-0.153	-0.360	-0.395	0.038	-0.076	0.591	-0.062	-0.217
Sb	0.333	0.878	-0.250	0.186	-0.155	-0.253	-0.257	-0.132	-0.102	0.590	-0.301	-0.464
Sc	-0.351	-0.395	0.327	-0.277	0.132	0.526	0.890	0.015	0.567	-0.372	0.492	0.648
Se	0.340	0.833	-0.294	0.226	-0.159	-0.308	-0.492	-0.070	-0.176	0.508	-0.231	-0.393
Sn	0.017	-0.030	-0.006	0.091	-0.099	-0.456	-0.121	0.588	0.034	-0.086	0.325	0.180
Sr	-0.154	0.159	0.287	0.164	-0.071	0.172	0.430	0.013	0.545	0.169	0.449	0.159
Ta	-0.195	0.331	0.462	0.089	-0.161	-0.370	-0.122	0.323	0.459	0.408	0.069	-0.105
Te	0.693	0.814	-0.245	0.288	-0.045	-0.444	-0.453	-0.057	-0.229	0.599	-0.389	-0.548
Th	-0.421	-0.426	0.482	-0.517	0.043	0.139	0.591	0.305	0.433	-0.287	0.931	0.900
Ti	-0.132	0.171	0.200	0.057	-0.103	0.379	0.447	-0.220	0.372	0.159	-0.002	0.014
Tl	0.840	0.391	-0.062	0.124	0.187	-0.212	-0.317	0.053	-0.378	0.390	-0.184	-0.347
U	-0.094	0.276	0.328	0.169	0.001	-0.485	-0.576	0.575	-0.133	0.364	0.109	-0.068
V	-0.022	0.199	0.520	0.184	0.386	-0.090	-0.339	0.508	-0.135	0.500	0.069	-0.080
W	0.100	-0.204	-0.360	0.066	-0.104	-0.051	-0.072	-0.360	0.076	-0.099	-0.330	-0.435
Y	-0.007	0.240	0.693	-0.008	0.235	-0.107	0.003	0.455	0.251	0.397	0.543	0.217
Zn	-0.065	0.314	0.490	-0.056	0.108	-0.325	-0.173	0.112	0.250	0.775	0.359	0.035
Zr	-0.292	-0.124	0.748	-0.189	0.194	-0.057	-0.121	0.363	0.230	0.331	0.438	0.279

Table 2. A correlation matrix generated from multi element assay data from available intercepts of Type I mineralization >0.300 opt (n=24).

Cr	Cs	Cu	Fe	Ga	Ge	Hf	Hg	In	K	La	Li	Mg
1.000												
-0.086	1.000											
0.121	-0.053	1.000										
-0.176	0.004	0.387	1.000									
0.138	-0.009	0.143	0.502	1.000								
0.205	-0.122	0.337	-0.094	0.132	1.000							
0.066	0.025	0.173	0.190	0.668	0.158	1.000						
0.092	0.148	0.920	0.165	-0.013	0.323	0.170	1.000					
-0.094	0.319	0.476	-0.109	0.003	0.657	0.330	0.645	1.000				
-0.070	0.594	-0.018	0.376	0.273	-0.433	-0.031	-0.077	-0.289	1.000			
0.072	-0.002	-0.090	0.581	0.633	0.075	0.301	-0.240	-0.052	0.006	1.000		
-0.002	-0.066	-0.173	0.383	0.741	-0.067	0.392	-0.320	-0.249	0.149	0.573	1.000	
-0.158	0.194	-0.100	0.072	0.162	-0.347	-0.133	-0.192	-0.312	0.530	-0.093	0.412	1.000
-0.159	0.230	-0.356	0.128	0.325	-0.368	0.083	-0.394	-0.323	0.388	0.236	0.642	0.650
0.275	-0.378	0.244	-0.119	0.337	0.526	0.573	0.140	0.287	-0.417	0.092	0.019	-0.312
0.047	0.274	0.100	0.423	0.625	0.065	0.138	-0.029	-0.064	0.458	0.421	0.754	0.463
0.019	0.277	0.210	-0.141	0.287	0.592	0.591	0.337	0.733	-0.214	0.000	0.127	-0.114
0.121	-0.257	0.083	0.221	0.569	0.330	0.592	-0.091	0.119	-0.172	0.508	0.255	-0.228
0.360	-0.232	0.286	-0.182	0.341	0.518	0.289	0.266	0.366	-0.304	0.136	0.023	-0.193
-0.178	0.158	0.087	0.349	0.237	-0.174	-0.134	-0.008	-0.170	0.330	0.233	0.359	0.424
-0.076	0.558	0.034	0.476	0.333	-0.423	-0.056	-0.058	-0.305	0.976	0.144	0.190	0.491
0.204	-0.194	0.153	-0.198	0.327	0.314	0.764	0.143	0.301	-0.320	0.018	0.042	-0.258
-0.171	0.158	0.385	-0.007	-0.098	0.730	0.107	0.510	0.860	-0.381	-0.018	-0.208	-0.292
-0.082	0.407	0.306	-0.321	-0.252	0.591	-0.114	0.509	0.770	-0.176	-0.263	-0.331	-0.192
-0.253	0.352	-0.295	0.488	0.302	-0.477	-0.045	-0.388	-0.385	0.639	0.395	0.499	0.603
-0.024	0.027	0.281	-0.279	-0.245	0.844	-0.147	0.370	0.726	-0.433	-0.182	-0.310	-0.237
-0.144	-0.297	-0.024	0.024	0.059	0.033	0.393	-0.073	0.093	-0.516	0.341	0.039	-0.268
0.335	0.182	-0.078	0.000	0.286	0.056	-0.046	-0.107	0.033	0.097	0.434	0.298	0.229
-0.039	0.192	-0.155	-0.255	0.324	0.222	0.555	0.004	0.304	-0.160	0.097	0.296	-0.127
-0.032	0.075	0.666	-0.136	-0.211	0.523	0.020	0.810	0.755	-0.311	-0.347	-0.417	-0.241
-0.150	0.093	-0.271	0.638	0.574	-0.205	0.245	-0.430	-0.276	0.261	0.895	0.628	0.143
-0.162	0.467	-0.062	-0.101	0.170	-0.154	-0.014	-0.010	0.054	0.380	-0.074	0.346	0.848
0.044	-0.108	0.951	0.322	0.042	0.215	0.151	0.941	0.463	-0.116	-0.154	-0.245	-0.183
0.101	-0.414	0.094	-0.207	0.371	0.512	0.584	0.049	0.348	-0.543	0.189	0.120	-0.335
0.277	-0.098	0.370	0.082	0.604	0.366	0.720	0.302	0.307	-0.019	0.139	0.116	-0.206
0.339	-0.157	-0.084	-0.378	-0.428	-0.208	-0.389	-0.015	-0.272	-0.199	-0.331	-0.231	-0.066
0.349	-0.074	0.339	0.283	0.792	0.442	0.579	0.228	0.300	-0.020	0.588	0.468	-0.050
0.183	0.095	0.246	0.066	0.546	0.480	0.505	0.274	0.588	-0.233	0.433	0.296	-0.323
0.427	-0.071	0.073	0.208	0.775	0.292	0.797	-0.002	0.118	-0.050	0.505	0.552	-0.223

Table 2. Continued

Mn	Mo	Na	Nb	Ni	P	Pb	Rb	Re	S	Sb	Sc	Se
1.000												
-0.476	1.000											
0.565	-0.180	1.000										
0.039	0.416	0.128	1.000									
-0.259	0.803	0.003	0.247	1.000								
-0.370	0.606	-0.033	0.338	0.581	1.000							
0.202	-0.135	0.513	-0.184	0.040	-0.039	1.000						
0.388	-0.424	0.520	-0.266	-0.126	-0.304	0.364	1.000					
-0.293	0.875	-0.267	0.494	0.742	0.540	-0.246	-0.375	1.000				
-0.268	0.157	-0.036	0.687	0.057	0.337	-0.141	-0.380	0.093	1.000			
-0.305	0.003	-0.047	0.455	-0.189	0.287	-0.152	-0.210	0.013	0.701	1.000		
0.777	-0.590	0.491	-0.241	-0.184	-0.478	0.304	0.669	-0.463	-0.315	-0.357	1.000	
-0.349	0.210	-0.101	0.541	-0.022	0.421	-0.164	-0.455	0.051	0.851	0.800	-0.448	1.000
-0.057	0.452	-0.292	0.117	0.515	0.081	-0.198	-0.453	0.503	0.079	-0.174	-0.137	-0.080
0.336	-0.114	0.370	0.025	0.145	0.459	0.113	0.124	-0.083	0.064	0.101	0.272	0.083
0.208	0.232	0.105	0.629	0.302	0.400	-0.004	-0.211	0.498	0.279	0.210	-0.130	0.161
-0.402	0.131	-0.151	0.435	-0.128	0.393	0.043	-0.340	0.122	0.726	0.719	-0.492	0.701
0.474	-0.128	0.472	-0.159	0.365	-0.165	0.291	0.375	-0.124	-0.208	-0.458	0.689	-0.421
0.560	-0.210	0.414	0.257	-0.195	-0.068	0.357	0.344	-0.122	-0.004	0.142	0.436	0.002
-0.382	0.136	-0.040	0.123	-0.034	0.237	0.028	-0.068	0.105	0.366	0.289	-0.339	0.213
-0.334	0.876	-0.177	0.457	0.805	0.758	-0.116	-0.546	0.835	0.270	0.065	-0.533	0.284
-0.261	0.739	0.002	0.500	0.735	0.678	-0.138	-0.040	0.799	0.120	0.027	-0.357	0.065
0.028	-0.265	-0.329	-0.326	-0.378	-0.232	-0.275	-0.198	-0.172	-0.303	-0.068	-0.160	-0.180
0.067	0.465	0.430	0.368	0.611	0.725	0.121	0.039	0.436	0.209	0.091	-0.018	0.158
-0.082	0.409	0.306	0.529	0.483	0.558	0.065	-0.199	0.389	0.403	0.295	-0.241	0.269
0.071	0.575	0.374	0.473	0.657	0.423	0.014	-0.024	0.600	0.015	-0.217	-0.081	-0.128

Table 2. Continued

Sn	Sr	Ta	Te	Th	Ti	Tl	U	V	W	Y	Zn	Zr
1.000												
0.042	1.000											
0.170	0.165	1.000										
-0.050	0.007	0.193	1.000									
0.287	0.324	0.026	-0.566	1.000								
-0.200	0.255	0.132	-0.027	0.045	1.000							
0.010	-0.141	-0.127	0.705	-0.318	-0.143	1.000						
0.501	0.085	0.509	0.198	-0.037	-0.199	0.060	1.000					
0.156	0.083	0.477	0.181	-0.055	-0.089	0.276	0.717	1.000				
-0.121	-0.126	-0.115	-0.094	-0.345	-0.092	0.017	-0.285	-0.247	1.000			
0.167	0.547	0.413	0.181	0.351	0.016	0.248	0.582	0.668	-0.372	1.000		
0.140	0.426	0.447	0.324	0.161	-0.065	0.208	0.562	0.563	-0.245	0.692	1.000	
0.220	0.144	0.547	-0.133	0.351	-0.138	-0.013	0.577	0.693	-0.257	0.727	0.591	1.000

Table 2. Continued

Type II	Au	Ag	Al	As	B	Ba	Be	Bi	Ca	Cd	Ce	Co
Au	1.000											
Ag	0.172	1.000										
Al	-0.597	-0.025	1.000									
As	0.879	0.169	-0.665	1.000								
B	-0.064	-0.061	0.059	0.104	1.000							
Ba	-0.183	0.127	0.146	-0.144	0.409	1.000						
Be	-0.597	0.123	0.492	-0.766	-0.198	-0.034	1.000					
Bi	-0.100	-0.066	0.313	-0.202	0.518	0.559	-0.029	1.000				
Ca	0.257	-0.023	0.540	0.039	0.032	-0.081	0.068	0.071	1.000			
Cd	-0.079	0.363	-0.029	-0.058	-0.338	-0.312	0.352	-0.260	-0.167	1.000		
Ce	-0.575	0.191	0.458	-0.560	-0.025	0.071	0.359	0.259	-0.197	0.055	1.000	
Co	0.221	-0.257	-0.049	0.159	-0.035	0.347	-0.249	0.105	0.185	-0.090	0.094	1.000
Cr	0.601	-0.237	-0.029	0.330	-0.142	-0.142	-0.288	0.245	0.504	-0.109	-0.059	0.614
Cs	-0.340	0.125	0.172	-0.102	-0.053	0.495	0.015	-0.284	-0.111	-0.084	-0.149	-0.001
Cu	0.731	0.339	-0.185	0.450	-0.125	-0.169	-0.178	0.026	0.506	0.174	-0.539	-0.013
Fe	0.273	0.305	-0.301	0.486	0.029	0.033	-0.335	-0.345	-0.165	0.465	-0.435	0.032
Ga	-0.681	0.010	0.974	-0.739	0.028	0.146	0.511	0.297	0.410	0.036	0.603	-0.016
Ge	0.486	0.193	0.033	0.486	0.305	0.364	-0.521	0.068	0.517	-0.273	-0.210	0.575
Hf	-0.619	0.001	0.799	-0.656	-0.022	-0.138	0.475	0.361	0.210	0.304	0.666	-0.156
Hg	0.866	0.365	-0.583	0.822	-0.100	-0.144	-0.609	-0.049	0.000	-0.023	-0.521	-0.123
In	0.501	0.430	-0.145	0.550	-0.321	-0.248	-0.307	-0.180	0.094	0.550	-0.304	-0.053
K	-0.164	-0.015	-0.224	-0.058	0.339	0.555	0.117	-0.105	-0.239	-0.188	0.051	0.441
La	-0.525	0.180	0.448	-0.483	0.020	0.030	0.231	0.313	-0.187	0.056	0.982	0.068
Li	-0.604	0.001	0.657	-0.669	0.253	0.355	0.203	0.632	0.016	-0.128	0.598	-0.091
Mg	0.684	-0.022	-0.125	0.492	0.186	-0.040	-0.278	-0.068	0.724	-0.233	-0.491	0.379
Mn	0.603	-0.101	0.089	0.381	0.122	-0.087	-0.205	0.012	0.864	-0.254	-0.430	0.344
Mo	0.060	0.318	-0.183	0.273	-0.191	-0.148	-0.362	-0.227	-0.360	0.165	-0.215	-0.560
Na	0.140	0.156	0.270	0.136	-0.223	-0.223	0.103	-0.241	0.514	0.339	-0.539	-0.372
Nb	0.116	-0.051	-0.445	0.218	-0.143	-0.346	0.168	-0.502	-0.252	0.603	-0.142	0.239
Ni	0.652	-0.215	-0.304	0.487	-0.133	-0.068	-0.415	0.117	0.229	-0.142	-0.063	0.753
P	-0.094	-0.064	0.188	-0.051	0.023	0.620	-0.069	-0.133	0.263	-0.242	-0.143	0.591
Pb	-0.349	0.005	-0.067	-0.308	0.005	0.175	0.385	-0.022	-0.276	0.595	0.166	0.258
Rb	-0.472	-0.043	0.018	-0.302	0.165	0.488	0.330	-0.237	-0.244	-0.005	0.126	0.308
Re	0.314	0.225	0.157	0.225	-0.153	-0.153	-0.141	0.073	0.362	0.213	0.170	0.411
S	0.181	0.373	-0.308	0.402	-0.004	0.087	-0.242	-0.391	-0.244	0.533	-0.300	0.099
Sb	0.503	0.057	-0.163	0.227	0.107	0.065	-0.421	0.413	0.222	-0.235	0.048	0.341
Sc	0.608	-0.191	-0.135	0.474	0.219	0.070	-0.330	-0.080	0.659	-0.293	-0.513	0.529
Se	0.807	0.170	-0.370	0.495	-0.204	-0.224	-0.242	0.049	0.351	0.032	-0.314	0.183
Sn	0.429	0.528	-0.289	0.562	-0.300	-0.264	-0.338	-0.312	-0.090	0.218	-0.318	-0.483
Sr	-0.263	-0.008	0.897	-0.416	-0.099	-0.080	0.421	0.166	0.801	0.047	0.200	-0.012
Ta	0.495	-0.071	0.188	0.226	-0.337	0.101	-0.142	0.113	0.682	-0.167	-0.149	0.633
Te	0.677	0.545	-0.626	0.680	-0.100	-0.178	-0.479	-0.030	-0.278	0.027	-0.177	-0.271
Th	-0.700	0.092	0.425	-0.662	0.147	0.081	0.327	0.353	-0.363	-0.012	0.829	-0.272
Ti	0.017	-0.103	0.037	0.148	0.306	0.499	-0.200	-0.220	0.276	-0.303	-0.353	0.431
Tl	0.945	0.191	-0.705	0.874	-0.188	-0.233	-0.578	-0.187	0.023	-0.056	-0.436	0.198
U	-0.723	-0.038	0.709	-0.666	-0.009	-0.074	0.553	0.070	0.131	0.490	0.589	0.053
V	-0.034	-0.223	0.485	-0.086	0.220	0.359	-0.023	0.035	0.719	-0.278	-0.159	0.507
W	0.602	0.101	-0.367	0.548	-0.260	-0.191	-0.430	-0.105	0.063	0.036	-0.030	0.505
Y	0.228	0.000	0.232	0.145	-0.158	0.004	-0.147	-0.073	0.534	-0.227	0.248	0.666
Zn	-0.647	0.105	0.500	-0.591	-0.042	0.032	0.427	0.176	-0.154	0.530	0.697	0.045
Zr	-0.679	-0.030	0.918	-0.735	0.022	0.008	0.483	0.376	0.304	0.163	0.606	-0.137

Table 3. A correlation matrix generated from multi element assay data from available intercepts of Type II mineralization >0.300 opt (n=13).

Cr	Cs	Cu	Fe	Ga	Ge	Hf	Hg	In	K	La	Li	Mg
1.000												
-0.570	1.000											
0.441	-0.348	1.000										
-0.175	0.435	0.219	1.000									
-0.060	0.152	-0.284	-0.299	1.000								
0.414	0.193	0.385	0.363	-0.012	1.000							
-0.013	-0.217	-0.238	-0.353	0.847	-0.308	1.000						
0.299	-0.171	0.659	0.423	-0.651	0.304	-0.556	1.000					
0.201	0.051	0.515	0.708	-0.187	0.230	-0.052	0.670	1.000				
-0.226	0.378	-0.387	0.049	-0.170	0.242	-0.434	-0.364	-0.525	1.000			
-0.026	-0.206	-0.500	-0.405	0.590	-0.180	0.706	-0.450	-0.229	-0.064	1.000		
-0.101	-0.005	-0.266	-0.283	0.744	-0.054	0.683	-0.428	-0.276	-0.170	0.632	1.000	
0.610	-0.243	0.622	0.030	-0.223	0.681	-0.387	0.317	0.051	0.133	-0.489	-0.379	1.000
0.680	-0.260	0.606	-0.075	-0.031	0.629	-0.195	0.249	0.076	-0.044	-0.418	-0.268	0.961
-0.435	0.378	0.035	0.564	-0.178	-0.123	-0.116	0.501	0.592	-0.464	-0.134	0.013	-0.433
-0.088	0.265	0.440	0.331	0.133	0.027	0.107	0.205	0.537	-0.467	-0.506	-0.229	0.217
-0.014	-0.145	-0.034	0.289	-0.416	-0.174	-0.205	-0.105	0.124	0.332	-0.190	-0.655	0.056
0.868	-0.471	0.339	-0.080	-0.325	0.445	-0.261	0.348	0.175	0.006	-0.045	-0.329	0.496
-0.012	0.715	-0.126	0.228	0.173	0.608	-0.284	-0.259	-0.155	0.616	-0.216	-0.010	0.293
-0.177	0.000	-0.221	0.045	0.034	-0.240	0.178	-0.511	-0.196	0.455	0.121	-0.003	-0.143
-0.462	0.594	-0.550	0.071	0.069	0.045	-0.192	-0.605	-0.489	0.897	0.004	-0.098	-0.116
0.454	-0.298	0.452	0.075	0.125	0.420	0.225	0.196	0.426	-0.297	0.218	-0.058	0.204
-0.223	0.469	0.107	0.970	-0.265	0.334	-0.329	0.303	0.622	0.202	-0.293	-0.263	-0.014
0.672	-0.569	0.498	-0.150	-0.112	0.445	-0.079	0.388	0.027	-0.161	0.110	0.281	0.465
0.597	-0.105	0.462	0.077	-0.229	0.718	-0.446	0.210	-0.021	0.278	-0.521	-0.391	0.963
0.739	-0.569	0.707	-0.039	-0.396	0.265	-0.307	0.628	0.309	-0.229	-0.295	-0.306	0.669
-0.167	0.195	0.302	0.460	-0.340	-0.016	-0.235	0.722	0.733	-0.474	-0.251	-0.361	-0.080
0.215	0.013	0.150	-0.272	0.813	0.129	0.684	-0.354	0.060	-0.390	0.201	0.354	0.181
0.789	-0.108	0.491	-0.130	0.097	0.543	-0.063	0.230	0.247	-0.140	-0.161	-0.163	0.588
0.097	-0.272	0.443	0.233	-0.628	0.061	-0.424	0.882	0.510	-0.305	-0.112	-0.329	0.043
-0.304	-0.091	-0.568	-0.331	0.575	-0.389	0.638	-0.472	-0.352	-0.070	0.833	0.807	-0.648
-0.113	0.660	-0.082	0.340	-0.007	0.659	-0.439	-0.171	-0.184	0.666	-0.404	-0.168	0.445
0.537	-0.314	0.535	0.257	-0.753	0.326	-0.650	0.867	0.497	-0.125	-0.402	-0.658	0.484
-0.157	0.029	-0.380	-0.104	0.787	-0.211	0.852	-0.768	-0.108	-0.051	0.584	0.497	-0.335
0.276	0.352	0.061	0.039	0.422	0.672	0.025	-0.320	-0.174	0.320	-0.187	0.127	0.596
0.515	-0.330	0.399	0.083	-0.389	0.369	-0.249	0.453	0.374	-0.125	0.009	-0.426	0.248
0.524	-0.093	0.130	-0.255	0.203	0.564	0.072	-0.089	-0.033	0.102	0.242	-0.137	0.440
-0.118	-0.011	-0.448	-0.022	0.651	-0.264	0.763	-0.588	-0.032	-0.023	0.700	0.604	-0.458
-0.058	-0.030	-0.239	-0.304	0.951	-0.180	0.953	-0.596	-0.105	-0.368	0.629	0.786	-0.343

Table 3. Continued

Mn	Mo	Na	Nb	Ni	P	Pb	Rb	Re	S	Sb	Sc	Se
1.000												
-0.434	1.000											
0.330	0.353	1.000										
-0.070	-0.275	-0.033	1.000									
0.482	-0.434	-0.326	0.216	1.000								
0.255	-0.216	0.040	-0.073	0.055	1.000							
-0.236	-0.383	-0.095	0.615	-0.133	0.148	1.000						
-0.232	-0.349	-0.245	0.367	-0.257	0.658	0.566	1.000					
0.249	-0.168	0.006	0.141	0.592	-0.042	-0.133	-0.319	1.000				
-0.146	0.482	0.231	0.373	-0.112	0.295	0.216	0.232	0.020	1.000			
0.430	-0.191	-0.352	-0.348	0.549	-0.094	-0.195	-0.495	0.276	-0.173	1.000		
0.919	-0.476	0.149	0.104	0.528	0.460	-0.080	0.048	0.139	0.043	0.383	1.000	
0.641	-0.162	0.095	0.006	0.567	-0.200	-0.148	-0.526	0.143	-0.065	0.686	0.544	1.000
-0.081	0.803	0.528	-0.100	-0.183	-0.270	-0.391	-0.435	-0.017	0.391	-0.160	-0.191	0.225
0.409	-0.236	0.520	-0.314	-0.092	0.128	-0.144	-0.180	0.331	-0.320	-0.096	0.125	-0.065
0.689	-0.372	0.184	-0.130	0.721	0.376	-0.241	-0.232	0.560	-0.181	0.385	0.593	0.519
-0.058	0.503	-0.049	-0.066	0.216	-0.474	-0.394	-0.537	0.152	0.181	0.338	-0.105	0.504
-0.591	0.079	-0.469	-0.375	-0.415	-0.290	0.059	0.008	-0.202	-0.245	0.056	-0.677	-0.403
0.360	-0.176	0.098	0.027	-0.031	0.900	0.091	0.652	-0.151	0.374	-0.142	0.602	-0.204
0.391	0.140	-0.007	0.183	0.650	-0.174	-0.348	-0.425	0.232	0.197	0.405	0.423	0.753
-0.220	-0.237	0.094	0.161	-0.309	0.032	0.518	0.244	0.156	-0.011	-0.295	-0.312	-0.474
0.654	-0.415	0.244	-0.183	0.112	0.787	0.025	0.338	0.055	0.045	0.085	0.701	-0.006
0.202	-0.121	-0.220	0.295	0.808	-0.064	-0.182	-0.277	0.819	0.039	0.330	0.224	0.322
0.486	-0.497	-0.141	0.049	0.640	0.377	-0.128	0.055	0.707	-0.233	0.225	0.458	0.134
-0.390	-0.062	-0.102	0.066	-0.302	-0.056	0.555	0.174	-0.052	0.117	-0.085	-0.443	-0.291
-0.139	-0.089	0.144	-0.377	-0.336	-0.082	0.068	-0.118	0.163	-0.297	-0.075	-0.377	-0.379

Table 3. Continued

Sn	Sr	Ta	Te	Th	Ti	Tl	U	V	W	Y	Zn	Zr
1.000												
-0.133	1.000											
-0.065	0.454	1.000										
0.719	-0.498	-0.036	1.000									
-0.253	0.069	-0.501	-0.159	1.000								
-0.218	0.009	0.171	-0.410	-0.406	1.000							
0.506	-0.422	0.392	0.772	-0.585	-0.104	1.000						
-0.392	0.569	-0.151	-0.672	0.497	-0.083	-0.754	1.000					
-0.387	0.534	0.501	-0.625	-0.274	0.786	-0.234	0.222	1.000				
0.102	-0.155	0.535	0.436	-0.418	-0.136	0.623	-0.295	-0.164	1.000			
-0.239	0.386	0.722	-0.137	-0.253	0.251	0.176	0.104	0.460	0.658	1.000		
-0.249	0.278	-0.270	-0.413	0.692	-0.223	-0.588	0.858	0.016	-0.376	-0.124	1.000	
-0.293	0.763	-0.012	-0.540	0.640	-0.248	-0.747	0.824	0.214	-0.360	0.068	0.709	1.000

Table 3. Continued

Type III	Au	Ag	Al	As	B	Ba	Be	Bi	Ca	Cd	Ce	Co
Au	1.000											
Ag	0.131	1.000										
Al	-0.121	-0.290	1.000									
As	0.247	0.336	0.031	1.000								
B	-0.132	-0.145	0.445	-0.112	1.000							
Ba	-0.266	-0.315	0.050	-0.515	-0.024	1.000						
Be	-0.037	-0.175	0.631	-0.162	0.414	0.254	1.000					
Bi	0.010	-0.026	0.413	0.239	0.259	-0.136	0.181	1.000				
Ca	-0.235	0.060	-0.568	-0.056	-0.246	0.160	-0.283	-0.428	1.000			
Cd	0.116	0.150	0.038	0.292	-0.025	0.019	-0.087	0.215	0.074	1.000		
Ce	-0.036	-0.183	0.686	0.147	0.136	-0.096	0.297	0.608	-0.539	0.187	1.000	
Co	0.061	-0.196	0.765	0.087	0.255	-0.128	0.388	0.478	-0.743	0.062	0.836	1.000
Cr	0.148	-0.015	0.284	0.090	0.017	-0.101	0.013	0.210	-0.321	0.213	0.367	0.349
Cs	0.149	0.892	-0.185	0.377	-0.113	-0.326	-0.155	-0.053	-0.013	0.111	-0.158	-0.135
Cu	0.096	0.021	0.343	0.067	0.080	-0.152	0.080	0.190	-0.354	0.345	0.381	0.448
Fe	0.212	-0.198	0.593	0.119	0.226	-0.179	0.282	0.530	-0.695	0.015	0.664	0.800
Ga	0.053	-0.137	0.930	0.166	0.332	-0.090	0.509	0.460	-0.620	0.161	0.747	0.793
Ge	0.367	0.595	0.036	0.386	-0.115	-0.331	0.010	0.242	-0.197	0.210	0.108	0.035
Hf	-0.164	-0.221	0.576	0.089	0.316	0.025	0.265	0.666	-0.382	0.295	0.621	0.452
Hg	0.175	0.895	-0.253	0.411	-0.157	-0.354	-0.216	-0.036	0.003	0.167	-0.184	-0.175
In	0.389	0.354	0.072	0.461	-0.156	-0.310	0.014	0.342	-0.156	0.211	0.138	-0.009
K	-0.072	-0.233	0.815	-0.025	0.549	0.020	0.613	0.519	-0.648	-0.109	0.600	0.760
La	-0.002	-0.136	0.652	0.202	0.111	-0.108	0.260	0.632	-0.499	0.267	0.987	0.808
Li	-0.089	-0.155	0.512	-0.102	0.134	0.420	0.474	0.009	-0.051	0.093	0.180	0.156
Mg	0.073	-0.023	-0.435	-0.303	-0.237	0.268	-0.206	-0.224	0.247	-0.347	-0.414	-0.459
Mn	-0.061	-0.066	-0.498	-0.178	-0.262	0.128	-0.216	-0.335	0.580	-0.345	-0.497	-0.606
Mo	0.026	-0.164	0.208	0.009	0.028	0.002	-0.031	0.137	0.021	0.576	0.282	0.147
Na	0.009	0.244	0.056	-0.344	-0.148	0.184	0.032	-0.320	0.032	-0.252	-0.138	-0.082
Nb	0.115	0.147	0.078	0.177	-0.113	0.007	-0.045	0.307	0.027	0.264	0.063	-0.086
Ni	0.037	-0.210	0.516	-0.011	0.091	-0.100	0.143	0.265	-0.429	0.333	0.593	0.616
P	-0.028	-0.167	0.507	0.124	0.168	0.067	0.224	0.299	-0.223	0.319	0.552	0.389
Pb	0.162	-0.059	0.358	-0.056	0.176	-0.051	0.188	0.182	-0.569	0.042	0.264	0.482
Rb	-0.072	-0.204	0.849	0.088	0.484	-0.018	0.619	0.539	-0.679	-0.038	0.679	0.807
Re	-0.257	-0.300	0.265	-0.122	0.138	0.134	0.038	0.226	-0.120	0.463	0.337	0.206
S	0.426	0.437	0.225	0.584	-0.050	-0.468	0.082	0.456	-0.400	0.196	0.368	0.334
Sb	0.136	0.607	-0.198	0.437	-0.197	-0.326	-0.094	0.137	0.083	0.209	-0.143	-0.244
Sc	-0.062	-0.075	0.276	0.011	0.033	-0.040	0.393	0.303	0.069	-0.201	0.347	0.268
Se	0.191	0.560	-0.075	0.425	-0.168	-0.335	-0.111	0.242	-0.077	0.226	-0.027	-0.126
Sn	0.146	0.496	0.194	0.387	0.081	-0.281	-0.024	0.286	-0.212	0.245	0.286	0.230
Sr	-0.104	-0.025	-0.434	-0.104	-0.212	0.347	-0.155	-0.334	0.774	0.038	-0.458	-0.607
Ta	-0.126	0.564	-0.171	0.154	0.013	-0.153	-0.153	0.071	0.078	0.144	-0.116	-0.157
Te	0.442	0.156	0.042	0.390	-0.064	-0.233	0.052	0.301	-0.142	0.152	0.112	-0.008
Th	-0.098	-0.215	0.746	0.051	0.170	-0.052	0.373	0.473	-0.611	0.024	0.913	0.880
Ti	-0.072	-0.132	0.209	-0.292	-0.094	0.334	0.063	-0.092	-0.007	-0.072	0.021	0.074
Tl	0.520	0.553	0.039	0.579	-0.062	-0.423	-0.070	0.299	-0.341	0.211	0.280	0.284
U	0.138	-0.084	0.299	0.105	-0.027	-0.019	0.030	0.224	-0.081	0.603	0.442	0.263
V	0.042	-0.111	-0.021	-0.090	-0.065	0.065	-0.044	-0.038	0.318	0.439	-0.011	-0.243
W	0.149	-0.016	0.043	0.301	-0.119	-0.131	0.019	0.232	-0.038	0.460	0.268	0.183
Y	-0.147	-0.258	0.533	0.115	0.081	-0.119	0.181	0.405	-0.172	0.222	0.723	0.534
Zn	0.171	0.072	0.051	0.286	-0.081	0.028	-0.044	0.149	0.138	0.934	0.220	0.065
Zr	-0.006	-0.187	0.624	0.086	0.283	-0.045	0.200	0.633	-0.577	0.370	0.705	0.634

Table 4. A correlation matrix for Type III mineralization (n=89)

Cr	Cs	Cu	Fe	Ga	Ge	Hf	Hg	In	K	La	Li	Mg
1.000												
0.034	1.000											
0.338	0.097	1.000										
0.288	-0.216	0.484	1.000									
0.402	-0.040	0.394	0.647	1.000								
0.139	0.658	0.139	-0.008	0.248	1.000							
0.393	-0.200	0.287	0.404	0.594	0.117	1.000						
0.080	0.974	0.096	-0.231	-0.089	0.653	-0.169	1.000					
0.156	0.403	-0.009	-0.033	0.248	0.780	0.247	0.455	1.000				
0.175	-0.179	0.184	0.641	0.716	-0.031	0.497	-0.230	-0.001	1.000			
0.401	-0.131	0.393	0.657	0.741	0.148	0.623	-0.148	0.195	0.547	1.000		
0.173	-0.103	0.011	0.103	0.455	-0.007	0.214	-0.144	-0.020	0.236	0.179	1.000	
-0.286	-0.188	-0.360	-0.152	-0.434	-0.284	-0.336	-0.177	-0.234	-0.342	-0.398	-0.057	1.000
-0.365	-0.149	-0.269	-0.263	-0.536	-0.299	-0.408	-0.140	-0.257	-0.486	-0.495	-0.118	0.707
0.325	-0.144	0.519	0.115	0.278	0.029	0.371	-0.103	0.015	-0.125	0.318	0.162	-0.320
-0.004	0.218	-0.012	-0.103	0.019	0.106	-0.217	0.184	-0.041	-0.005	-0.177	0.254	0.197
0.255	0.158	-0.095	-0.046	0.208	0.460	0.414	0.205	0.580	0.048	0.112	0.258	-0.095
0.392	-0.157	0.710	0.488	0.563	0.037	0.438	-0.161	-0.057	0.301	0.579	0.125	-0.453
0.347	-0.092	0.473	0.329	0.523	0.095	0.645	-0.076	0.127	0.312	0.549	0.300	-0.359
-0.054	-0.034	0.409	0.468	0.332	0.052	0.162	-0.067	-0.152	0.360	0.206	0.021	-0.166
0.224	-0.122	0.272	0.657	0.781	0.019	0.528	-0.184	0.046	0.941	0.641	0.220	-0.371
0.277	-0.264	0.511	0.183	0.232	-0.202	0.561	-0.230	-0.231	0.032	0.338	0.173	-0.278
0.259	0.465	0.255	0.419	0.436	0.767	0.245	0.490	0.780	0.220	0.417	-0.026	-0.306
-0.053	0.588	-0.103	-0.264	-0.067	0.727	-0.063	0.626	0.705	-0.172	-0.099	-0.090	-0.176
0.012	-0.104	-0.081	0.285	0.219	0.007	0.107	-0.149	0.017	0.369	0.330	0.157	-0.121
0.033	0.606	0.024	-0.139	0.081	0.792	0.031	0.636	0.810	-0.091	0.016	-0.093	-0.215
0.177	0.502	0.208	0.172	0.365	0.634	0.256	0.484	0.449	0.120	0.326	0.061	-0.242
-0.255	-0.139	-0.392	-0.478	-0.484	-0.241	-0.244	-0.121	-0.161	-0.475	-0.412	0.180	0.490
-0.065	0.561	-0.024	-0.201	-0.056	0.540	-0.009	0.514	0.122	-0.127	-0.102	-0.077	-0.080
0.120	0.181	-0.085	0.004	0.206	0.590	0.162	0.239	0.823	0.021	0.163	-0.024	-0.174
0.249	-0.166	0.378	0.679	0.750	0.029	0.508	-0.208	-0.007	0.685	0.858	0.221	-0.425
0.139	-0.108	-0.094	0.063	0.196	-0.087	-0.058	-0.145	-0.124	0.219	0.005	0.519	0.103
0.211	0.560	0.207	0.372	0.246	0.512	0.037	0.595	0.487	0.145	0.335	-0.133	-0.093
0.398	-0.070	0.553	0.259	0.443	0.186	0.495	-0.023	0.210	-0.040	0.496	0.206	-0.272
0.204	-0.173	0.307	-0.082	0.039	-0.028	0.287	-0.126	0.037	-0.283	0.042	0.082	0.052
-0.002	-0.081	0.198	0.197	0.109	0.061	0.114	-0.060	0.045	0.090	0.291	-0.118	-0.169
0.326	-0.186	0.403	0.394	0.567	0.029	0.581	-0.189	0.068	0.304	0.713	0.157	-0.450
0.197	0.030	0.326	0.025	0.172	0.192	0.206	0.079	0.195	-0.149	0.298	0.110	-0.360
0.500	-0.126	0.471	0.546	0.693	0.157	0.881	-0.115	0.194	0.505	0.714	0.233	-0.384

Table 4. Continued

Mn	Mo	Na	Nb	Ni	P	Pb	Rb	Re	S	Sb	Sc	Se
1.000												
-0.247	1.000											
0.148	-0.090	1.000										
-0.148	0.085	0.110	1.000									
-0.461	0.731	0.017	-0.017	1.000								
-0.342	0.439	-0.035	0.163	0.489	1.000							
-0.306	0.138	0.135	-0.234	0.456	0.194	1.000						
-0.524	-0.043	-0.119	-0.007	0.389	0.381	0.366	1.000					
-0.258	0.752	-0.118	0.016	0.630	0.504	0.209	0.081	1.000				
-0.311	0.022	-0.071	0.393	0.153	0.172	0.112	0.291	-0.202	1.000			
-0.110	-0.118	0.010	0.409	-0.216	-0.166	-0.130	-0.151	-0.316	0.655	1.000		
0.140	-0.217	0.072	0.075	-0.037	-0.005	-0.128	0.286	-0.161	0.213	0.076	1.000	
-0.203	-0.064	0.005	0.441	-0.110	-0.036	-0.046	-0.045	-0.288	0.741	0.911	-0.013	1.000
-0.238	0.063	0.062	0.224	0.096	0.201	0.136	0.157	-0.042	0.611	0.473	0.082	0.485
0.555	-0.082	0.116	0.114	-0.434	-0.080	-0.433	-0.497	-0.177	-0.362	-0.027	0.040	-0.144
-0.049	-0.068	0.083	0.177	-0.114	-0.087	0.038	-0.128	-0.083	0.225	0.455	-0.012	0.377
-0.232	0.088	-0.123	0.455	-0.017	0.009	-0.160	0.058	-0.259	0.670	0.572	0.023	0.637
-0.477	0.177	-0.008	-0.058	0.615	0.434	0.423	0.719	0.277	0.260	-0.210	0.335	-0.110
-0.018	-0.064	0.429	0.447	0.011	-0.028	-0.053	0.087	-0.081	-0.145	-0.121	0.135	-0.121
-0.206	-0.118	-0.086	0.143	-0.009	0.085	0.065	0.225	-0.269	0.753	0.431	0.093	0.504
-0.238	0.830	-0.040	0.217	0.647	0.671	0.158	0.056	0.665	0.220	-0.068	-0.150	0.047
0.132	0.709	-0.013	0.210	0.349	0.329	-0.165	-0.251	0.518	-0.092	-0.109	-0.172	-0.080
-0.171	0.081	-0.213	0.055	0.205	0.097	0.152	0.115	0.080	0.159	0.082	0.118	0.065
-0.251	0.439	-0.115	0.023	0.554	0.695	0.171	0.385	0.452	0.168	-0.176	0.298	-0.071
-0.284	0.624	-0.203	0.195	0.364	0.308	0.003	-0.086	0.426	0.176	0.150	-0.134	0.155
-0.541	0.485	-0.168	0.292	0.634	0.648	0.336	0.573	0.618	0.298	-0.132	0.009	0.004

Table 4. Continued

Sn	Sr	Ta	Te	Th	Ti	Tl	U	V	W	Y	Zn	Zr
1.000												
-0.214	1.000											
0.493	-0.013	1.000										
0.295	-0.136	-0.053	1.000									
0.204	-0.552	-0.136	-0.022	1.000								
-0.144	0.129	-0.045	-0.105	0.090	1.000							
0.515	-0.222	0.192	0.396	0.160	-0.179	1.000						
0.193	-0.083	-0.046	0.127	0.283	-0.058	0.096	1.000					
-0.082	0.252	-0.100	0.100	-0.160	-0.022	-0.193	0.666	1.000				
0.063	-0.042	-0.059	0.046	0.207	-0.104	0.155	0.134	0.074	1.000			
0.193	-0.201	-0.145	-0.013	0.608	-0.115	0.012	0.605	0.259	0.226	1.000		
0.216	0.059	0.049	0.181	0.061	-0.066	0.149	0.645	0.503	0.530	0.297	1.000	
0.300	-0.393	0.012	0.122	0.596	-0.037	0.148	0.604	0.217	0.095	0.584	0.270	1.000

Table 4. Continued

	Type I	Type II	Type III
Grade	Commonly ore grade, >0.300 oz/t Au, but mineralization is rarely > 1.000 oz/t	Commonly ore grade, >0.300 oz/t Au, mineralization is commonly >1.000 oz/t up to 2.59 oz/t)	Rarely ore grade >0.300 oz/t Au, typically low grade, 0.010 to 0.100 oz/t Au
Chemistry	Higher Ag (1-15 ppm), higher Hg (100-500 ppm), Sb (100-400ppm), Tl (100-200 ppm)	Very low Ag (<0.1 ppm), lower Hg (50-150 ppm), Sb (20-150ppm), and Th (15-40ppm) than in Type I	Defined by Au<Ag, Hg, Sb, and Tl are common along with Au but their concentrations are quite variable relative to Au
Hosts	Dominantly hosted in the limestone inter-bedded with the siliceous carbonaceous mudstones that have not been calc-silicate altered.	Hosted in strongly argillized argillaceous mudstone and limestone lithologies within a fault gouge.	Dominantly hosted in siliceous carbonaceous mudstones that are limestone poor.
Controls	Mineralization occurs as fine grained pyrite in jasperoid altered limestones where ore fluids have spread out from ore fluid conduits into receptive limestone host rocks.	Ore stage sooty pyrite is very structurally controlled occurring within the argillized gouge a west dipping fault zone observed in Cross Section B.	Ore stage sooty pyrite and late stage quartz occur along formerly calcite filled tension gashes and veins that are common in the siliceous mudstones.
Alteration	Strong decalcification and silicification of limestone units, very little alteration in rocks adjacent to these mineralized zones. Commonly associated with abundant realgar.	Strong argillization of fault gouge with local silicification. Outside the mineralized zone areas of alteration, such as bleaching and argillization, is common. Abundant realgar is uncommon.	Decalcification and local silicification of formerly calcite filled tension gashes, mudstones often remain visibly unaltered. Commonly associated with abundant realgar.
Elemental Correlations	Strong correlation (R>0.75) of Au with Cu, Hg, and Tl; moderate correlation (0.50<R<0.75) of Au with Te; and a weak but notable correlation (0.40<R<0.50) of Au with Ag and S.	Strong correlation (R>0.75) of Au with As, Hg, Se and Tl; moderate correlation (0.50<R<0.75) of Au with Cr, Cu, In, Mg, Mn, Ni, Sb, Sc, Te, and W; and a weak but notable correlation (0.40<R <0.50) of Au with Ge, Sn, and Ta.	Moderate correlation (0.50<R<0.75) with Tl and a weak but notable correlation (0.40<R<0.50) with Te and S.

Table 5. A table summarizing the characteristics and differences between Type I, II, and III mineralization.

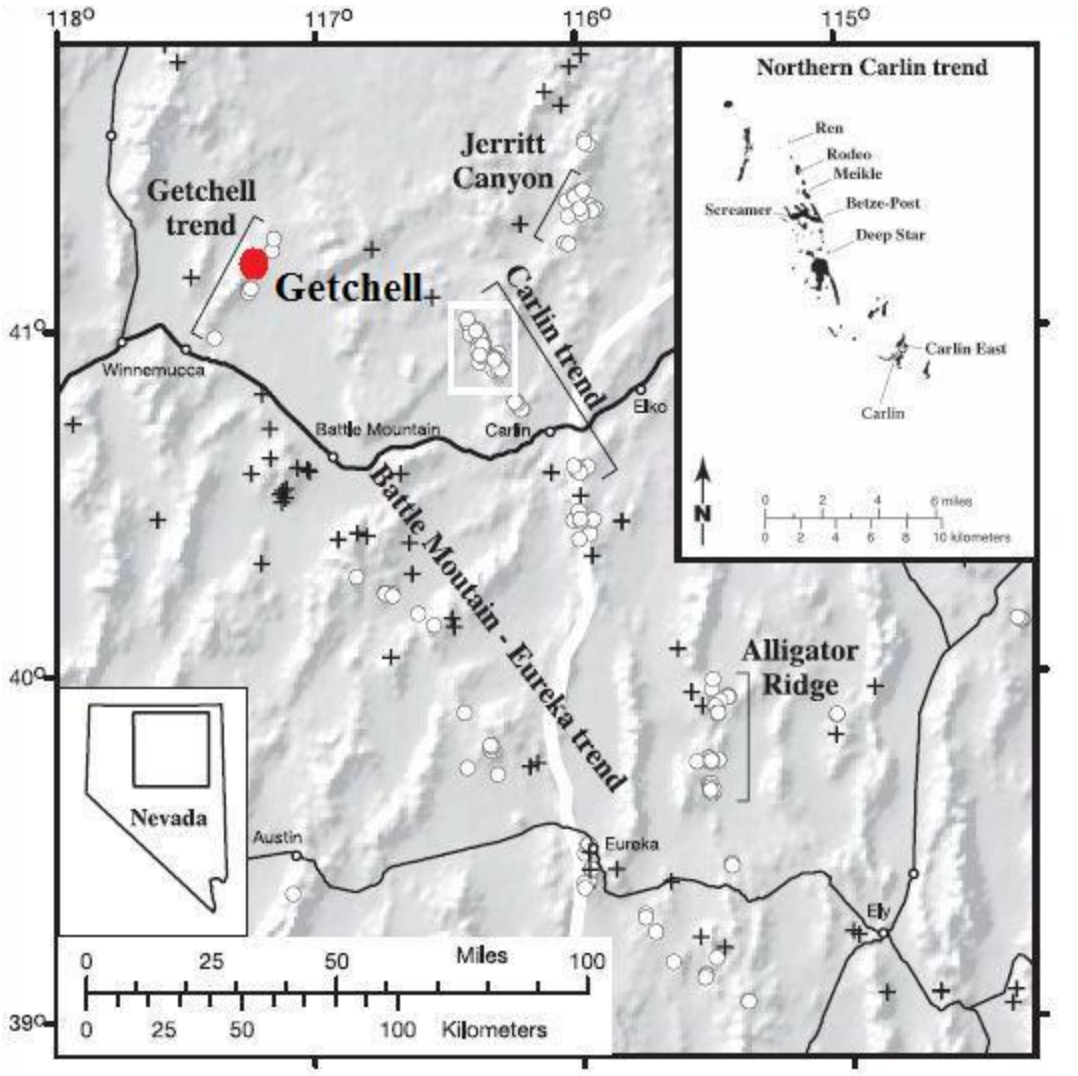

Figure 1. A map (modified from Cline et al., 2005) showing the five major trends of Carlin type deposits in Nevada. The Getchell and Turquoise Ridge deposits are circled in orange. Trends are interpreted as crustal scale faults (Tosdal et al., 2000) which served as conduits for these Carlin-type ore fluids. The Getchell and Turquoise Ridge deposits are located at the northern end of the Getchell trend.

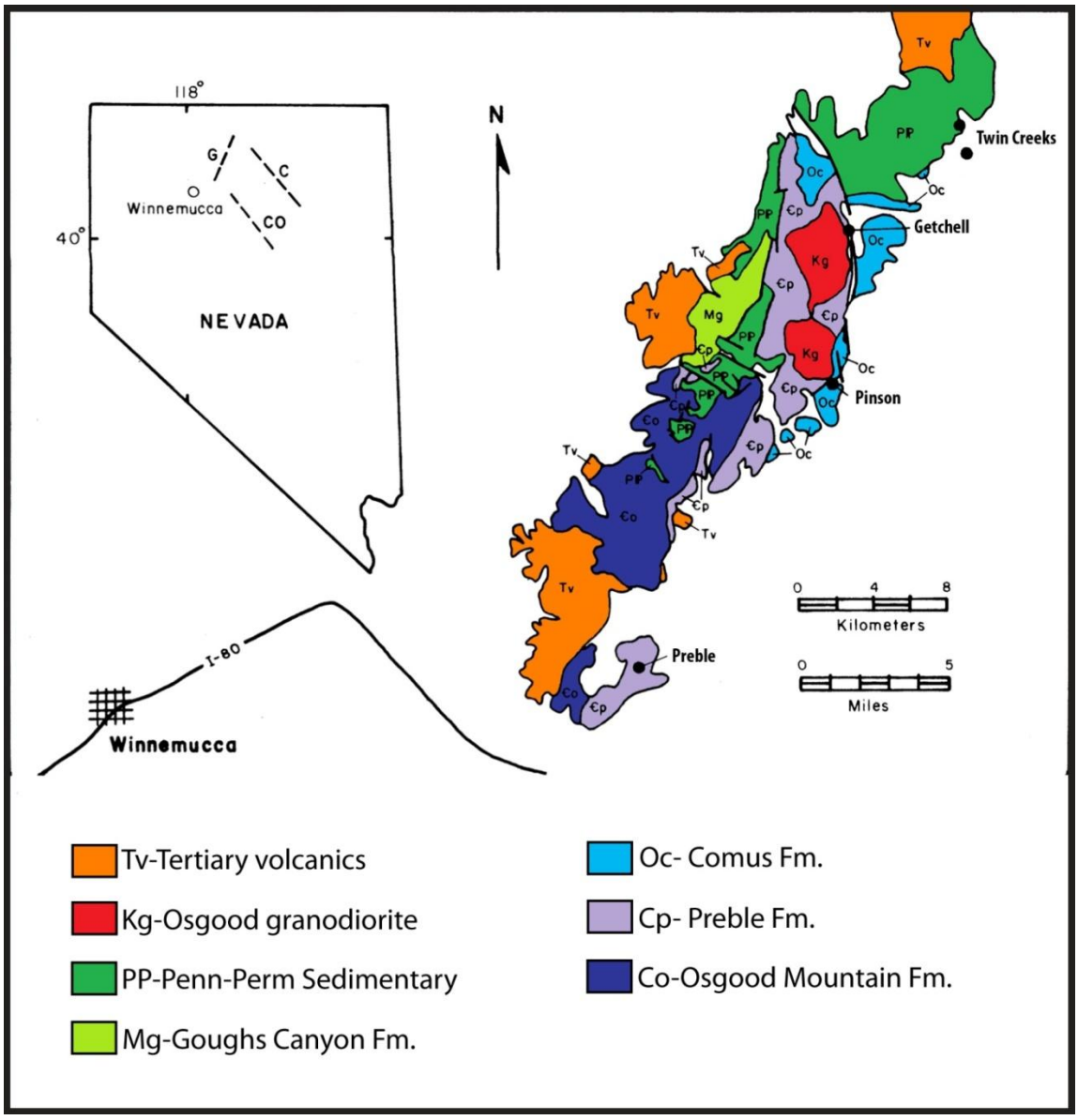

Figure 2. A geologic map of the Getchell trend (denoted G" on the insert), with the Preble, Pinson Getchell/Turquoise Ridge and Twin Creeks deposits, occurring along the eastern flank of the Osgood Mountains (modified from Foster and Kretshmer, 1991). The Getchell deposit is hosted in the Cambrian Preble Formation and the Ordovician Comus Formation. The Getchell Mine is located near the Osgood granodiorite (Kg) and many of the rocks have experienced moderate to strong contact metamorphism.

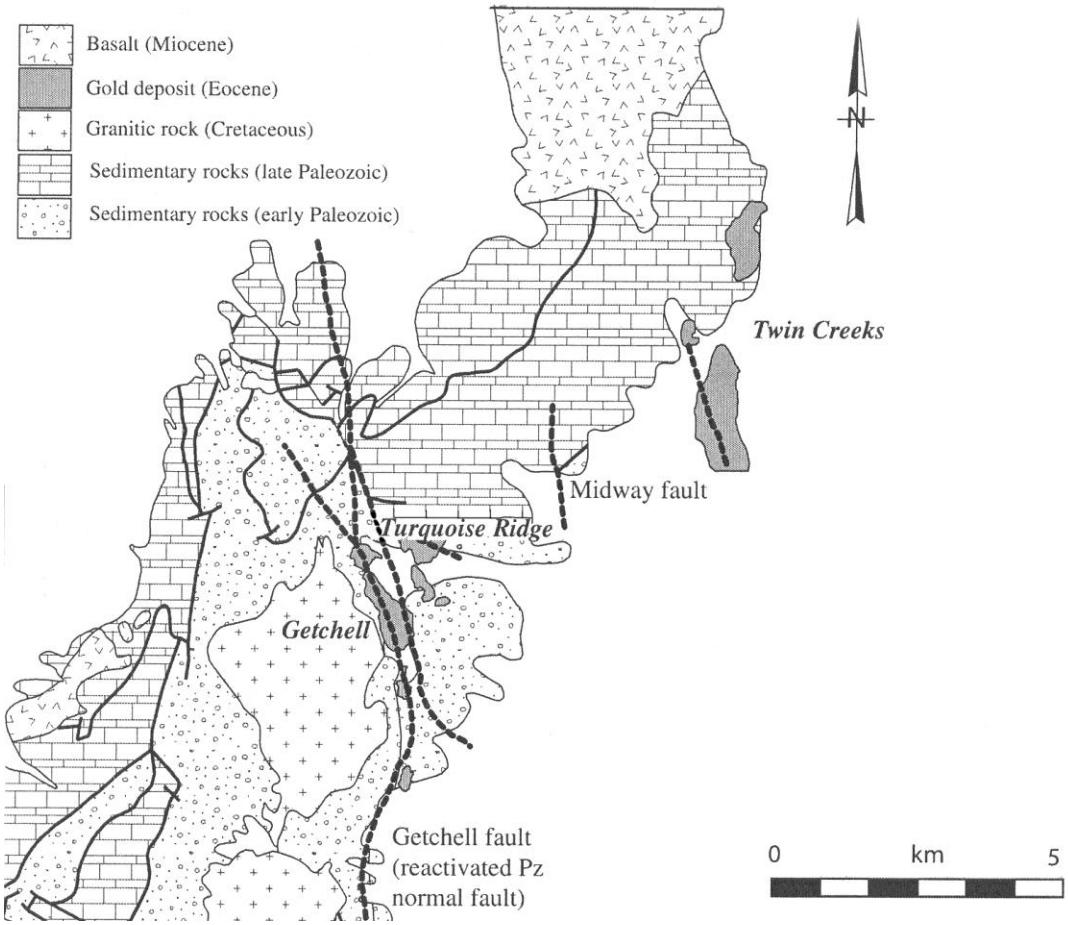

Figure 3. A geologic map (modified from Cline et al. 2005) showing the Carlin type gold deposits on the northern end of the Getchell trend. The Getchell Main Pit and North Pit are centered primarily on the Getchell fault; the Getchell Main Underground is located in the footwall adjacent to the open pits; the Turquoise Ridge deposit is located to the east in the hanging wall of the Getchell fault.

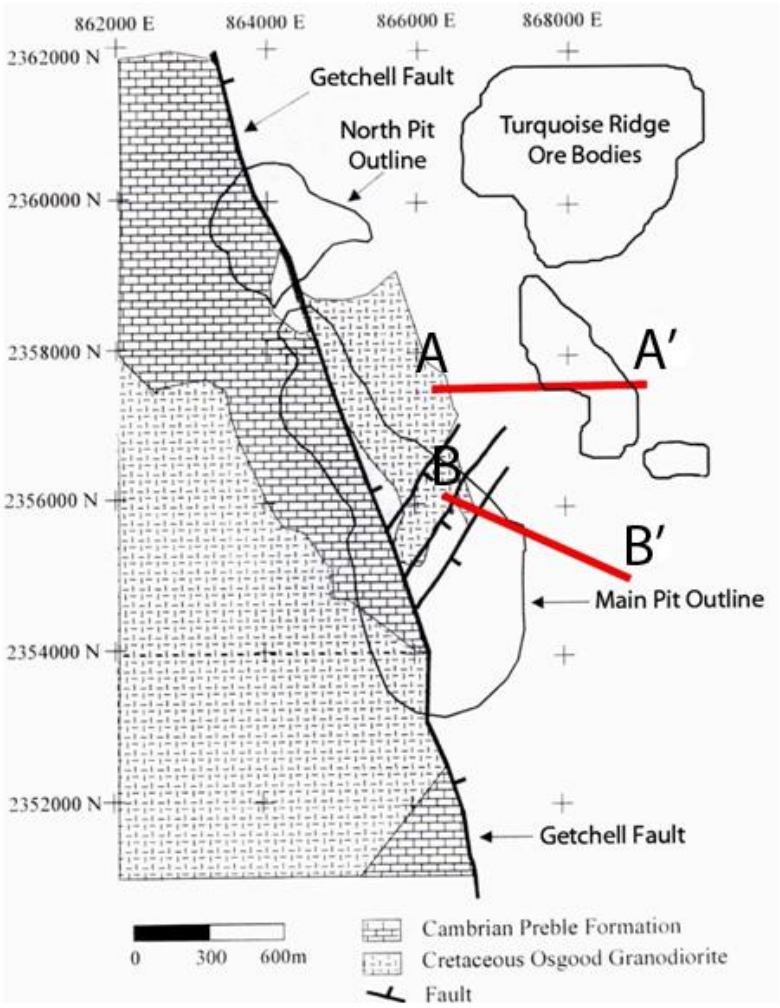

Figure 4. A map modified from Tretbar (2004) of the Getchell Deposit showing the locations of the cross sections produced by this study (red lines) in relation to the outlines of the Getchell open pits and the outline of the Turquoise Ridge (underground) deposit. Note the location of the lobe of the Osgood stock in the hanging wall of the Getchell Fault.

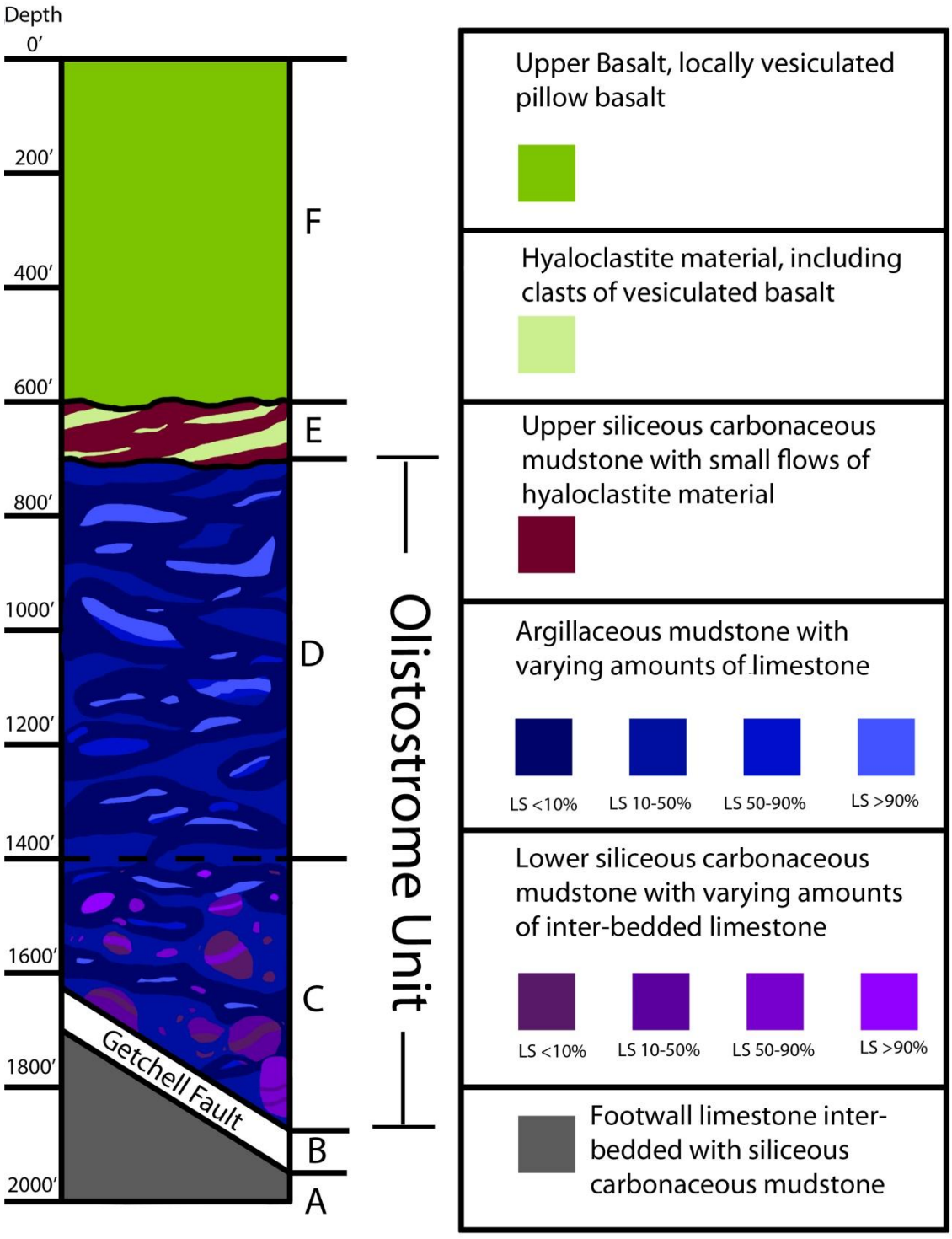

Figure 5. A generalized stratigraphic column for the study area. The depth to the Getchell fault is variable depending on location due to its moderate eastward dip.

Figure 6. Footwall carbonaceous limestones, gray to dark gray, with inter-beds of siliceous carbonaceous mudstones, black. The section is composed dominantly of limestone and shows little to no alteration to calc-silicate minerals. (63.5 mm diameter core, footage 1261' is upper left, footage 1270' is lower right)

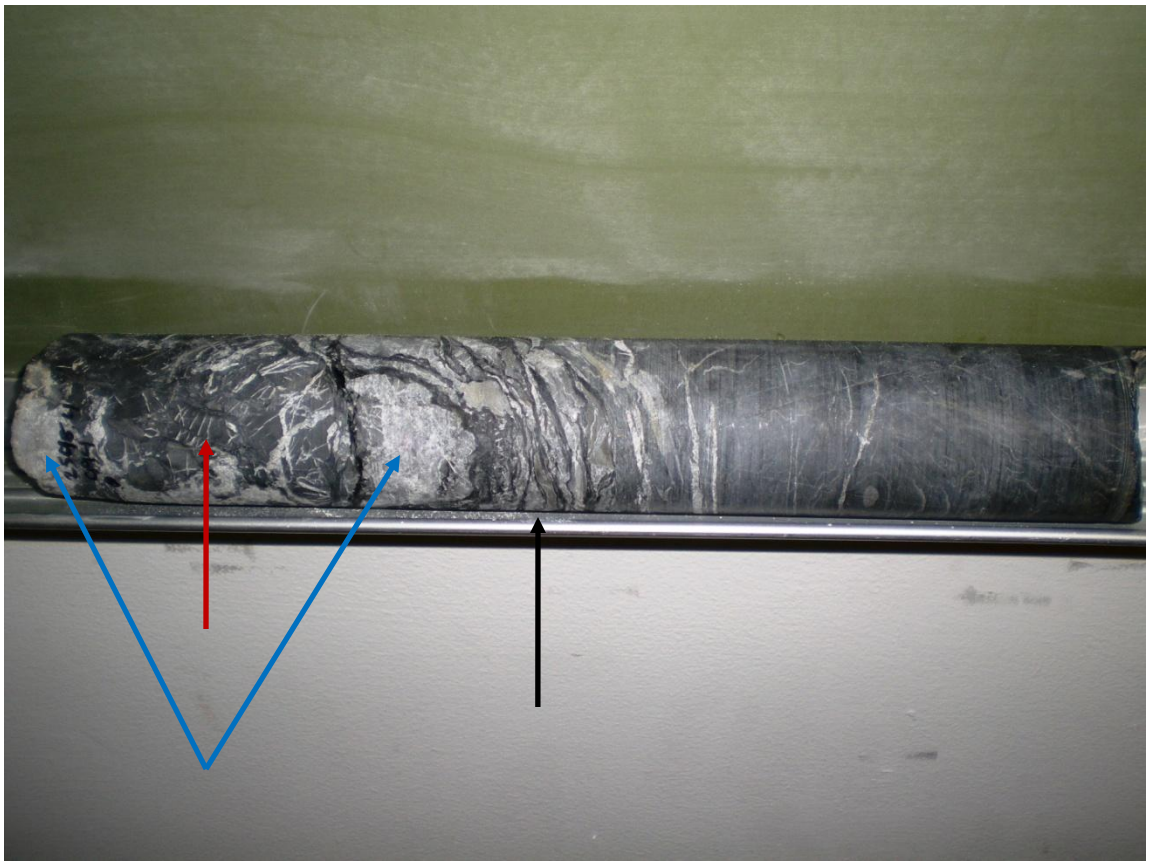

Figure 7. A sample of an intact contact between the siliceous carbonaceous mudstone clast (left) and the argillaceous mudstone matrix (right) in drill hole 95-094 2538'. At the contact there is a layer of limestones and carbon-rich mudstones foliated parallel to the contact (black arrow). Moving further into the siliceous carbonaceous clast there is an non-oriented broken jumble of clasts of siliceous carbonaceous mudstones and limestones (red arrow) in a matrix of coarse open space filling crystalline calcite (blue arrows). Moving further into the clast bedding becomes regular by 2558' (not shown). (63.5 mm diameter core)

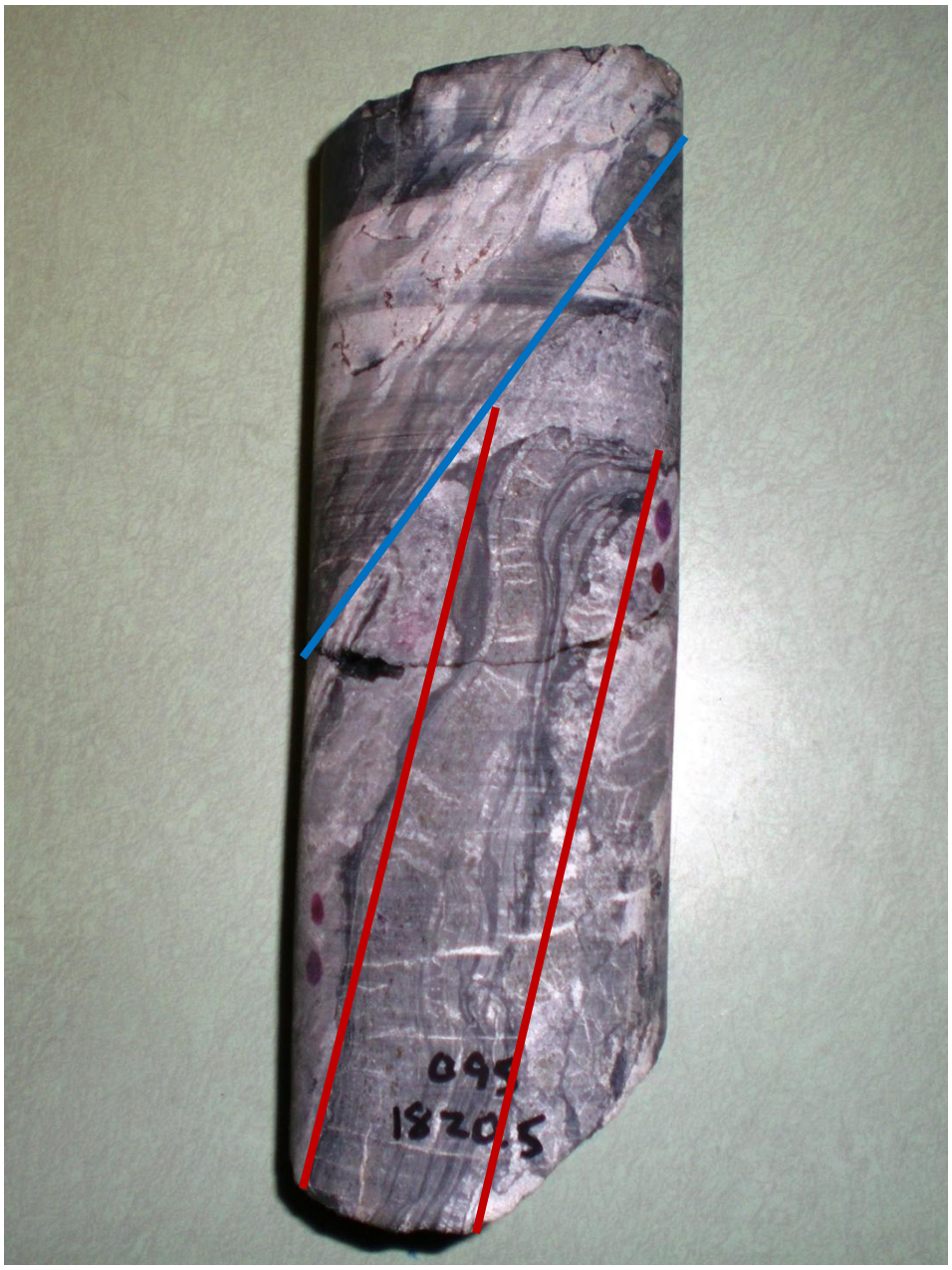

Figure 8. A sample of the contact, 30-40 degrees to core axis, (blue line) between argillaceous mudstone with calc-silicate altered limestone fragments (above) and a small clast (1.1’ interval) of non calc-silicate altered limestone and siliceous carbonaceous mudstone (below). One limestone bed (red lines) bounded by thin inter-beds of siliceous carbonaceous mudstone, 10 degrees to core axis, terminates into the contact between the lithologies (63.5 mm diameter core).

Figure 9. A section of siliceous carbonaceous mudstone with inter-beds of limestone turbidites. The limestones in the section locally have some alteration to calc-silicate minerals (red arrows) which is common in the upper intercepts of the siliceous carbonaceous mudstones in Cross Section B (63.5 mm diameter core).

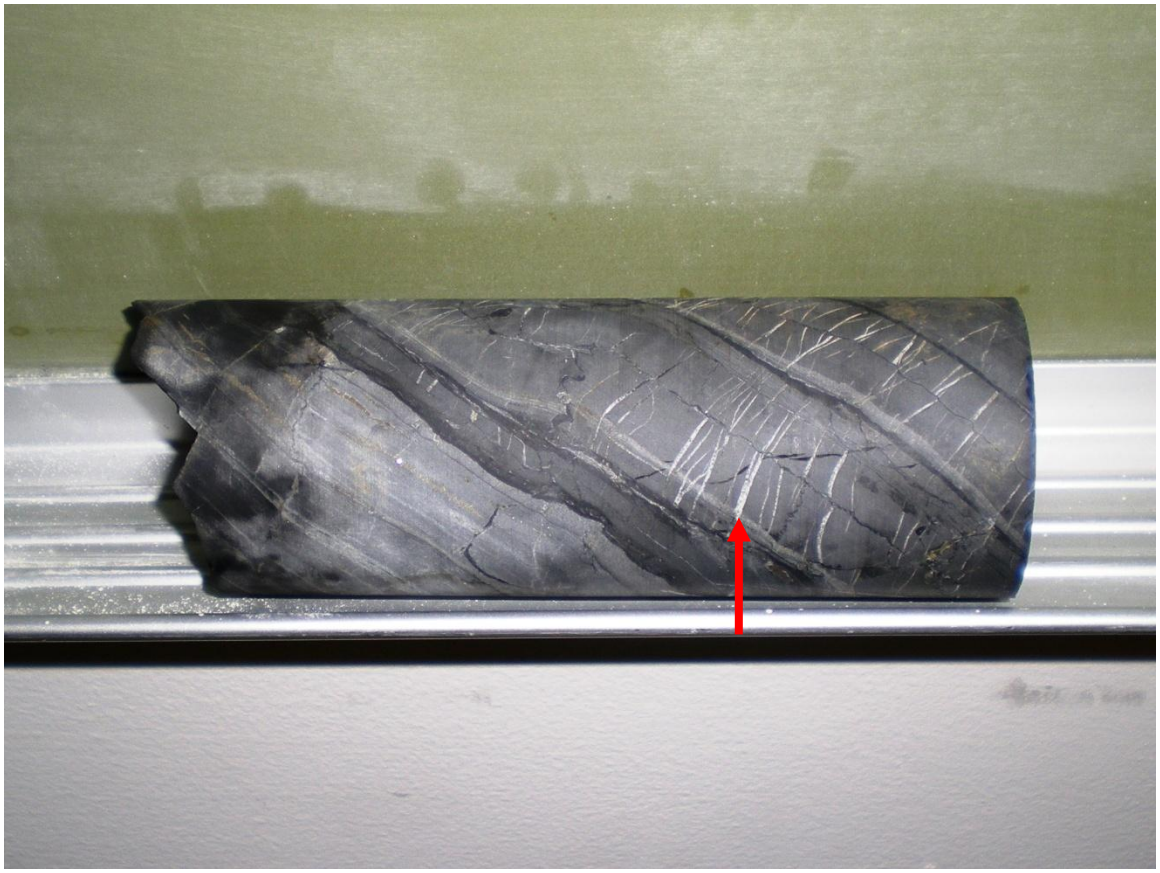

Figure 10. A sample of siliceous carbonaceous mudstone with well developed calcite fractures perpendicular, and restricted, to individual mudstone beds. Beds are bounded by thin carbon rich mudstone inter-beds at which the calcite filled fractures end. Locally the carbon-rich mudstone fills portions of the fractures suggesting that it remained ductile while the siliceous mudstones broke in a brittle manner (63.5 mm diameter core).

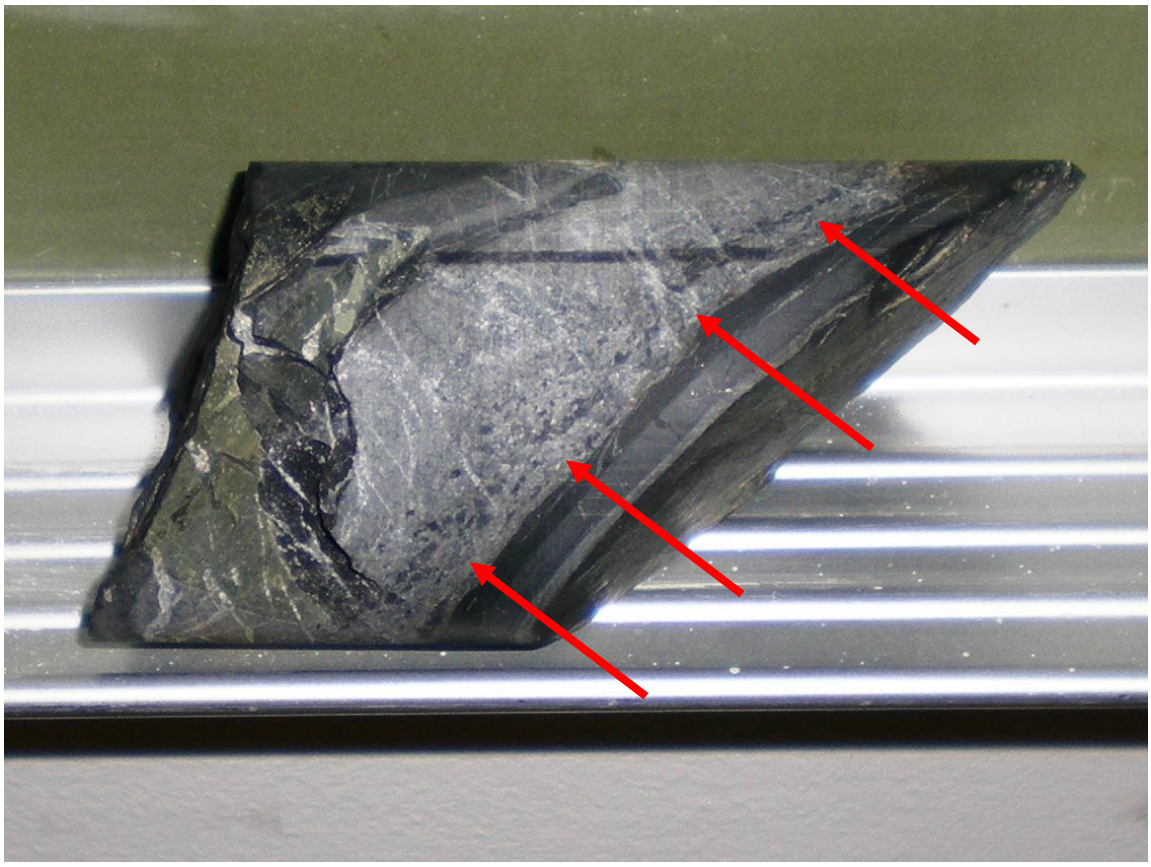

Figure 11. A sample of limestone turbidite (gray bed) with a basal conglomerate of rip-ups from the underlying siliceous carbonaceous bed (red arrows). The bed pictured is over-turned, however, other beds in the same drill core have normal bedding indicators. It is unclear if this is a result of internal folding of the clast or whether the clast is over-turned (63.5 mm diameter core).

Figure 12. A sample of core from a limestone (left, lighter grey) inter-bedded with thin carbon rich calcareous mudstone beds (right, darker grey). Note the calcite veins are bounded by these carbon rich inter-beds. Also note the injection of the carbon rich mudstone into the void later filled with calcite (orange arrow) (63.5 mm diameter core).

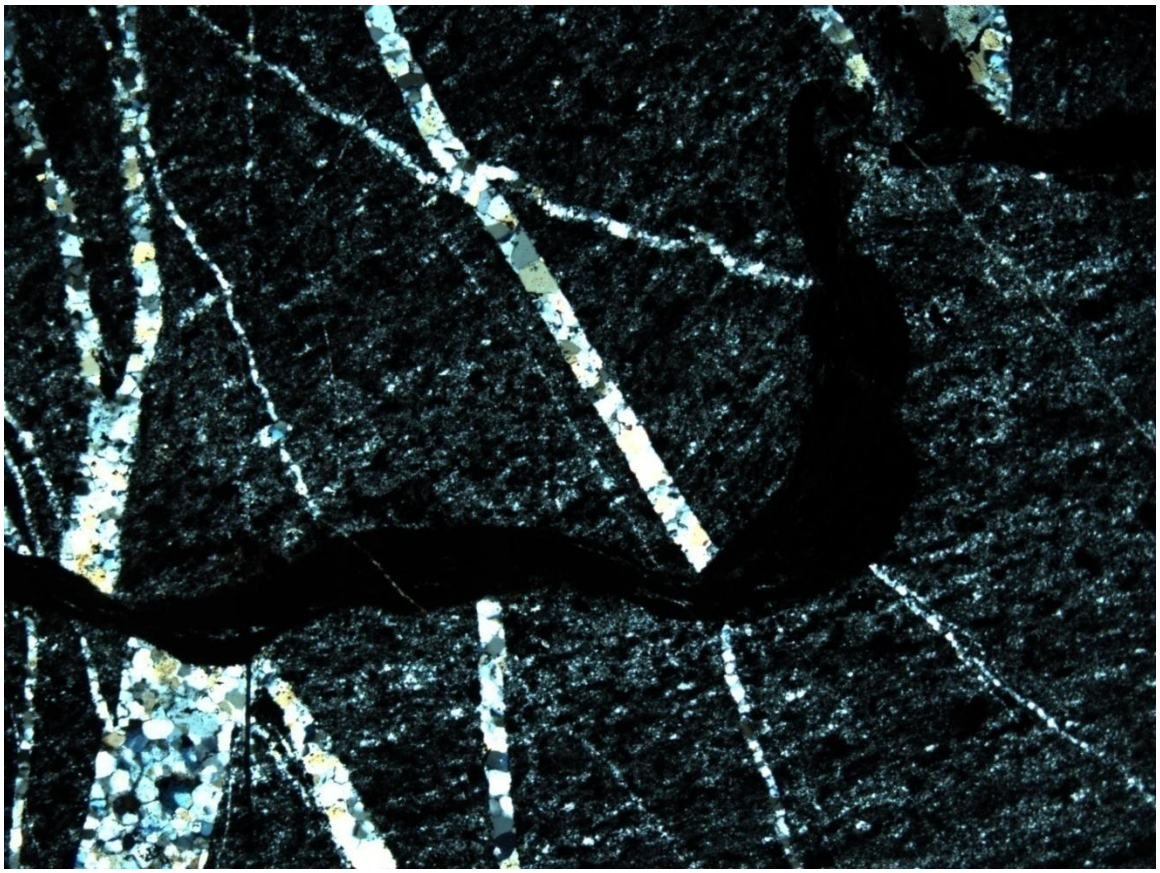

Figure 13. A photomicrograph of a sample of siliceous carbonaceous mudstone from the lower potions of the debris flow (95-088-1627 crossed polars at 40x, field of view 0.25 mm). The sample is cut by several bedding perpendicular quartz replaced calcite veinlets which terminate at a carbon rich mudstone bed, the opaque horizontal feature. The sample is from the margins of a mineralized area and the former calcite veins that have been decalcified and replaced with quartz.

Figure 14. Samples, spanning 150 feet of core, composed of siliceous carbonaceous mudstone inter-bedded with limestone from one interval in core representing one clast. Bedding angles vary from near perpendicular to near parallel to core axis. This change in bedding orientation is likely due to folding within the clast of siliceous carbonaceous mudstone. Changes in bedding orientation may vary from clast to clast but also may be variable within one clast (63.5 mm diameter core).

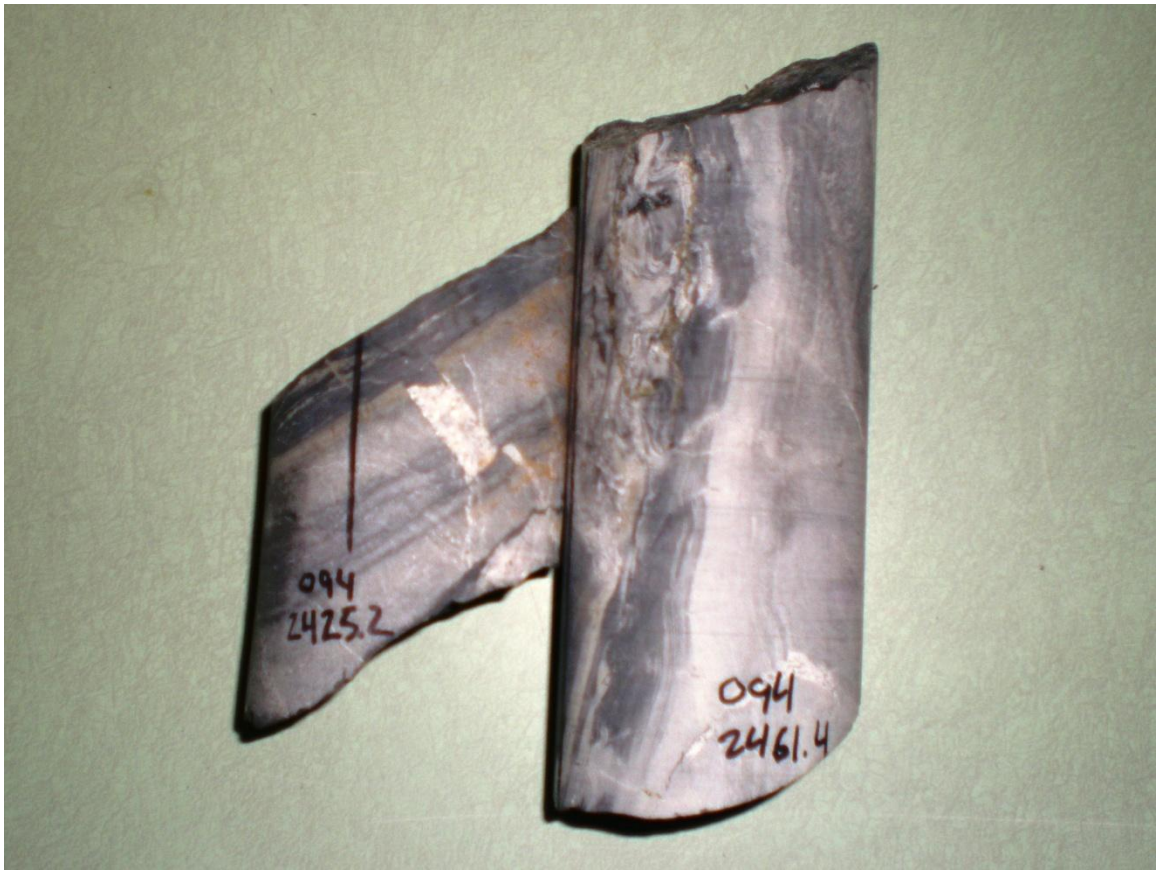

Figure 15. Two samples of the siliceous carbonaceous mudstone inter-bedded with limestone from two separate intercepts of the lithology separated by a 15’ interval of argillaceous mudstone matrix. In this case the clasts appear to have very different bedding orientations 60-70 degrees to core axis on the left 0-10 degrees on the right (63.5 mm diameter core).

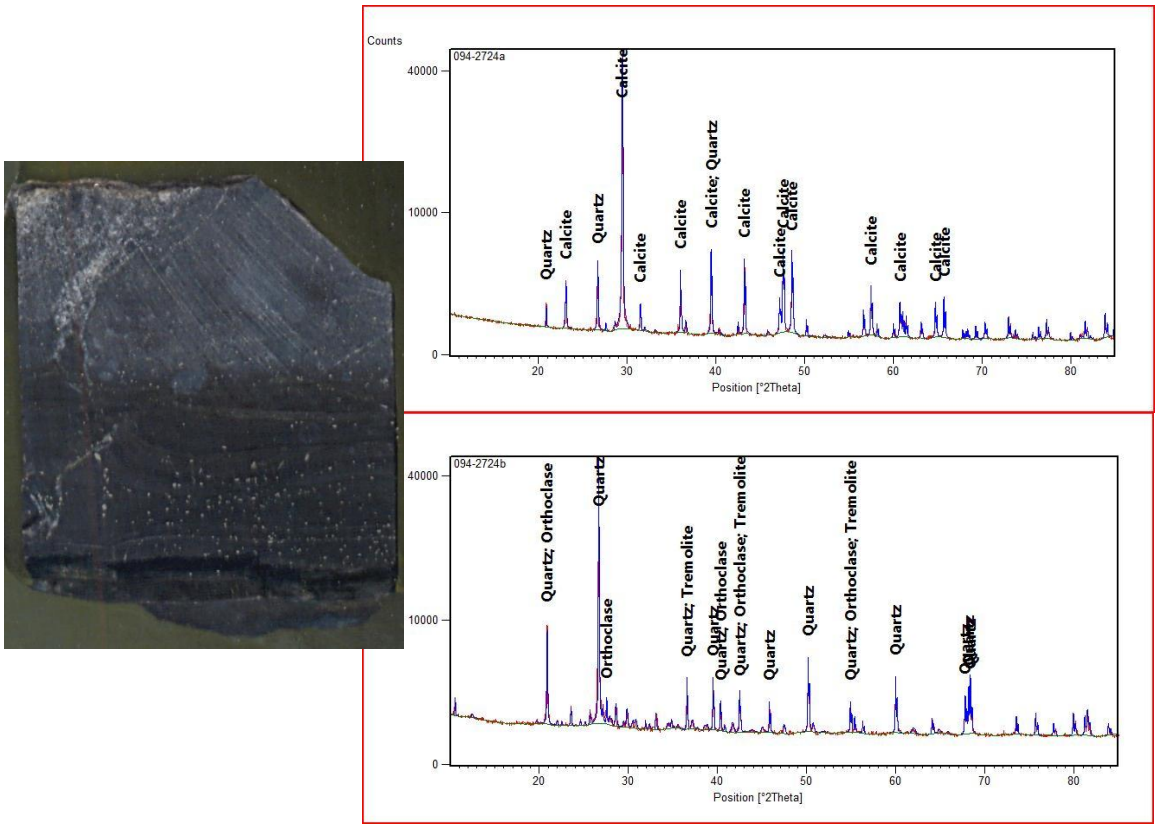

Figure 16. A sample of the contact between a siliceous carbonaceous mudstone bed and an overlying limestone turbidite. Samples were taken from each component and analyzed via XRD. The limestone turbidite is dominantly calcite with no calc-silicate minerals present. A minor quartz signature confirms observations of small quartz grains in the limestone and possibly some material incorporated into the turbidite from the underlying siliceous mud. The lower spectrum is from the siliceous carbonaceous mudstone and shows a dominant signature of quartz with lesser orthoclase, tremolite, and pyrite. Diagenetic pyrite is visible as the small brassy spots in the mudstone bed in the photo above.

Figure 17. A section of argillaceous mudstone with weak metamorphism to fine grained biotite hornfels resulting in the maroon brown color that is common in the argillaceous mudstones in the study area. The mudstone is thinly bedded in this section but is often massive to locally chaotically bedded due to soft-sediment deformation elsewhere (63.5 mm diameter core).

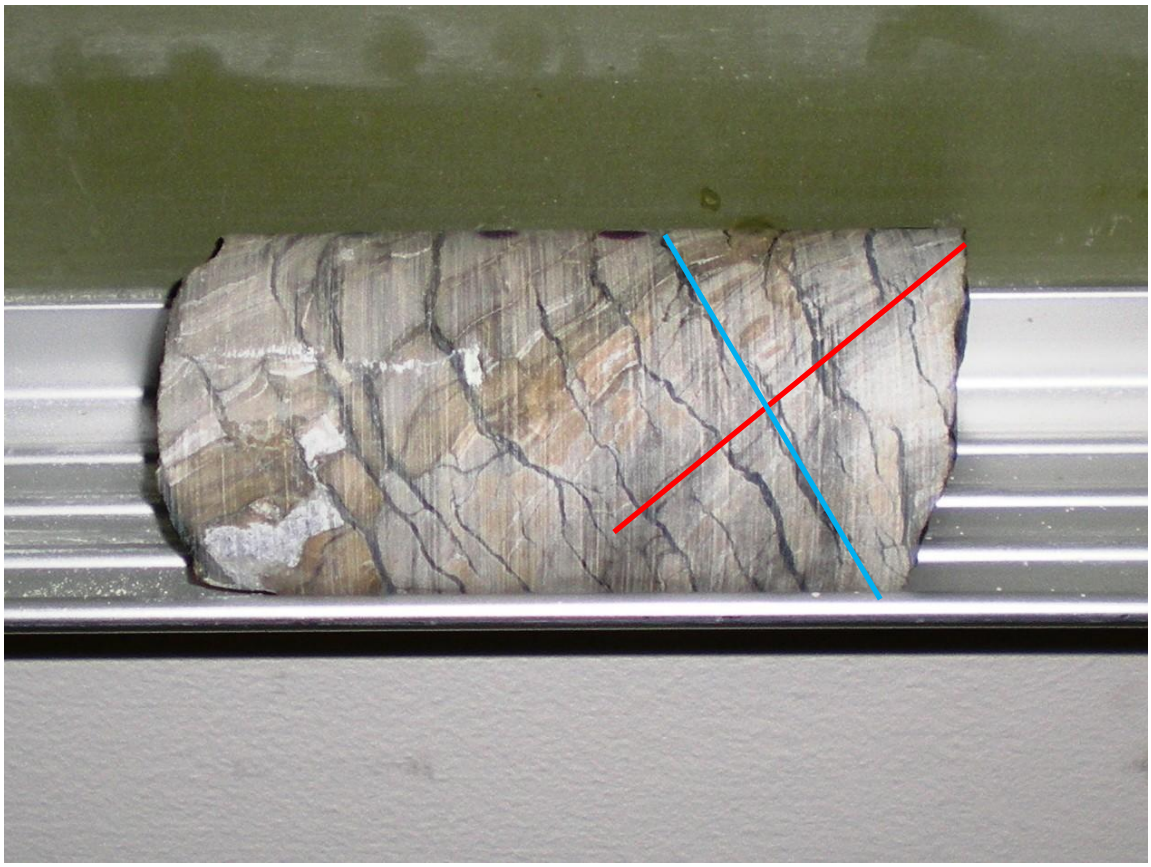

Figure 18. A sample of argillaceous limestone, locally known as the Powder Hill Limestone with weak calc-silicate alteration. The bedding (red line) is cut by a later well developed cleavage fabric (blue line) which is common in this unit. The cleavage planes cause minor offset in the limestone beds (63.5 mm diameter core).

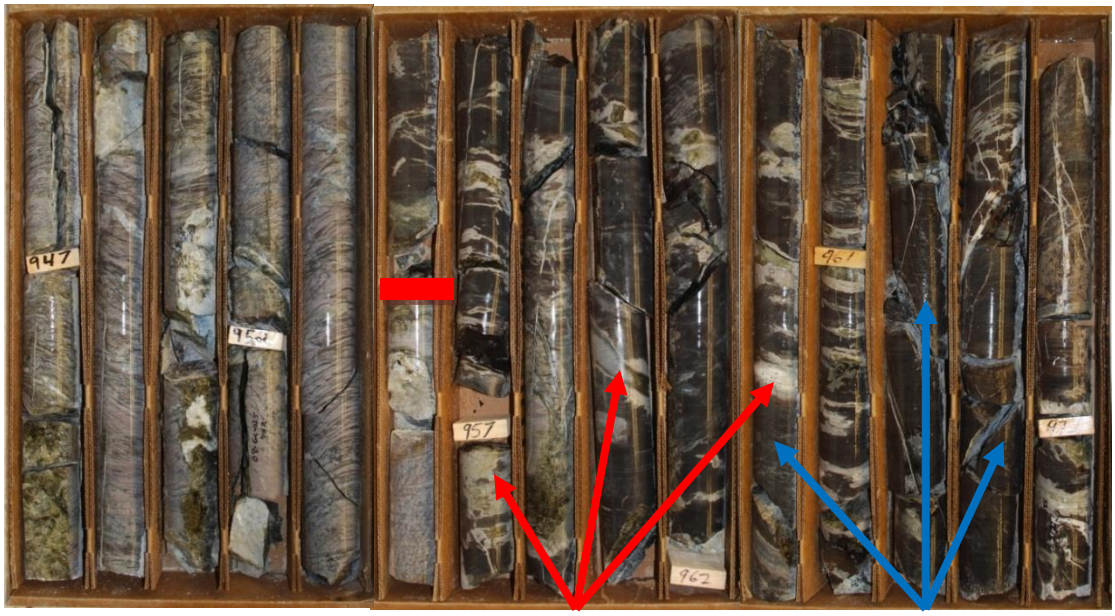

Limestone **Limestone Clasts** **Mudstone Matrix**

(Pink/Grey) (Grey/White) (Brown/Dark-gray)

Drill hole 08-GC-035 from 946’ to 973’ moving down-hole left to right

Figure 19. A section of limestone with thin argillaceous mudstone inter-beds, and weak calc-silicate alteration ending ~955’. At 955’ (red bar) there is a transition to dominantly argillaceous mudstone (blue arrows) with clasts of calc-silicate altered limestone (red arrows), interpreted as being ripped up from the larger dominantly limestone section 912’-955’ (63.5 mm diameter core).

Figure 20. A section of the upper siliceous carbonaceous mudstone unit. The unit is thinly bedded, < 1 cm thick, and commonly contains abundant pyrite. The unit forms a continuous layer just below the upper basalt in both Cross Sections. Locally the unit contains inter-beds of hyaloclastite (63.5 mm diameter core).

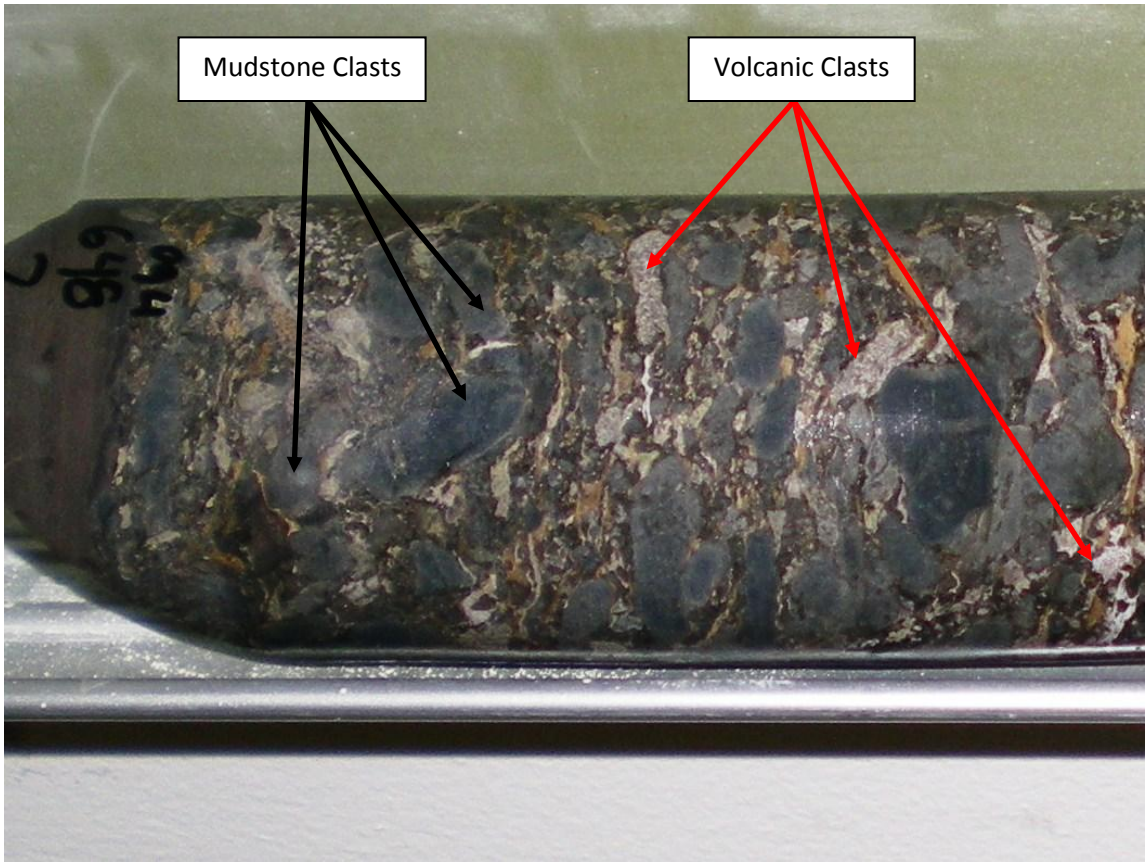

Figure 21. A 1 foot thick conglomeratic bed of hyaloclastite/scoria (red arrows) and rounded clasts of the upper siliceous carbonaceous mudstone (black arrows). The bed is located in the upper siliceous carbonaceous mudstone ~150 feet below the basalt mudstone contact. (63.5 mm diameter core)

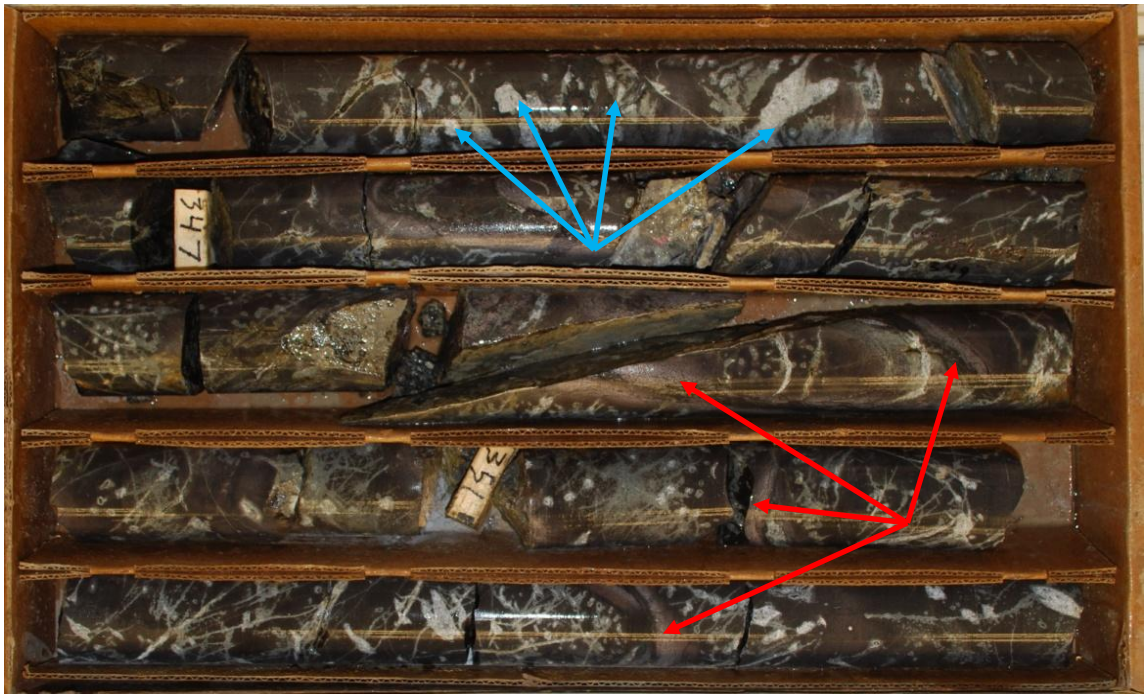

Figure 22. A section of vesiculated Upper Basalt which caps the stratigraphy in the study area. The vesicles have been filled with calcite (blue arrows). Several pillow margins are also visible (red arrows) (63.5 mm diameter core).

Figure 23. A contact (red line) between a section of argillaceous mudstone inter-bedded with limestone (above) with a diabase dike (below). The diabase is very fine grained and dark gray to green in color (63.5 mm diameter core).

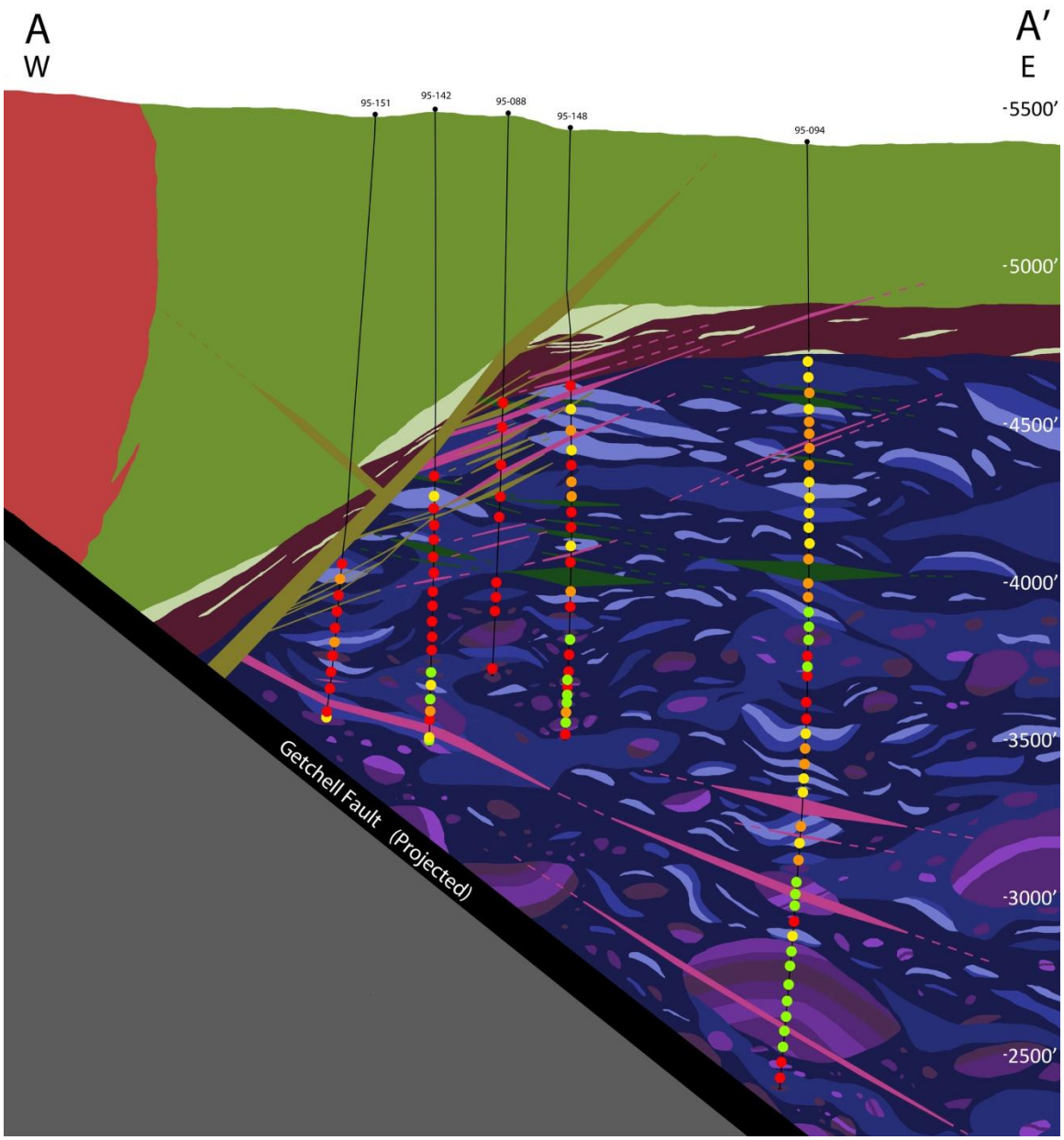

Figure 24. A diagram showing the intensity of calc-silicate alteration observed in drill cores along Cross Section A. Green dots represent limestone with no visible calc-silicate alteration. Yellow represent areas of limestone with minor calc-silicate alteration (<25% of limestone altered to calc-silicates). Orange represent areas of limestone with moderate calc-silicate alteration (25%-75% of limestone altered to calc-silicates). Red representing areas of limestone with strong calc-silicate alteration (>75% of limestone altered to calc-silicates) (no vertical exaggeration).

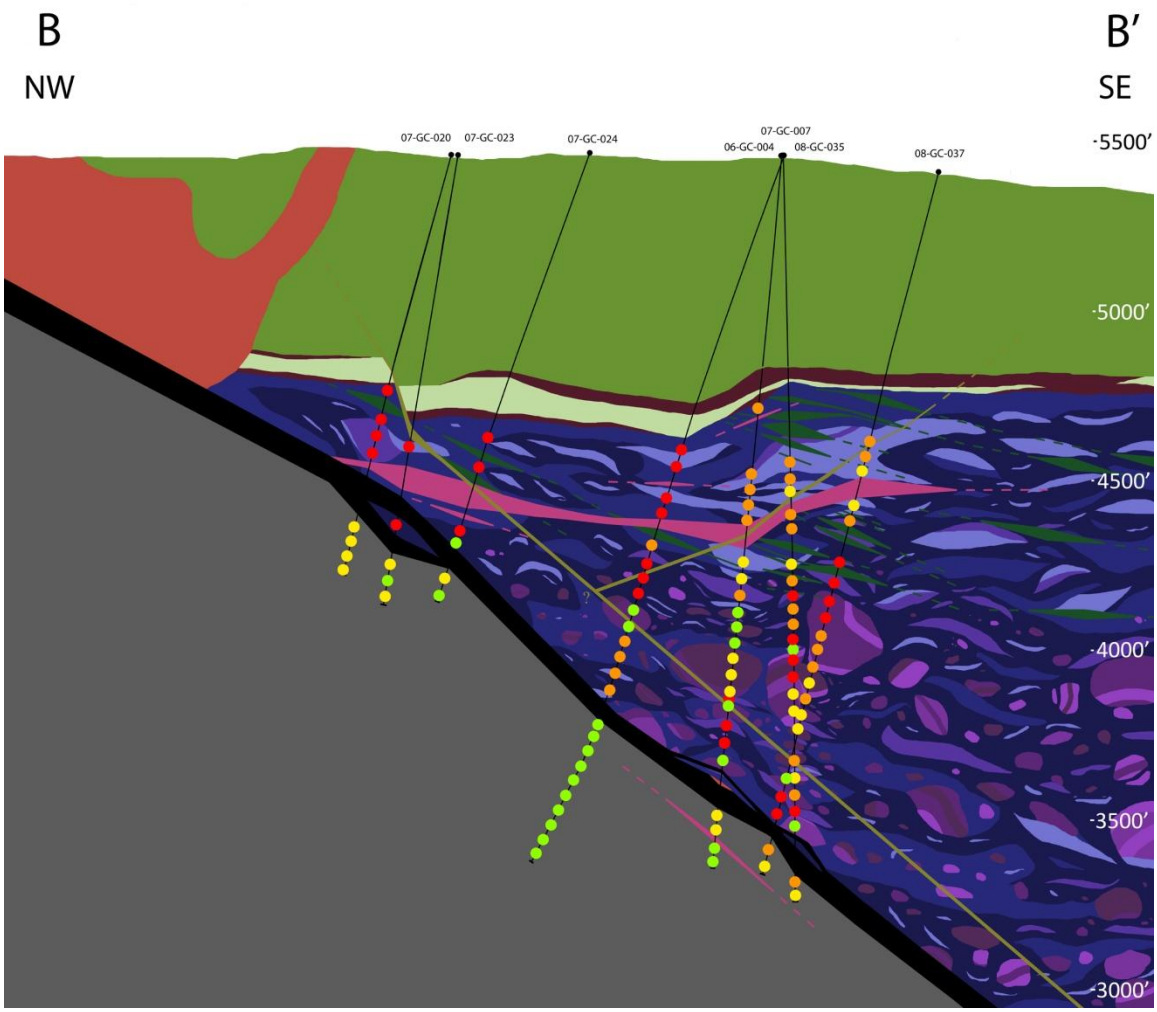

Figure 25. A diagram showing the intensity of calc-silicate alteration observed in drill cores along Cross Section B. Green dots represent limestone with no visible calc-silicate alteration. Yellow represent areas of limestone with minor calc-silicate alteration (<25% of limestone altered to calc-silicates). Orange represent areas of limestone with moderate calc-silicate alteration (25%-75% of limestone altered to calc-silicates). Red representing areas of limestone with strong calc-silicate alteration (>75% of limestone altered to calc-silicates) (no vertical exaggeration).

Figure 26. A small clast of limestone inter-bedded with siliceous carbonaceous mudstone (1311'-1317' between red lines) in a matrix of argillaceous mudstone and limestone. The argillaceous mudstone and limestone are strongly calc-silicate altered while the clast composed of the limestone inter-bedded with the siliceous carbonaceous mudstone is not (63.5 mm diameter core).

Figure 27. A sample of calc-silicate altered limestone inter-bedded with siliceous carbonaceous mudstone. The dominant calc-silicate mineral is wollastonite (white/gray) with minor amounts of vesuvianite (brown). The siliceous carbonaceous mudstone bed adjacent to the calc-silicate altered limestone bed (right of blue line) has been bleached (red arrow) (63.5 mm diameter core).

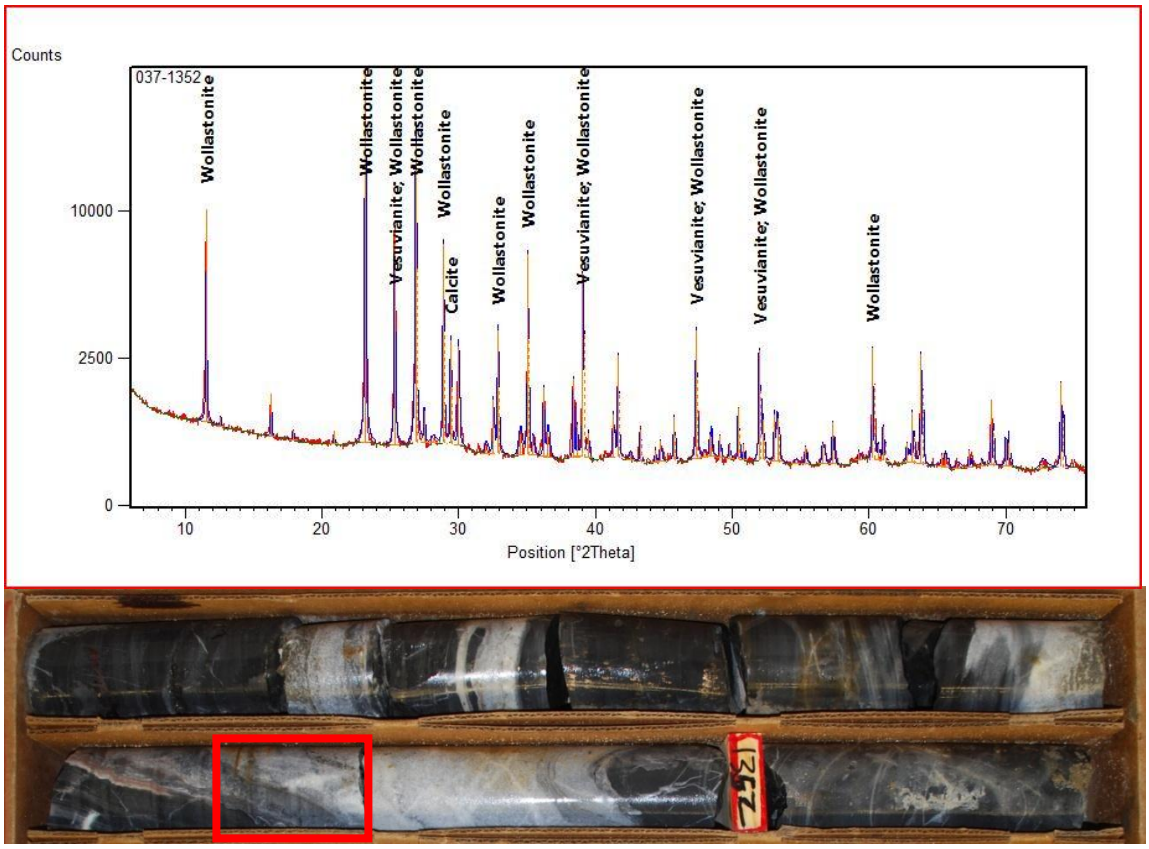

Figure 28. A section of calc-silicate altered siliceous carbonaceous mudstone with inter-bedded limestone. The limestone bed has been altered to dominantly wollastonite, with local minor vesuvianite and minor remaining calcite. This section of calc-silicate alteration is located above the mineralized zone in the northwest-southeast Cross Section. Sample is from a five-foot section that grades 0.0004 oz/t Au (63.5 mm diameter core).

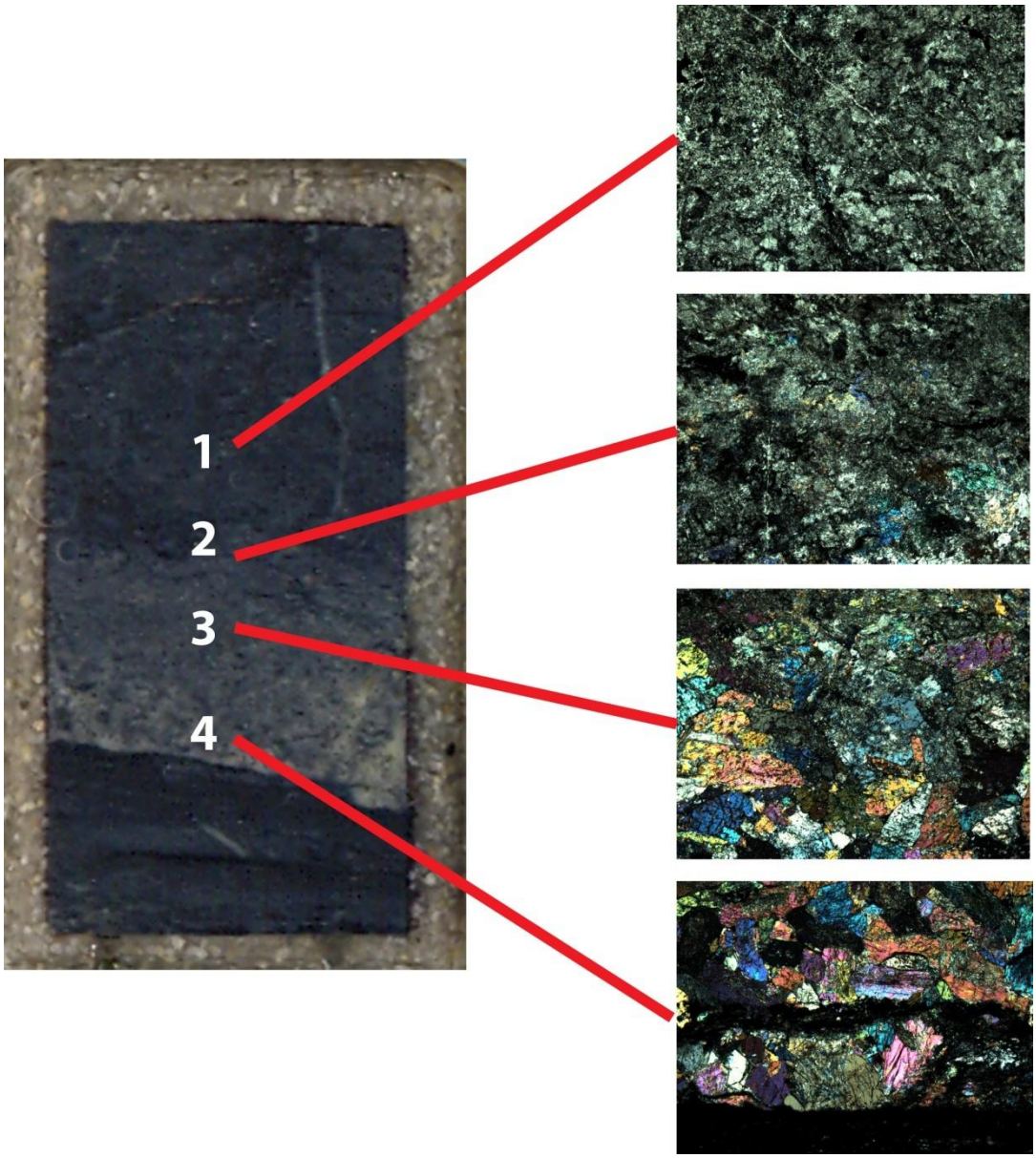

Figure 29. Thin section photomicrograph showing change in calc-silicate alteration extending from strongly calc-silicate (denoted by 2nd order colors in cross polarized light) altered limestone near the limestone siliceous mudstone contact to unaltered, locally recrystallized limestone near the center of the bed. Photomicrograph taken at 40x in cross polarized light, field of view is 0.25 mm.

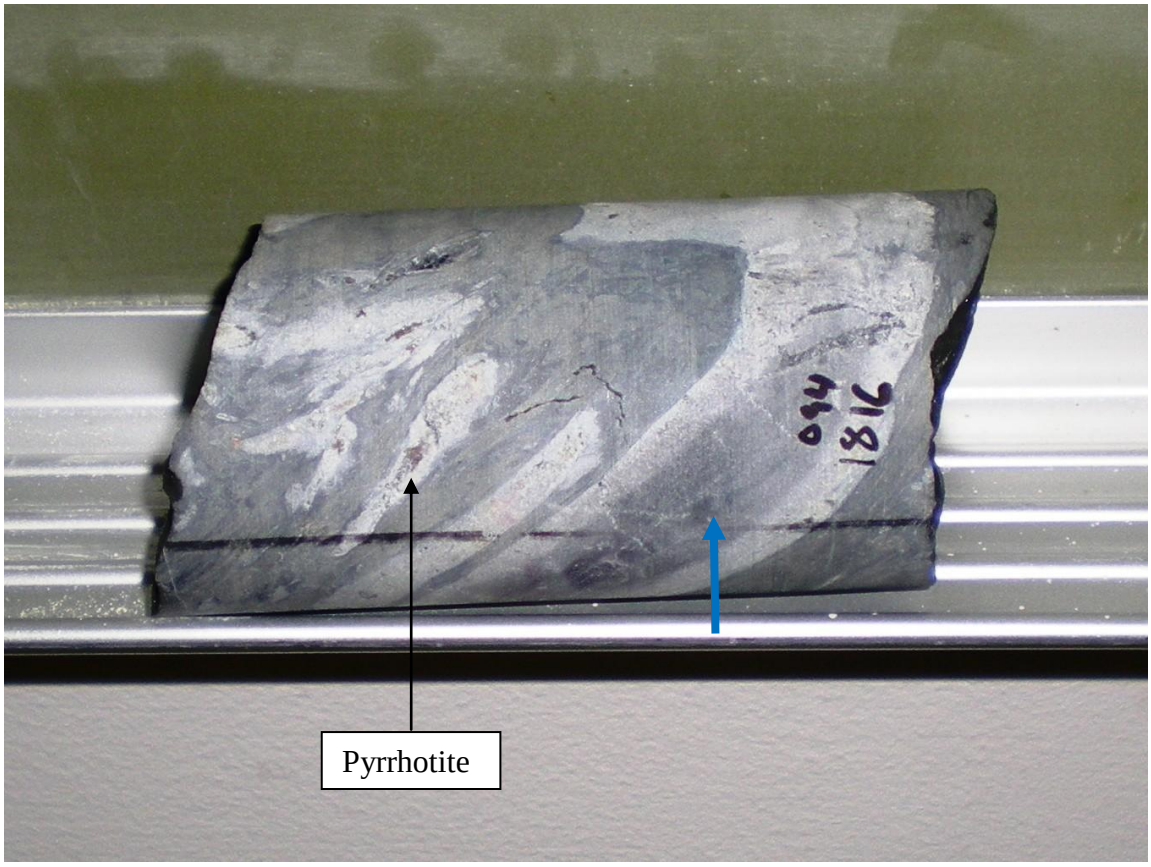

Figure 30. A sample of argillaceous mudstone with fragments of limestone now mostly altered to calc-silicates (off white) with pyrrhotite (bronze). As is common the smaller fragments are completely altered to calc-silicates while larger clast still has reactive limestone at the center (blue arrow) rimmed by a mantle of calc-silicates (63.5 mm diameter core).

Figure 31. A typical interval through the gouge of the Getchell Fault, with a strongly sheared carbonaceous dark matrix with clasts of limestone which have often been silicified where the gouge is weakly mineralized as shown above. The fault appears to have incorporated a large amount of footwall carbonaceous material. This section grades from 0.0335 to 0.0540 oz/t Au which is typical for the Getchell fault gouge where encountered in the study area (63.5 mm diameter core).

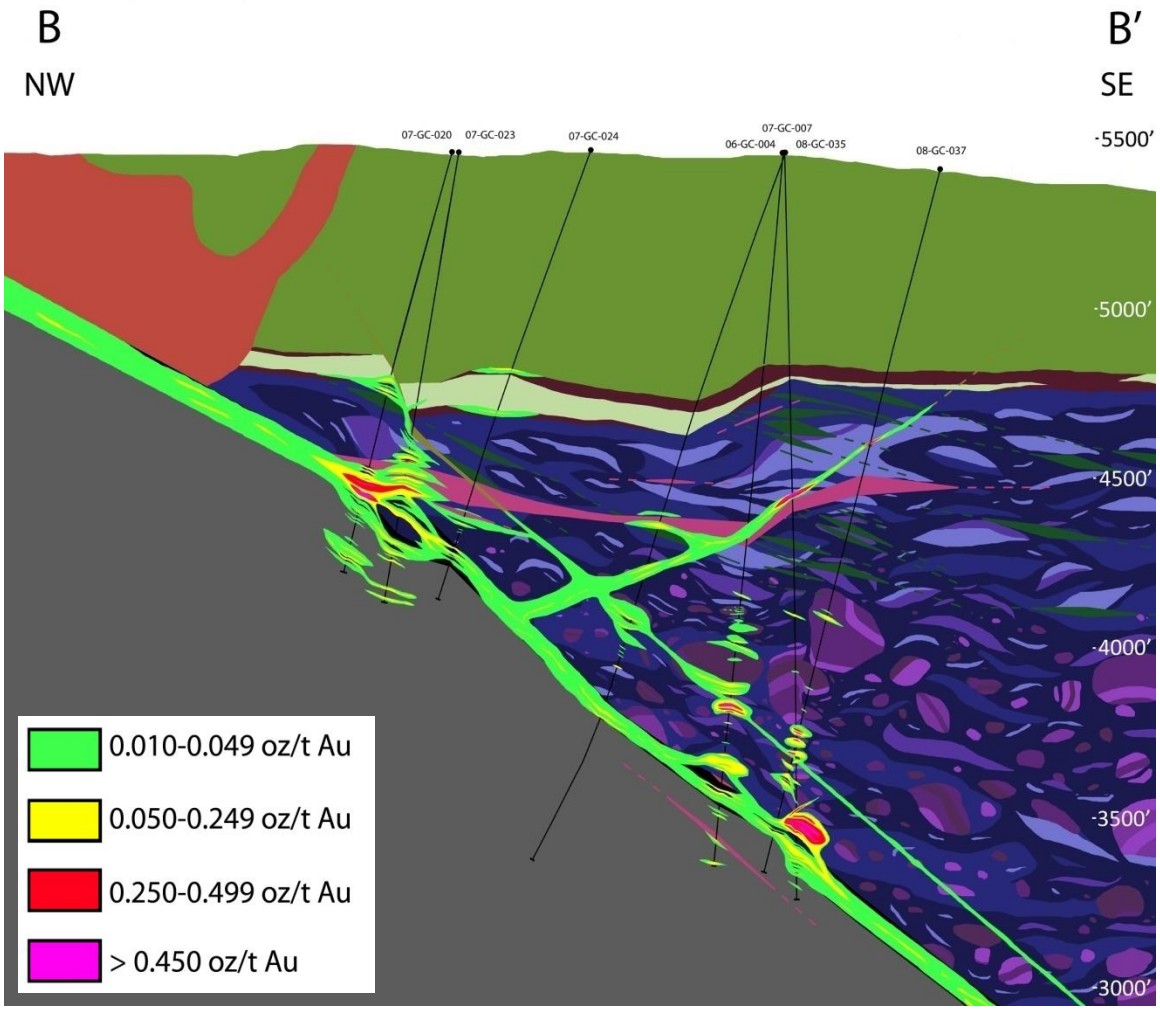

Figure 32. Hand drawn ore grade contours overlain on Cross Section B. Weak to moderate mineralization is common along and within the Getchell fault gouge. Where limestones inter-bedded with siliceous carbonaceous mudstones are in contact with the Getchell fault there is typically higher-grade mineralization. Other areas of higher grade mineralization are centered on heavily structurally disturbed zones such as the jog in the Getchell fault. Mineralization is also present along a Getchell parallel fault in the hanging wall 100-200 feet above the Getchell fault. A narrow, often high grade, zone of strongly fault controlled mineralization occurs along a west dipping hanging wall structure (no vertical exaggeration).

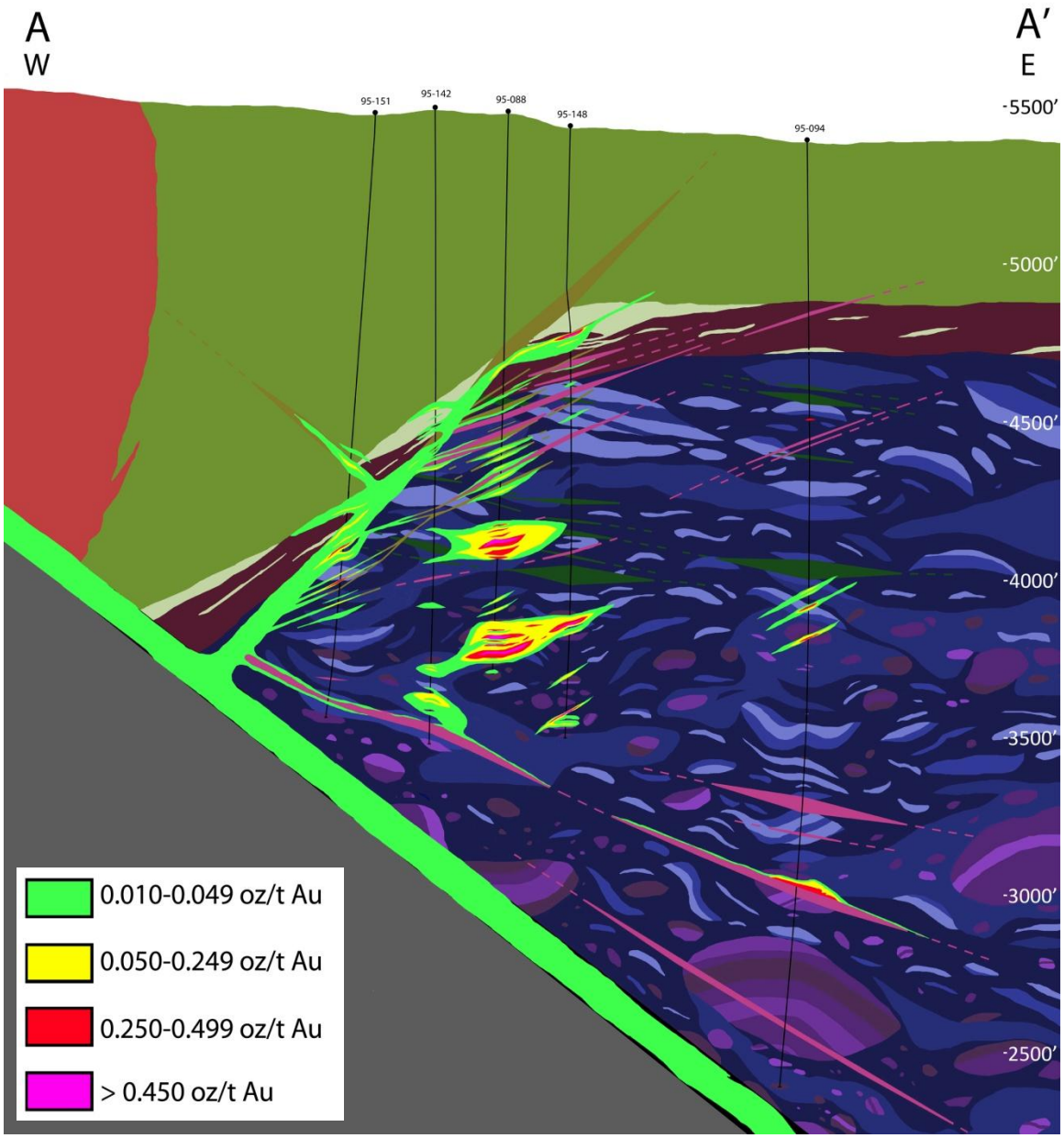

Figure 33. Hand drawn ore grade contours overlain on Cross Section A. Low grade mineralization along the Getchell fault is inferred to be similar to what is observed in Cross Section B as no drill hole in Cross Section A reached the Getchell fault. Controls on mineralization in Cross Section B are not as clear as the controls in Cross Section A. Mineralization along the west dipping fault in the hanging wall is typically low grade and confined to gouge. Mineralization is also channeled along a Getchell parallel dacite dike, expanding in areas of receptive host rock. The controls on the two most prominent areas of mineralization in Cross Section A are unclear, possibly related to some structure out of plane of the cross section (no vertical exaggeration).

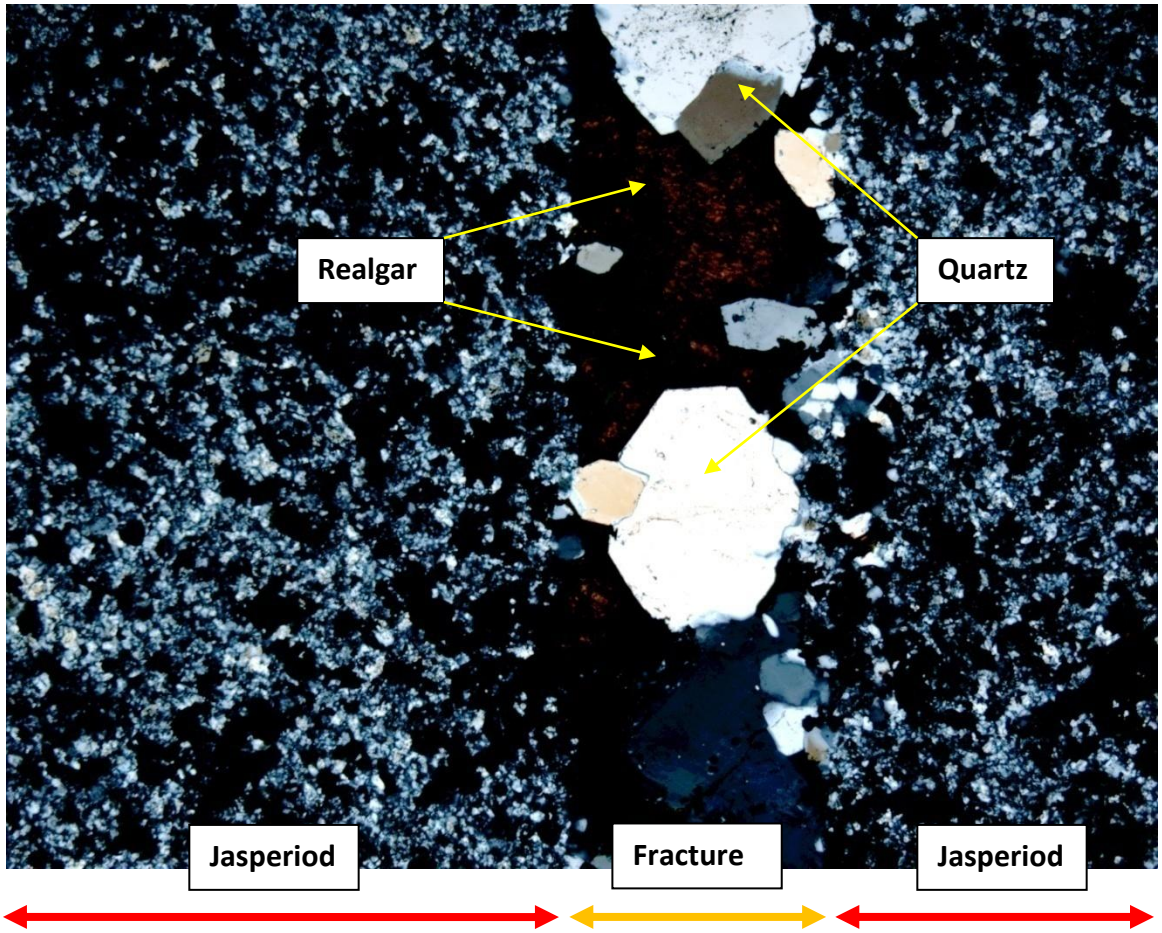

Figure 34. A photomicrograph of decalcified and silicified limestone from sample 088-1620 taken with crossed polars at 80x (0.125 mm field of view). Limestone (red arrows) has been replaced by fine grained quartz (grays) and sulfides (black). A late fracture (orange arrows) cuts through the sample and is incompletely filled with late euhedral coarser grained quartz and later realgar. Sample is from a section averaging 0.091 oz/t Au.

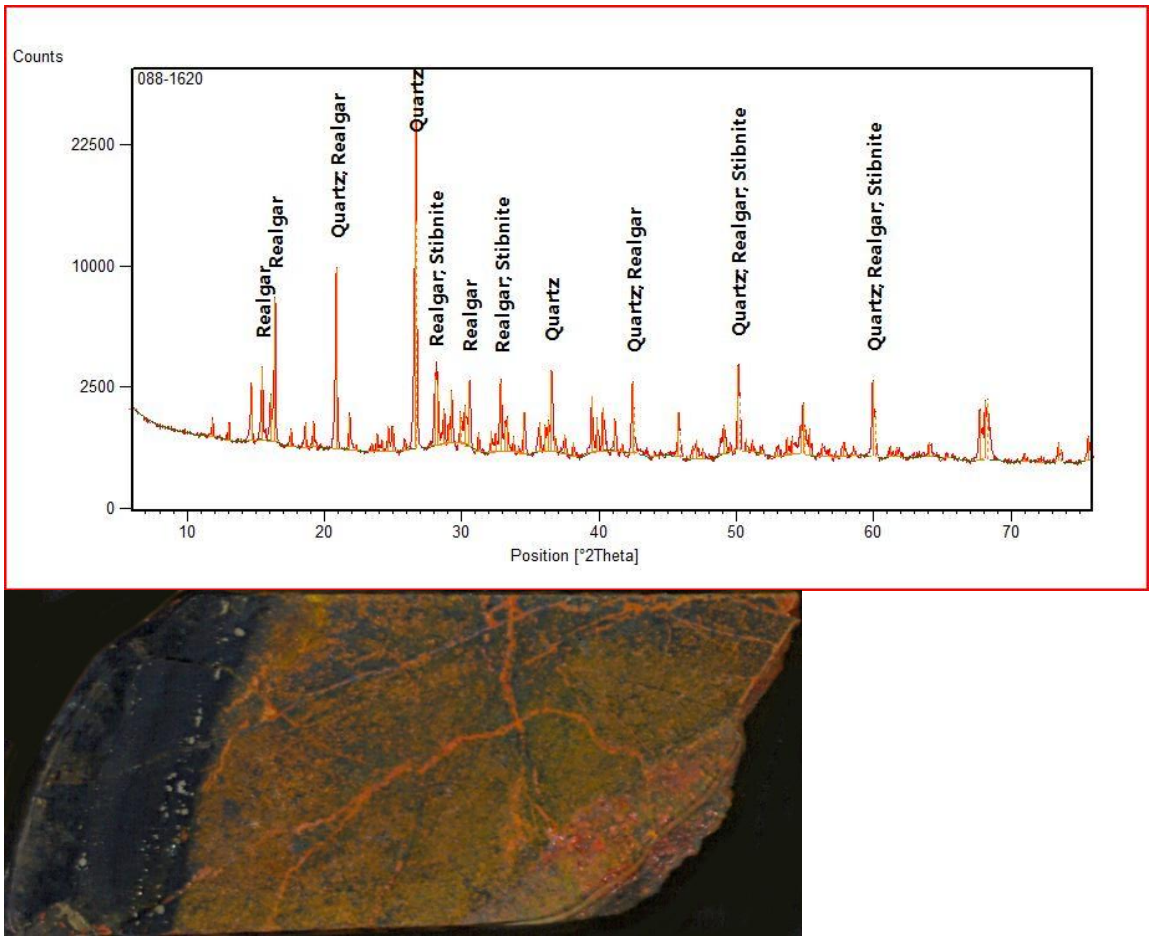

Figure 35. A sample (088-1620) of mineralized limestone (right) inter-bedded with siliceous carbonaceous mudstones (left). Sample has been completely decalcified and silicified by Carlin ore fluids with abundant late realgar (orange) and lesser stibnite (silver/gray) filling void space. The sample taken for the XRD spectra comes from the altered limestone (left) and shows the sample is dominantly quartz, 76%, with lesser realgar, 21%, and stibnite, 2%. Abundant realgar does not necessarily correlate to higher gold grade; this sample is from a section averaging 0.091 oz/t. The sample pictured is 1″ by 2“.

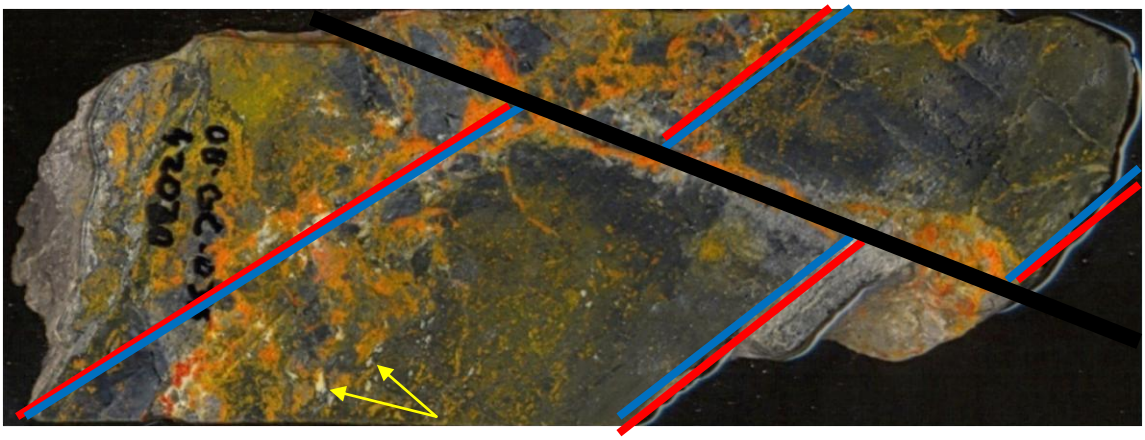

Figure 36. A sample of mineralized siliceous carbonaceous mudstone (outside redlines) with a limestone inter-bed (between blue lines) cut and offset by a small fault (black line). The brittle siliceous carbonaceous mudstones have been brecciated and are cemented by realgar. The limestone has been strongly decalcified and silicified with open pore space locally filled with realgar or white/tan clay, kaolinite (yellow arrows) (63.5 mm diameter core).

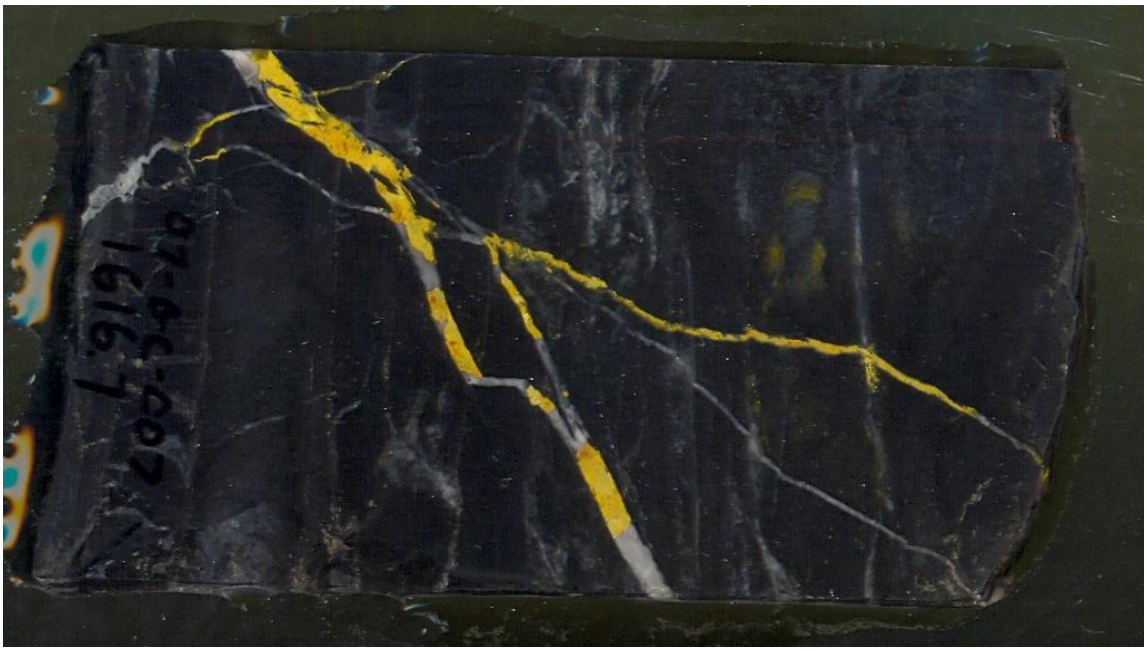

Figure 37. A sample of siliceous carbonaceous mudstone with late veins containing calcite (white) and orpiment (yellow). The sample comes from just above a mineralized zone in drill hole 07-GC-007 associated with the Getchell parallel fault in the hanging wall on Cross Section B.

Figure 38a. A section of core from drill hole 08-GC-035 (1974.5’-2010’). The argillaceous mudstones inter-bedded with limestones from 1974’-1988.8’ are intensely calc-silicate altered and are not mineralized, with the exception of a small fault 1980.3’-1982.7’. At 1988.8’ there is a transition to limestone inter-bedded with siliceous carbonaceous mudstone (63.5 mm diameter core).

Figure 38b. (Continued from 36a) Continuing down-hole the siliceous carbonaceous mudstones inter-bedded with limestones from 1988.8’-2010’ show strong decalcification and silicification indicating these rocks were not calc-silicate altered by the intrusion of the Osgood Stock. These rocks range in grade from 0.200 to 1.000 oz/t Au. The zone continues until it reaches the Getchell Fault at ~2046’ (63.5 mm diameter core).

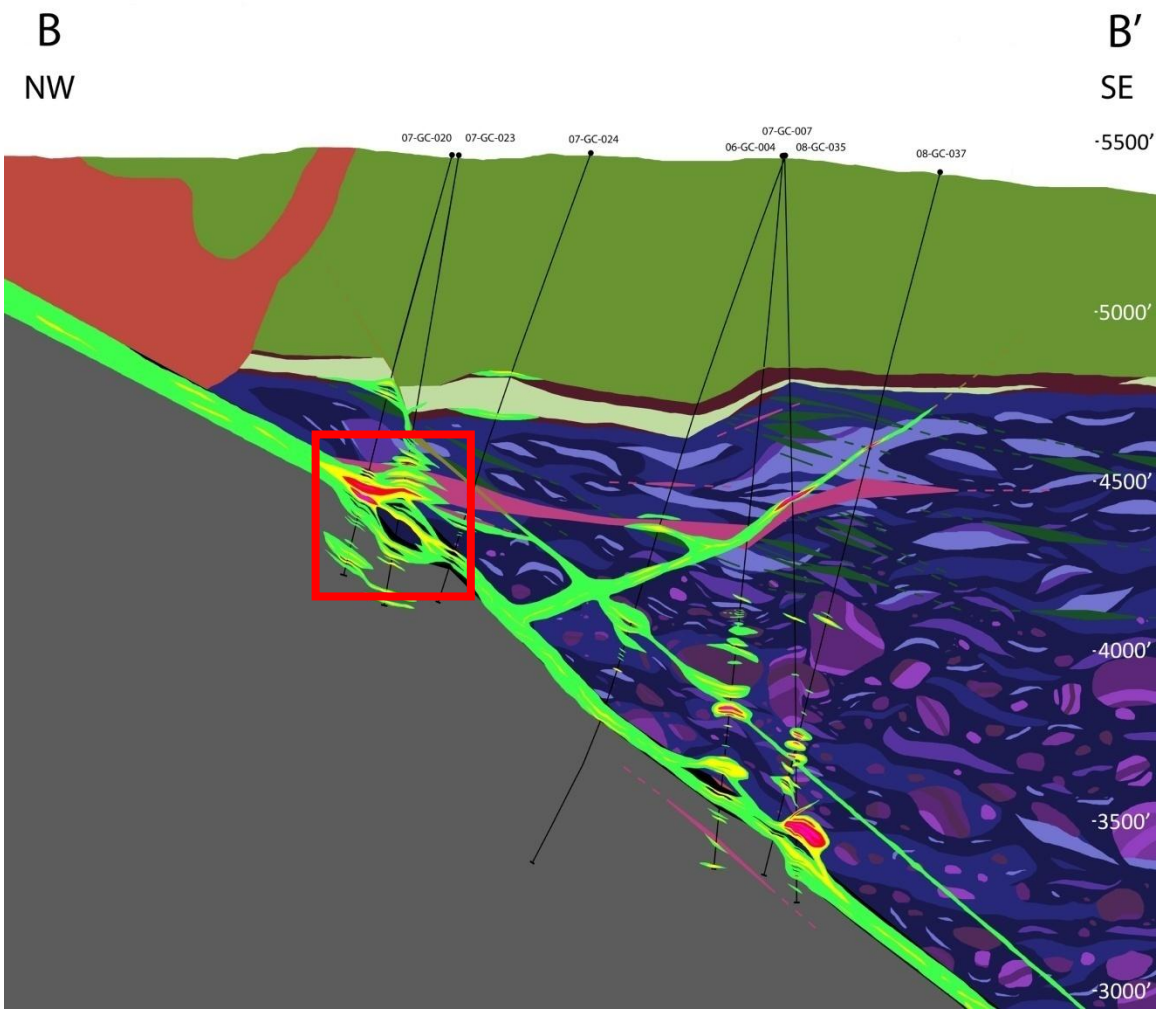

Figure 39. An area of thicker high grade mineralization (red box) in Cross Section B occurs in association with a jog in the Getchell fault which generates a wider zone of broken faulted material (07-GC-020 with 78' @ 0.300 oz/t Au from 1058’ to 1136’) (no vertical exaggeration).

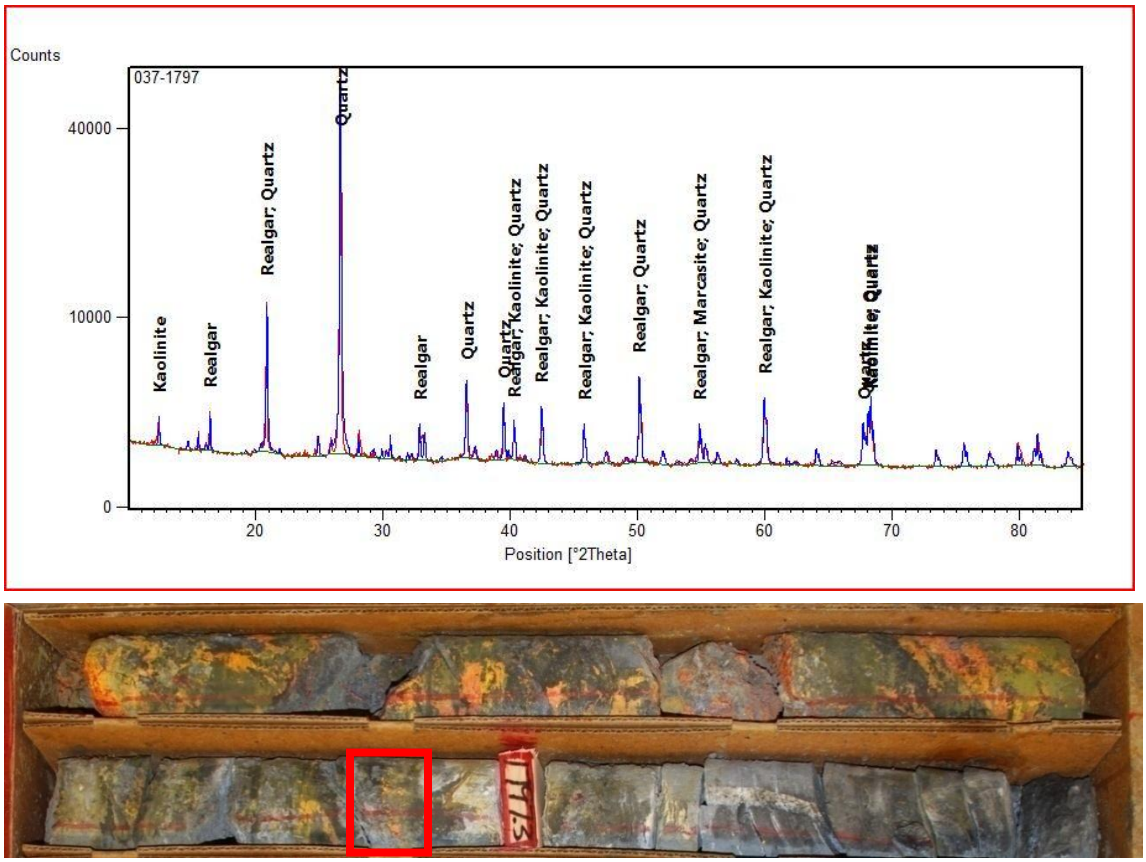

Figure 40. A sample taken from a strongly mineralized section 1795-1798.5 averaging 0.841 oz/t. The original rock was limestone inter-bedded with siliceous carbonaceous mudstone becoming all mudstone after 1797.5 (toward lower right). Limestone has been completely decalcified and silicified and cut by late abundant realgar mineralization. The XRD spectrum from the sample taken from 1797 (red box) shows the sample is dominantly quartz with lesser realgar, kaolinite, and marcasite. Based on the alteration (decalcification and silicification) from the Carlin-type ore fluids the lower portions of Cross Section B were not subject to calc-silicate alteration from the Osgood stock (63.5 mm diameter core).

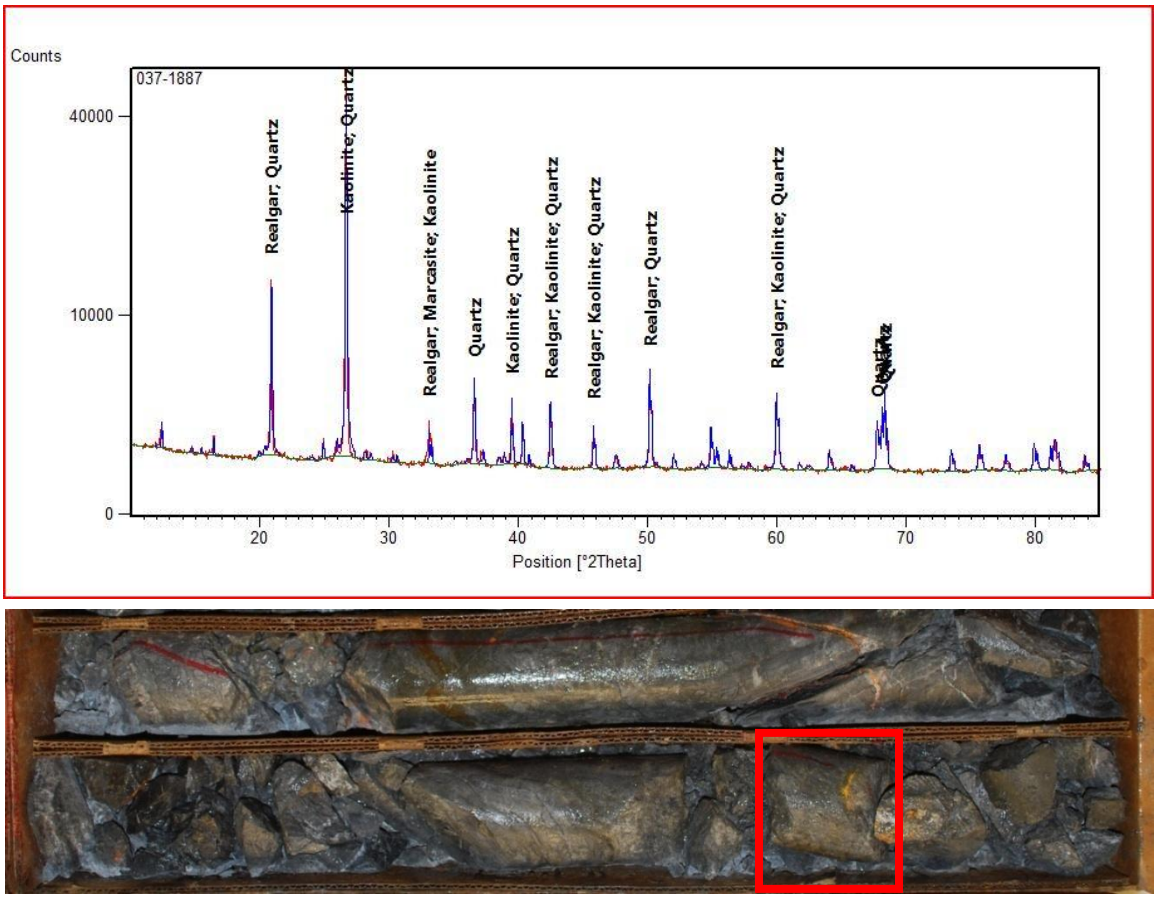

Figure 41. A sample from 1887' (red box) ten feet below the sample above. This sample is from a mineralized five foot section averaging 0.1255 oz/t. The rock is intensely decalcified, and silicified limestone inter-bedded with silicious carbonaceous mudstones with weak realgar mineralization. XRD spectrum indicates that the sample is dominantly quartz with lesser kaolinite, realgar, marcasite and pyrite (63.5 mm diameter core).

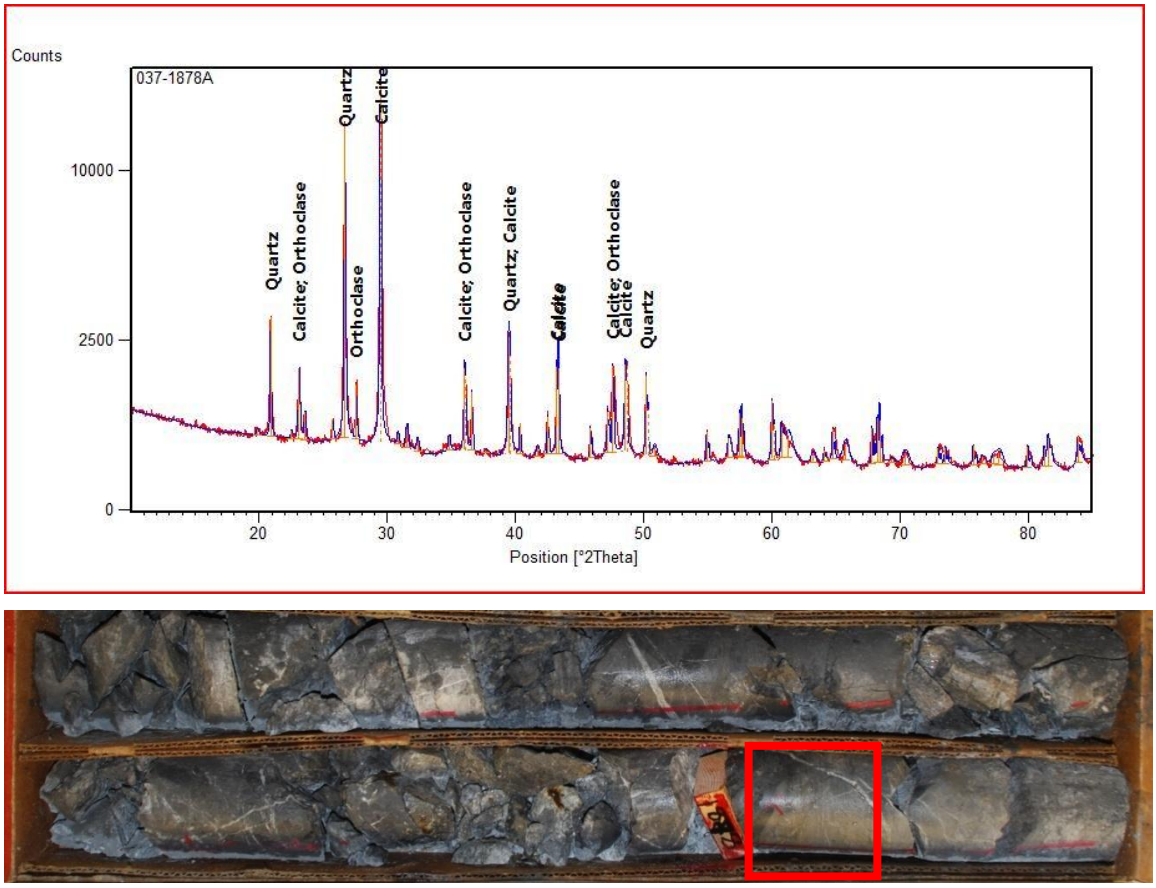

Figure 42. A sample (red box) from a section of weakly silicified limestone with local inter-beds of siliceous carbonaceous mudstone. XRD spectra show the sample is dominantly calcite with moderate quartz. The sample also notably shows an absence of calc-silicate minerals. The section is in a broader area of weak mineralization and the five foot section containing this sample grades 0.0057 oz/t (63.5 mm diameter core).

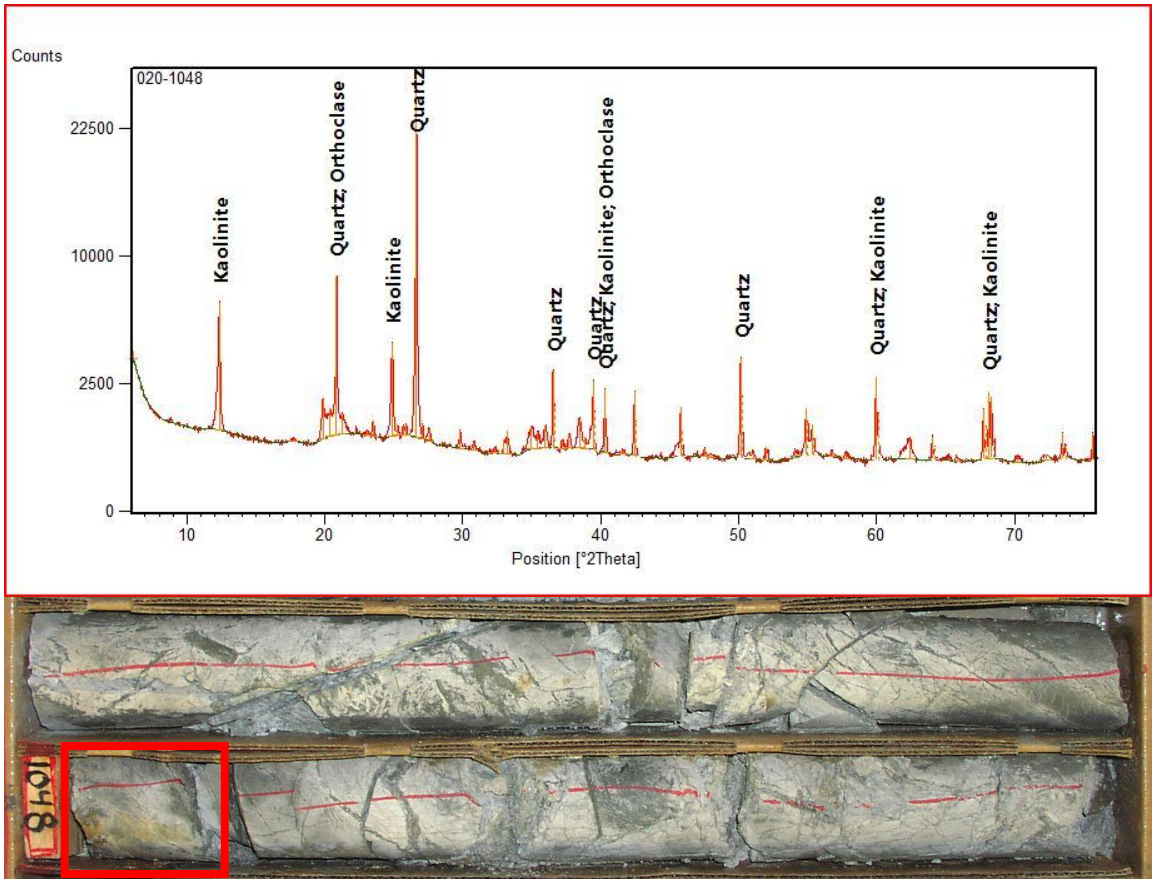

Figure 43. A sample (red box) taken from a five foot section averaging 0.059 oz/t. The sample is strongly altered to quartz and kaolinite and lesser marcasite and orthoclase. The sample is from Cross Section B above the jog in the Getchell Fault, just above a strongly mineralized zone that is characterized by strong argillization of argillaceous mudstone, in comparison to the dominant alteration types elsewhere which are decalcification and silicification of carbonate material in non calc-silicate altered rocks (63.5 mm diameter core).

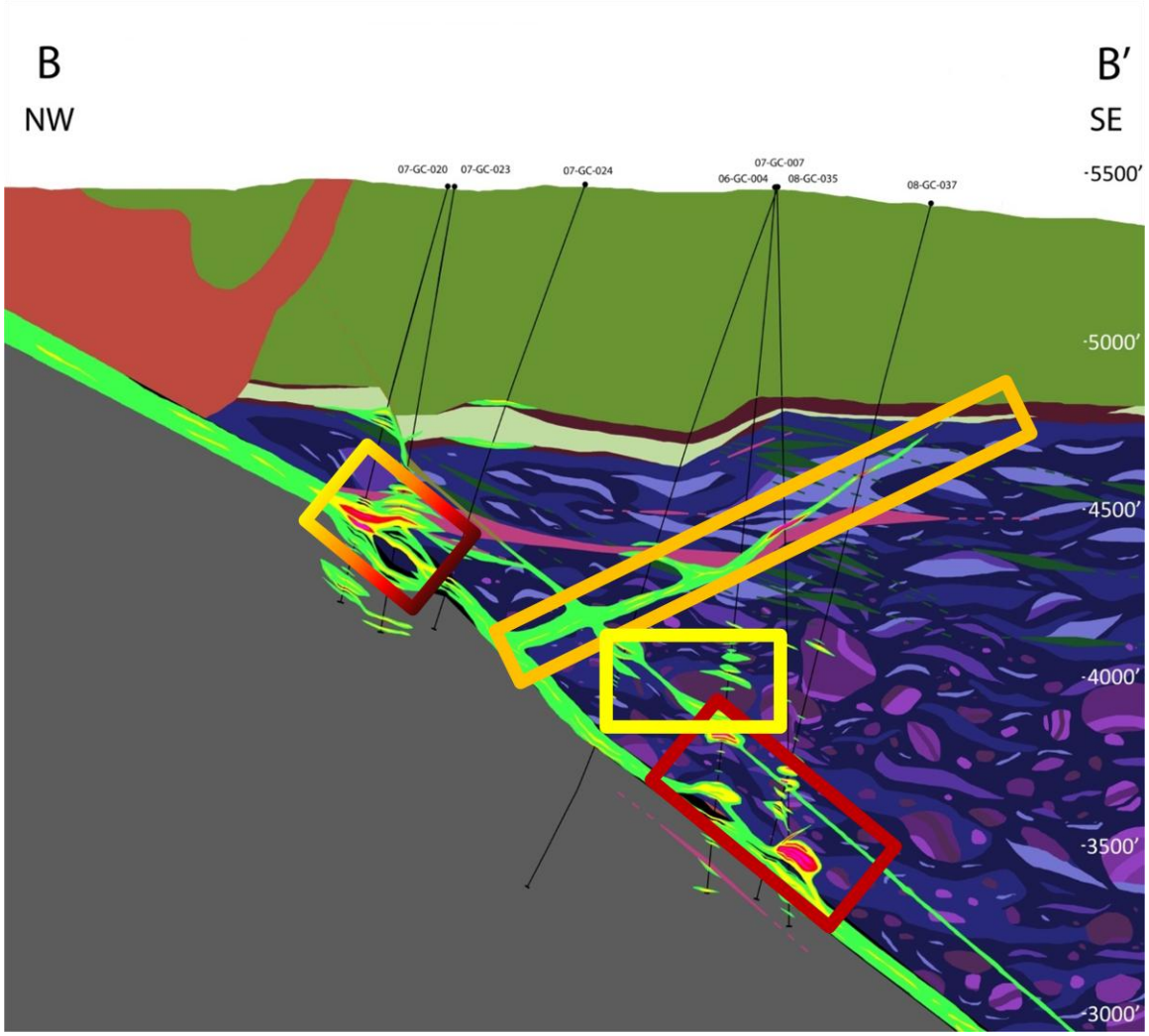

Figure 44. Mineralization overlay on Cross Section B showing Type I mineralization (red box) typically moderate (1.0 to 0.3 oz/t Au) to low grade (0.3 to 0.1 oz/t Au). This mineralization is found above the Getchell fault or the Getchell parallel fault in the hanging wall. Here ore fluids accessed reactive carbonate and generated wider areas of mineralization via carbonate dissolution. Type II mineralization (orange box) is high grade mineralization, commonly >1.0 oz/t Au, found along a west dipping hanging wall fault, mineralization is confined to gouge zone. Type III mineralization (yellow box) typically very low grade mineralization (<0.10 oz/t Au) often found above, or mantling, Type I mineralization. Mineralization in the multi-colored box, where the horizontal dacite dike intersects the Getchell fault, shares characteristics of both Type I (high Hg, Sb, and Tl) and Type II (low Ag) (no vertical exaggeration).

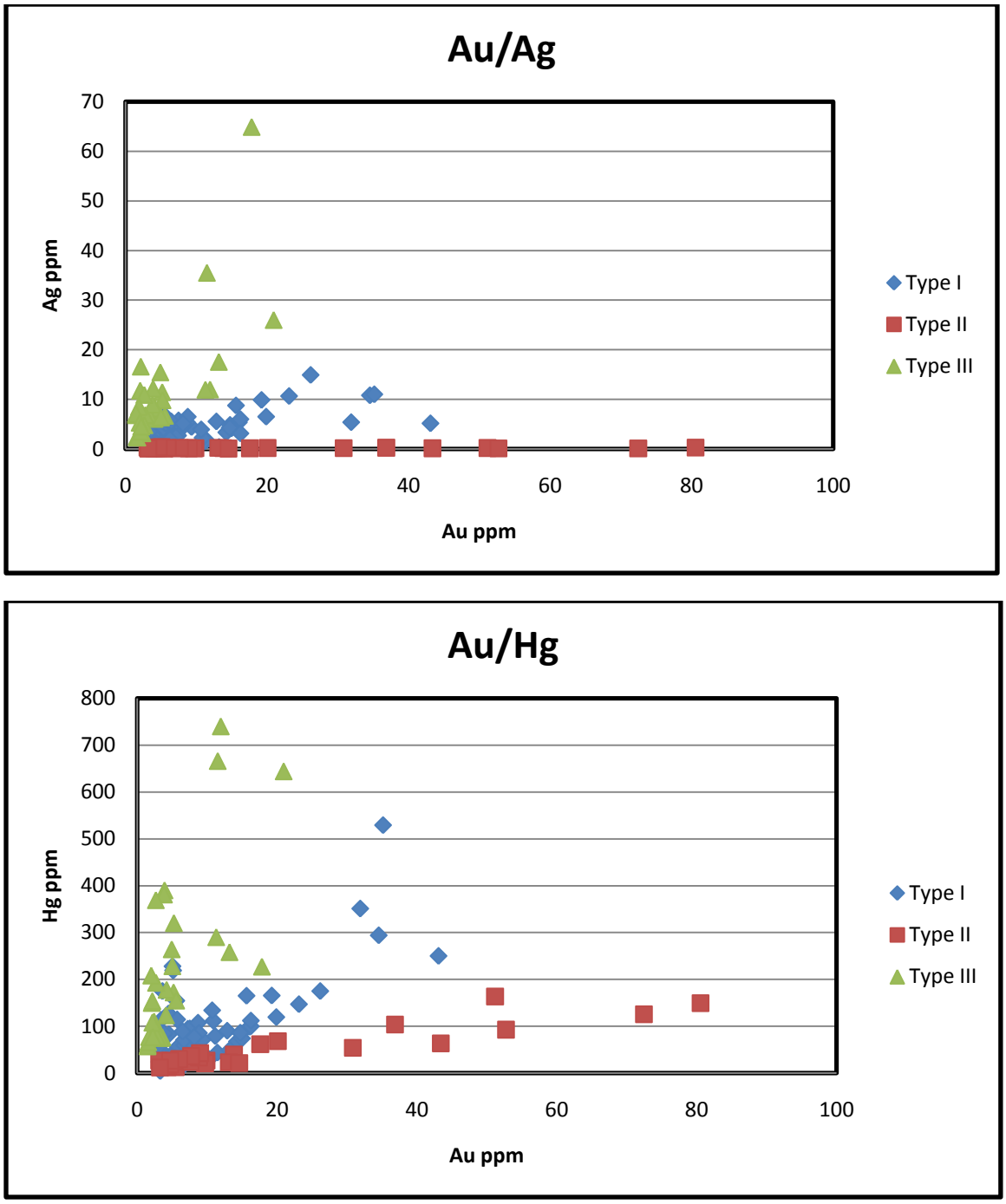

Figure 45. Graphs of Au verses Ag and Hg in Type I,II, and III mineralization showing the variation in chemistry between the three types.

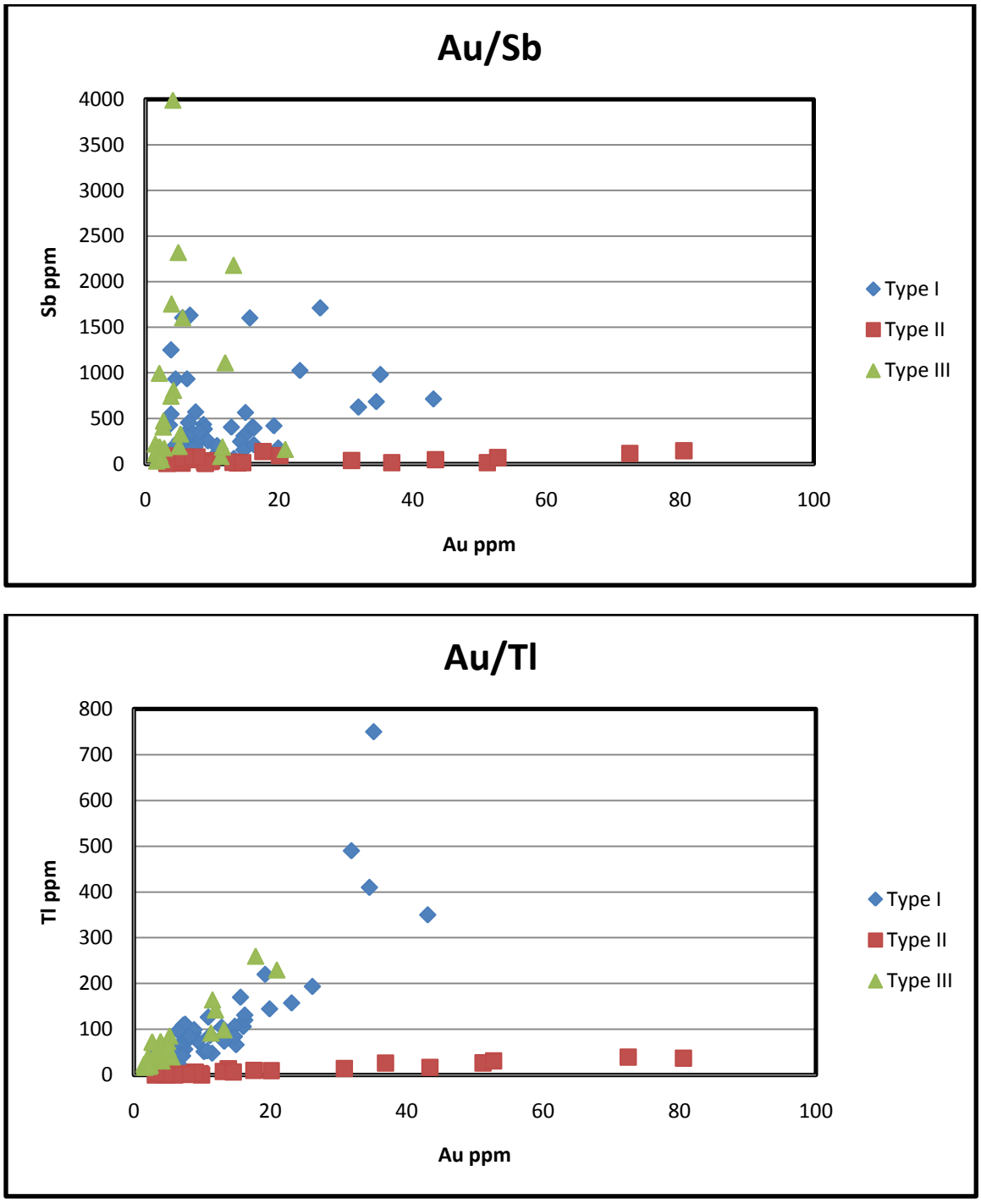

Figure 46. Graphs of Au verses Sb and Tl in Type I,II, and III mineralization showing the variation in chemistry between the three types.

Figure 47. An interval of type II mineralization from drill hole 08-GC-035. Strong bleaching occurs above the mineralized zone, starting at 997 and continuing to 1023, unlike the type I mineralization which generally has little to no bleaching. The bleached zone is not mineralized, grades <0.001 oz/t Au. High-grade mineralization starts abruptly in an argillized gouge zone with abundant sooty pyrite; 1023'-1027' grades 1.645 oz/t and 1027'-1032' averages 1.185 oz/t. There is some disseminated mineralization extending below the fault and 1032'-1037' averages 0.285 oz/t; below mineralization and alteration decline rapidly and 1037'-1042' averages 0.0375 oz/t, 1042'-1045.3' averages 0.005 oz/t (63.5 mm diameter core).

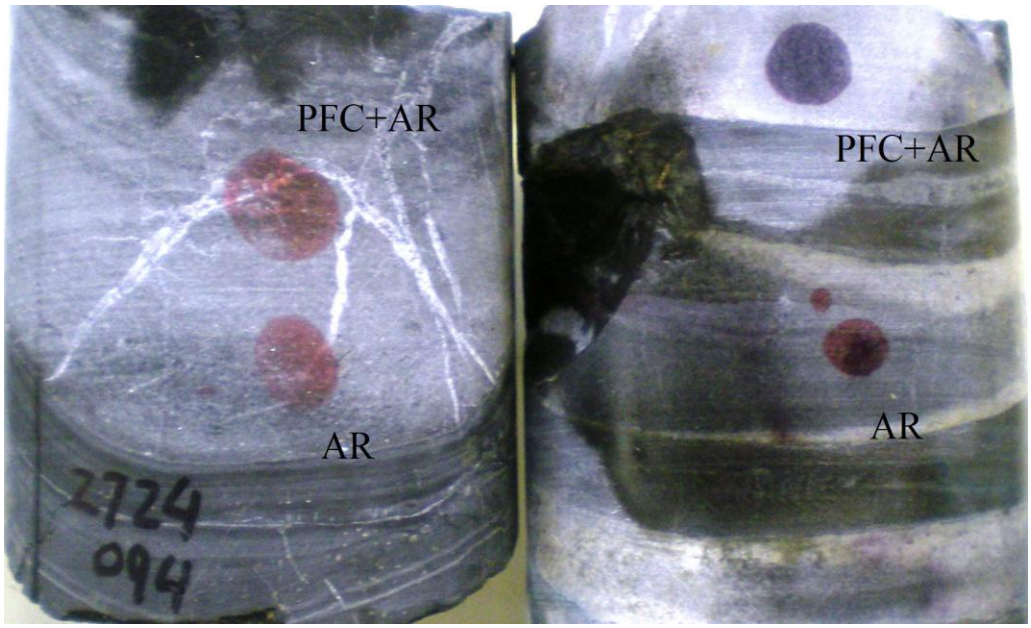

Figure 48. Staining results on limestone inter-bedded with siliceous carbonaceous mudstone and argillaceous mudstone (left and right respectively). The upper spot is 50/50 mixture of potassium ferricyanide and Alizarin red S, the lower spot is only a solution of Alizarin red S, both in a 2% HCl solution. The limestone inter-bedded with siliceous carbonaceous mudstone on the left stains red indicating no iron in the carbonate. The limestone inter-bedded with argillaceous mudstone on the right stains purple indicating the presence of iron in the carbonate (63.5 mm diameter core).

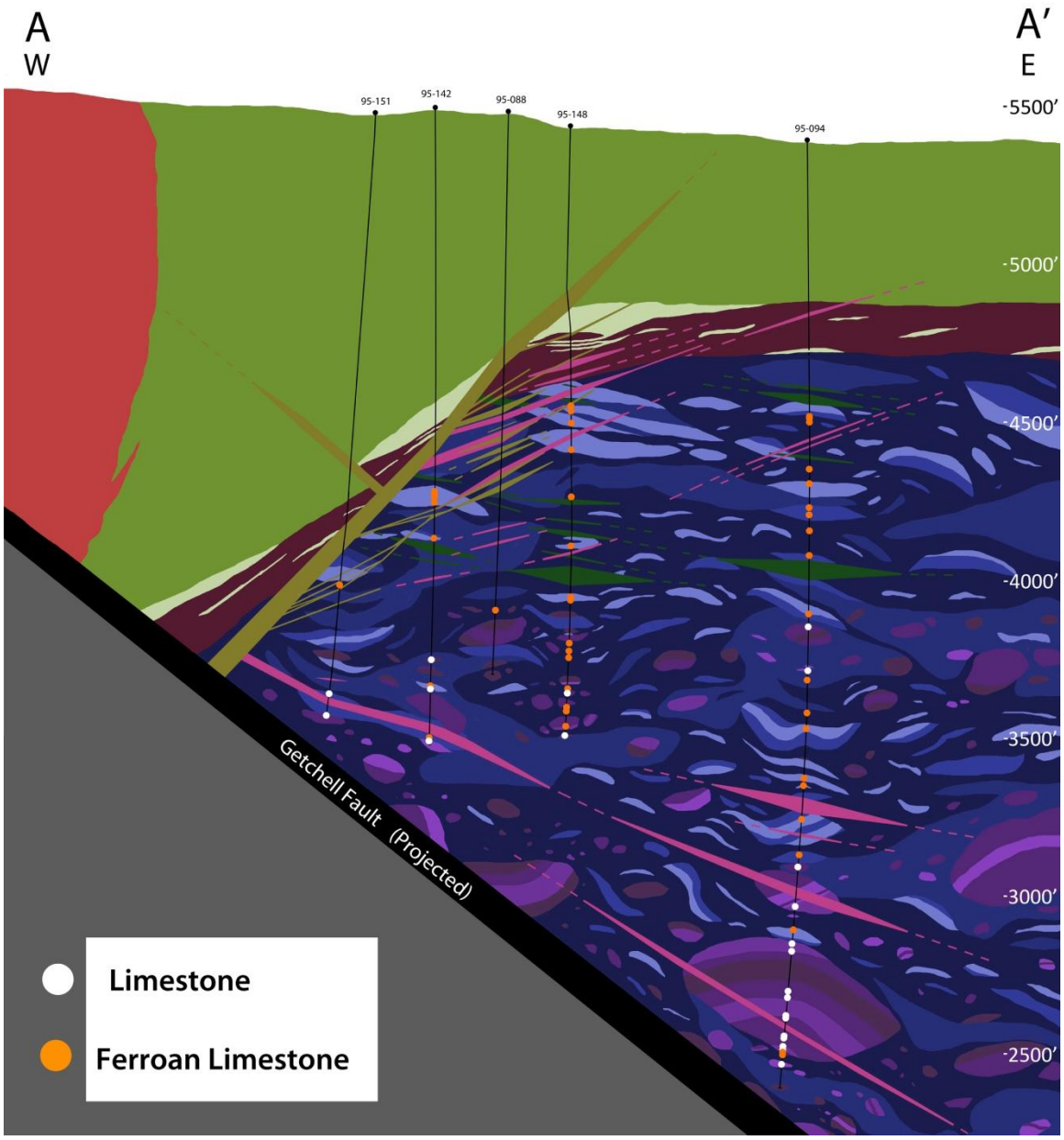

Figure 49. A staining overlay on Cross Section A, with samples of ferroan calcite denoted in orange and samples of iron poor calcite denoted in white (no vertical exaggeration).

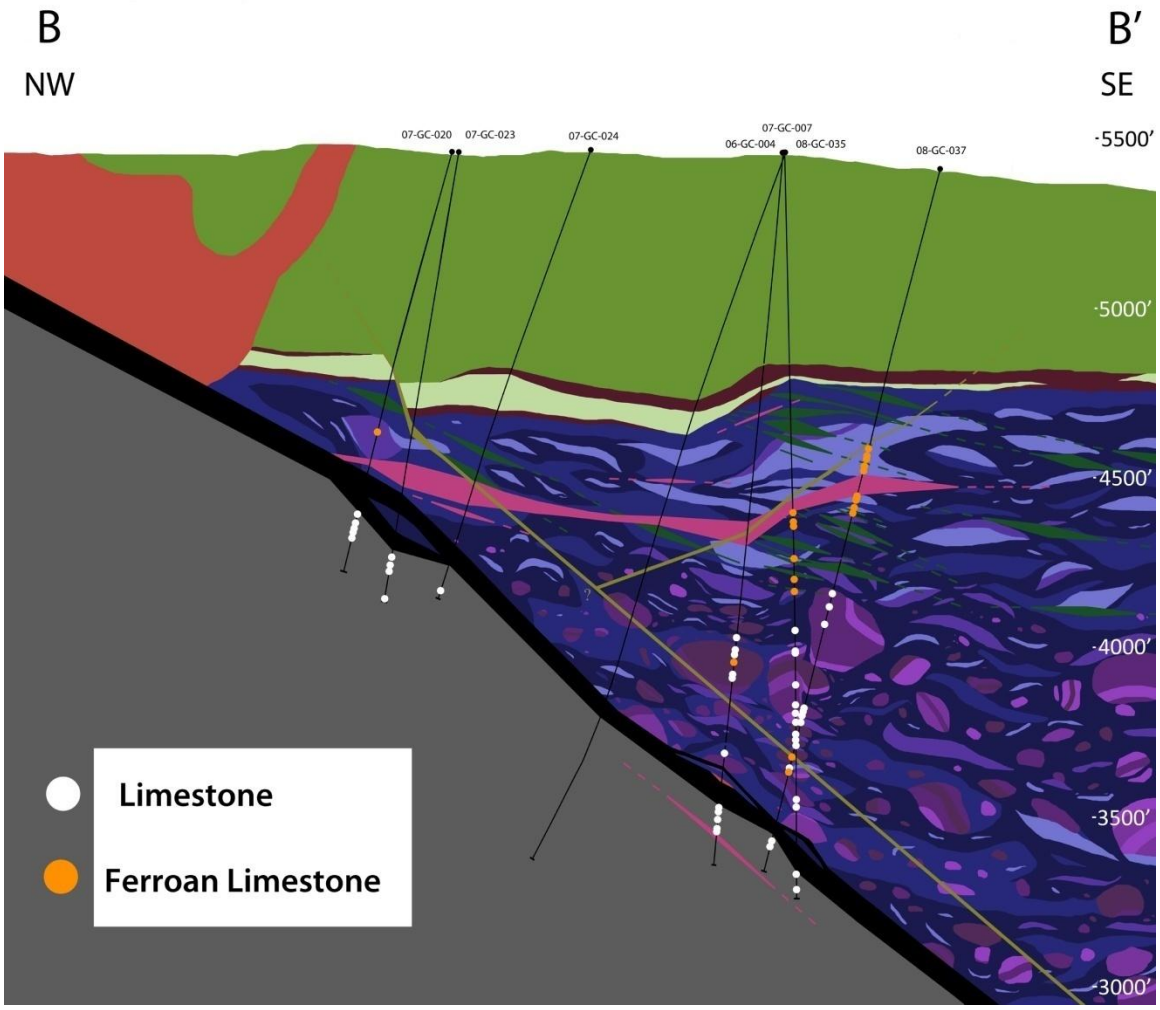

Figure 50. A staining overlay on Cross Section B, with samples of ferroan calcite denoted in orange and samples of iron poor calcite denoted in white (no vertical exaggeration).

BIBLIOGRAPHY

Barker, S., Hickey, K., Cline, J., Dipple, G., Kilburn, M., Vaughan, J., and Longo, T., 2009, Uncloaking invisible gold: Use of NanoSIMS to evaluate gold, trace elements and sulfur isotopes in pyrite from Carlin-type gold deposits: Economic Geology, v. 104, p. 897-904.

Boskie, R., 2001, Detailed structure and stratigraphy of the Lower Paleozoic rocks of the Getchell trend, Osgood Mountains, Humboldt County, Nevada: Unpublished master's thesis, University of Nevada, Reno.

Breit, F., Russel, M., Anderson, S., and Muirhead, E., 2005, Geology and gold deposits of the Twin Creeks Mine, Humboldt County, Nevada: Geological Society of Nevada Symposium 2005, Window to the World v. 1 p. 431-452.

Chevillion, V., Berentsen, E., Gingrich, M., Howald, B., and Zbinden, E., 2000, Geologic overview of the Getchell gold mine geology, exploration, and ore deposits, Humboldt County, Nevada: Society of Economic Geologists Guidebook Series, v. 32, p. 195-201.

Cline, J., and Hofstra, A., 2000, Ore-fluid evolution at the Getchell Carlin-type gold deposit, Nevada, USA: European Journal of Mineralogy, v. 12, p 195-212.

Cline, J., 2001, Timing of gold and arsenic sulfide mineral deposition at the Getchell Carlin-type gold deposit, North Central Nevada: Economic Geology, v. 96, p. 75-89.

Cline, J., Shields, D., Riciputi, L., Fayek, M., Copp, T., Muntean, J., and Hofstra, A., 2003, Trace element and isotope micro analysis support a deep ore fluid source at the Getchell Carlin-type gold deposit, northern Nevada: Geological Society of America *Abstracts with Programs*, v. 35, n. 6, p. 358.

Cline, J., Hofstra, A., Muntean, J., Tosdal, R., and Hickey, K., 2005, Carlin-type gold deposits in Nevada: Critical geologic characteristics and viable models: Economic Geology, 100th Anniversary Volume, p. 451-484.

Cline, J., Muntean, J., Longo, T., and Cassinerio, M., 2008, Collaborative research on fluid pathways and metal transport in Carlin-type gold deposits: Insights from the Getchell deposit, USGS Report.

Cook, H., 2005, Carbonate sequence stratigraphy: an exploration tool for sediment-hosted, disseminated gold deposits in the Great Basin: Geological Society of Nevada Symposium 2005, Window to the World, p. 19-24.

Crafford, A., and Grauch, V., 2002, Geologic and geophysical evidence for the influence of deep crustal structures on Paleozoic tectonics and the alignment of world-class gold deposits, north-central Nevada, USA: Ore Geology Reviews, v. 21, p. 157-184.

Dickinson, W., 2004, Evolution of the North American Cordillera: Annual Review Earth Planet Science, v. 32, p. 13–45.

Emsbo, P., Groves, D., Hofstra, A., and Bierlein, F., 2006, The giant Carlin gold province: a protracted interplay of orogenic, basinal and hydrothermal processes above and lithospheric boundary: Mineralium Deposita, v. 41, p.517-525.

Foster, J., and Kretchmer, E., 1991, Geology of the Mag deposit, Pinson Mine, Humboldt County Nevada: Geological Society of Nevada Geology and Ore deposits of the Great Basin, v. 2, p. 845-856.

Groff, J., Heizler, M., McIntosh, W., and Norman, D., 1997, $^{40}Ar/^{39}Ar$ dating and mineral paragenesis for the Carlin-type gold deposits along the Getchel trend, Nevada: Evidence for Cretaceous and Tertiary gold mineralization, Economic Geology, v. 92, p. 601-622.

Heitt, D., Thompson, T., and Jackson, R., 2003, Geology and Geochemistry of the Deep Star Gold Deposit, Carlin Trend Nevada: Economic Geology, v. 98, p. 1107-1135.

Hitzman, M., 1999, Routine staining of drill core to determine carbonate mineralogy and distinguish carbonate alteration textures: Mineralium Deposita, v. 34, p. 794-798.

Holtz, P. and Willden, R., 1964, Geology and mineral deposits of the Osgood Mountains quadrangle, Humboldt County, Nevada: U.S. Geological Survey Professional Paper 431, 128 p., scale 1:62,500.

Humphreys, E., 1995, Post Laramide removal of the Farallon slab, western United States: Geology, v. 23, p. 987-990.

Joralemon, P., 1951, The occurrence of gold at the Getchell Mine, Nevada: Economic Geology, v. 46, p.267-310.

Longo, A.A., Cline, J.C. and Muntean, J., 2008, Compositional variations in Au-bearing pyrite from a Carlin-type Au deposit, Getchell, Nevada. Geological Society of America Abstracts with Programs, v. 40, n. 1, p. 51

Madden-McGuire, D., and Marsh, S., 1990, Lower Paleozoic host rocks in the Getchell gold belt: Several distinct allocthons of a sequence of continuous sedimentation?: Geology, v. 19, p. 489-492.

Metcalf, R., 2004, Evolution and subduction polarity of the mid-Paleozoic Klamath-Sierra Volcanic Arc, Geological Society of America *Abstracts with Programs*, Vol. 36, No. 4, p. 70

Nevada Bureau of Mines and Geology, 2009, The Nevada mineral industry 2008: Nevada Bureau of Mines and Geology Special Publication MI-2008, 178p.

Roberts, R., Hotz, P., Gilluly, J., and Ferguson, H., 1958, Paleozoic rocks of north-central Nevada: American Association of Petroleum Geologists Bulletin, v. 42, no. 12, p. 2813-2857

Ressel, M., Noble, D., and Henry, C., 2000, Dike-hosted ores of the Beast deposit and the importance of Eocene magmatism in gold mineralization of the Carlin-trend: Economic Geology, v. 95, p. 1417-1444.

Ressel, M., and Henry, C., 2006, Igneous geology of the Carlin Trend, Nevada: Development of the Eocene plutonic complex and significance for Carlin-type gold deposits: Economic Geology, v. 101, p. 347–383.

Sillitoe, R., 2008, Major gold deposits of the North and South American Cordillera: Distribution, tectonomagmatic settings, and metallogenic considerations: Economic Geology, v. 103, p. 663-687.

Tretbar, D., 2004, The geology and geochemistry of the 194 orebody, Getchell Mine, Humboldt County, Nevada, Master's thesis, University of Nevada, Reno.

Stewart, J., 1980, Geology of Nevada: Nevada Bureau of Mines and Geology Special Publication 4, 136p.

Tosdal, R., Wooden, J., and Kistler, R., 2000, Geometry of the Neoproterozoic continental break-up, and implications for the location of Nevadan mineral belts: Geology of Ore Deposits 2000: The Great Basin and Beyond, v. 1, p. 451-466.

VITA

Graduate College
University of Nevada, Las Vegas

Nathan Eck

Degrees:
Bachelor of Science, Geology, 2008
University of Wisconsin – Madison

Thesis Title: The Effects of Contact Metamorphism on Host Rocks for Carlin-Type Mineralization at the Getchell Deposit, Nevada, USA

Thesis Examination Committee:
Co-Chairperson, Adam Simon, Ph. D.
Co-Chairperson, Jean Cline, Ph. D.
Committee Member, Wanda Taylor, Ph. D.
Committee Member, John Muntean, Ph. D.
Graduate Faculty Representative, Barbara Luke, Ph. D.